SKB

TECHNICAL REPORT 95-30

DECOVALEX I – Bench-Mark Test 3: Thermo-hydro-mechanical modelling

Jan Israelsson

Itasca Geomekanik AB

December 1995

SVENSK KÄRNBRÄNSLEHANTERING AB
SWEDISH NUCLEAR FUEL AND WASTE MANAGEMENT CO
P.O.BOX 5864 S-102 40 STOCKHOLM SWEDEN
PHONE +46 8 665 28 00 TELEX 13108 SKB
FAX +46 8 661 57 19

DECOVALEX I - BENCH-MARK TEST 3:

THERMO-HYDRO-MECHANICAL MODELLING

Jan Israelsson

Itasca Geomekanik AB

December 1995

DECOVALEX I

BENCH-MARK TEST 3: THERMO-HYDRO-MECANICAL MODELLING

Jan Israelsson

Itasca Geomekanik AB
Box 17
781 21 Borlänge
Sweden

December 1995

Keywords: DECOVALEX, Numerical modelling, Bench-Mark, Thermal, Hydraulic, Mechanical, Coupled

FOREWORD

This report is an integral part of SKB's engagement in the first part of the DECOVALEX project (DECOVALEX I). The work, that was made 1992-1994, is compiled in four reports and two articles.

The following SKB technical reports have been printed:

Börgesson, L. and Hernelind, J. (1995) "DECOVALEX I — Test Case 2: Calculation of the Fanay-Augères THM Test — Thermomechanical modelling of a fractured rock volume," SKB Technical Report TR 95-28.

Börgesson, L. and Hernelind, J. (1995) "DECOVALEX I — Test Case 3: Calculation of the Big Ben Experiment — Coupled modelling of the thermal, mechanical and hydraulic behaviour of water-unsaturated buffer material in a simulated deposition hole," SKB Technical Report TR 95-29.

Israelsson, J. (1995) "DECOVALEX I — Bench-Mark Test 3: Thermo-Hydro-Mechanical Modelling," SKB Technical Report TR 95-30.

Rosengren, L. and Christianson, M. (1995) "DECOVALEX I — Test Case 1: Coupled Stress-Flow Model," SKB Technical Report TR 95-31.

The following articles have been published:

Rehbinder, G. (1995) "Analytical Solutions of Stationary Coupled Thermo-Hydro-Mechanical Problems," *Int. J. Rock Mech. Min. Sci. & Geomech. Abstr.* Vol. 32, No. 5, pp. 453-463, 1995.

Claesson, J., Follin, S., Hellström, G. and Wallin, N-O. (1995) "On the use of diffusion equation in test case 6 of DECOVALEX," *Int. J. Rock Mech. Min. Sci. & Geomech. Abstr.*, Vol. 32, No. 5, pp. 525-528, 1995.

ABSTRACT

The second phase of DECOVALEX (DEvelopment of COupled models and their VALidation against EXperiments in nuclear waste isolation) involved continuation of the problem(s) initiated in phase I and one new problem, Bench-Mark Test 3 (BMT3). Bench-Mark Test 3 was formulated by the French research teams supported by ANDRA and CEC.

The bench-mark test concerns the excavation of a tunnel, located 500 m below the ground surface, and the establishment of mechanical equilibrium and steady-state fluid flow. Following this, a thermal heating due to nuclear waste, stored in a borehole below the tunnel, was simulated. The results are reported at (1) 30 days after tunnel excavation, (2) steady state, (3) one year after thermal heating, and (4) at the time of maximum temperature.

The problem specification included the excavation and waste geometry, material properties for intact rock and joints, location of more than 6500 joints observed in the 50 by 50 m area, and calculated hydraulic conductivities. However, due to the large number of joints and the lack of dominating orientations, it was decided to treat the problem as a continuum using the computer code *FLAC* /Itasca, 1992a/.

The problem was modeled using a vertical symmetry plane through the tunnel and the borehole. The rock mass was modeled as an elastic - ideally plastic material with a Mohr-Coulomb failure criterion. Equivalent continuum material properties were calculated using Rock Mass Rating by Bieniawski, (1979) and Rock Mass Strength by Stille et al., (1982).

Flow equilibrium was obtained approximately 40 days after the opening of the tunnel. Since the hydraulic conductivity was set to be stress dependent, a noticeable difference in the horizontal and vertical conductivity and flow was observed. After 40 days, an oedometer-type consolidation of the model was observed.

Approximately four years after the initiation of the heat source, a maximum temperature of 171°C was obtained. The stress-dependent hydraulic conductivity and the temperature-dependent dynamic viscosity caused minor changes to the flow pattern.

The specified mechanical boundary conditions imply that the tunnel is part of a system of parallel tunnels (which is the case for many storage concepts). However, the fixed temperature at the top boundary maintains the temperature below the temperature anticipated for an equivalent repository. The combination of mechanical and hydraulic boundary conditions cause the model to behave like an oedometer test in which the consolidation rate goes asymptotically to zero.

SAMMANFATTNING

I den andra fasen av DECOVALEX (DEvelopment of COupled models and their VALidation against EXperiments in nuclear waste isolation) ingick Bench-Mark Test 3, vilket var formulerat av de franska forskningsteamen under support av ANDRA och CEC.

Bench-Mark testet omfattar utbrytningen av en tunnel, placerad 500 m under markytan, med den påföljande beräkningen av mekanisk jämvikt och flödesjämvikt. Så snart jämvikten uppnåtts, vidtog en termisk upphettning av bergmassan på grund av det kärnavfall som lagrats i ett borrhål under tunneln. Förutom för jämviktsläget, redovisas resultat för 30 dagar efter tunnelutbrytning, ett år av termisk upphettning och tillfället för maximal temperatur i modellen.

Problemspecifikationen innehöll, förutom geometrier, dessutom materialparametrar för intakt material och sprickor, strukturdata rörande mer än 6500 sprickor inom ett 50*50 [m] område och beräknade hydrauliska konduktiviteter. På grund av det stora antalet sprickor och avsaknaden av dominerande sprickorienteringar, valdes att behandla problemet som ett kontinuum-problem varför finita differens programmet *FLAC*, /Itasca, 1992a/ användes.

Modellen utformades med ett symmetriplan genom tunneln och borrhålet. Bergmassan tilldelades ett elastiskt-idealt plastiskt brottkriterium enligt Mohr-Coulomb. Materialparametrarna beräknades med hjälp av "Rock Mass Rating" /Bieniawski (1979)/ och "Rock Mass Strength" /Stille et al. (1982)/.

Flödesjämvikt erhölls 40 dagar efter öppningen av tunneln. Eftersom den hydrauliska konduktiviteten tilldelats ett spänningsberoende beteende, erhölls stora variationer i fördelningen av den horisontella och den vertikala konduktiviteten, vilket också kunde observeras i flödesfältet. I ett sent skede dominerades aktiviteten i modellen av en ödometerliknande konsolidering, vilken asymtotiskt gick mot noll.

Ungefär fyra år efter installationen av värmekällan, uppnåddes den maximala temperaturen 171°C. Den spänningsberoende konduktiviteten och temperaturberoendet av den dynamiska viskositeten, medförde en påverkan på flödesbilden, dock ej markant.

De randvillkor som använts, motsvaras av att tunneln ingår i ett system av tunnlar, (vilket är fallet i många lagringskoncept). Dock medför den fixerade temperaturen i den övre randen att temperaturen styrs av randen. Kombinationen av mekaniska och hydrauliska randvillkor i modellen medförde att modellen, i ett sent skede, konsoliderades typ konsolidering i en ödometer.

TABLE OF CONTENTS

SUMMARY AND CONCLUSIONS

The second phase of DECOVALEX (DEvelopment of COupled models and their VALidation against EXperiments in nuclear waste isolation) involved continuation of the problem(s) initiated in phase I and one new problem, Bench-Mark Test 3 (BMT3). Bench-Mark Test 3 was formulated by the French research teams supported by ANDRA and CEC.

The bench-mark test concerns the excavation of a tunnel, located 500 m below the ground surface, and the establishment of mechanical equilibrium and steady-state fluid flow. Following this, a thermal heating due to nuclear waste, stored in a borehole below the tunnel, was simulated. The results are reported at (1) 30 days after tunnel excavation, (2) steady state, (3) one year after thermal heating, and (4) at the time of maximum temperature.

The problem specification included the excavation and waste geometry, material properties for intact rock and joints, location of more than 6500 joints observed in the 50 by 50 m area, and calculated hydraulic conductivities. However, due to the large number of joints and the lack of dominating orientations, it was decided to treat the problem as a continuum using the computer code *FLAC* /Itasca, 1992a/.

The problem was modeled using a vertical symmetry plane through the tunnel and the borehole. The rock mass was modeled as an elastic - ideally plastic material with a Mohr-Coulomb failure criterion. Equivalent continuum material properties were calculated using Rock Mass Rating by Bieniawski, (1979) and Rock Mass Strength by Stille et al., (1982).

Flow equilibrium was obtained approximately 40 days after the opening of the tunnel. Since the hydraulic conductivity was set to be stress dependent, a noticeable difference in the horizontal and vertical conductivity and flow was observed. After 40 days, an oedometer-type consolidation of the model was observed.

Approximately four years after the initiation of the heat source, a maximum temperature of 171°C was obtained. The stress-dependent hydraulic conductivity and the temperature-dependent dynamic viscosity caused minor changes to the flow pattern.

The specified mechanical boundary conditions imply that the tunnel is part of a system of parallel tunnels (which is the case for many storage concepts). However, the fixed temperature at the top boundary maintains the temperature below the temperature anticipated for an equivalent repository. The combination of mechanical and hydraulic boundary conditions cause the model to behave like an oedometer test in which the consolidation rate goes asymptotically to zero.

1 INTRODUCTION

This report presents the results of the Bench-Mark Test (BMT3), of the second phase of DECOVALEX. BMT3, which was formulated and proposed by ANDRA of France and CEC of Belgium, concerns the hydro-thermo-mechanical relation in a rock mass /DECOVALEX, 1992/. The model simulates the opening of a tunnel, establishing the fluid flow equilibrium and thermally loading the rock mass around a nuclear waste canister located in a borehole beneath the tunnel.

The BMT specification describes a 50 by 50 m rock matrix with a tunnel and a borehole in the center. The character of the rock mass was that of the Stripa Granite (i.e., high uniaxial compressive strength and low hydraulic conductivity). The problem specification, described the temperature dependence on the fluid flow characteristics. A conceptual figure of the model geometry and the properties of the solid material and the joints are found in Figure 1-1 and Table 2-1, respectively.

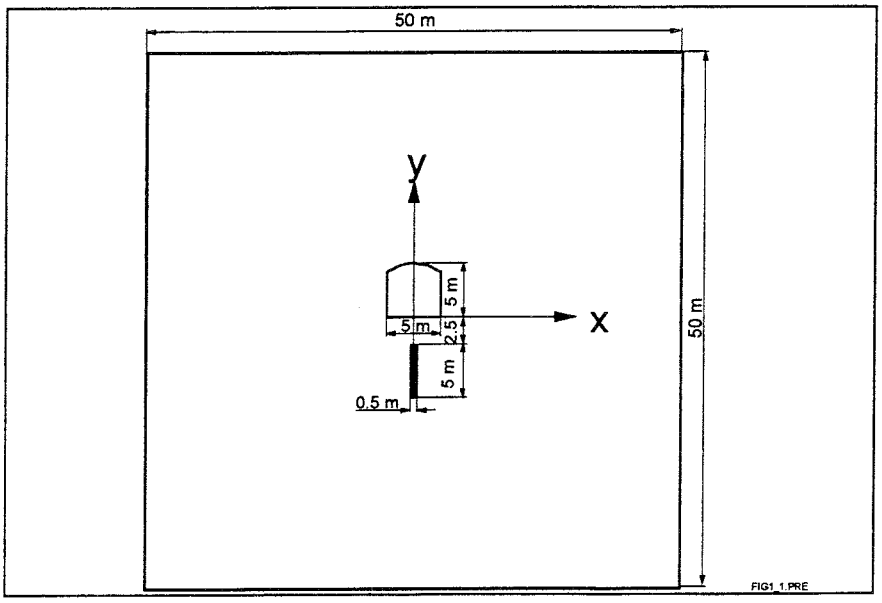

Fig. 1-1 *Conceptual figure of BMT3 problem size and geometry.*

The problem specification provided joint geometry for 6580 joints which was considered too many to model explicitly.

By plotting the frequency of joint orientations, it was found that there were no dominating orientations among the joints listed — i.e., a continuum approach could therefore give a reasonably good representation of the rock mass (see Figure 1-2). Figure 1-3 shows a 20 by 20 m jointed part, centered

in the 50x50 m problem area. Also, there were no concentrations of joint orientations in different regions — i.e., all orientations are represented over the entire problem area. This observation was assumed to be valid for the whole 50x50 m problem domain.

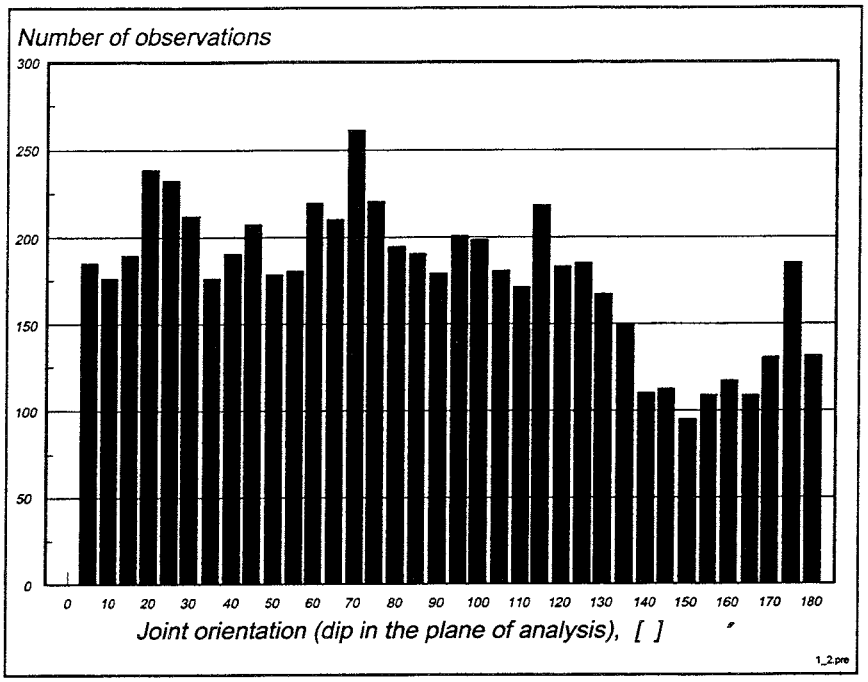

Fig. 1-2 *Frequency of joint dip in the entire problem area (plane). Joint dip measured counter-clockwise from positive x-axis.*

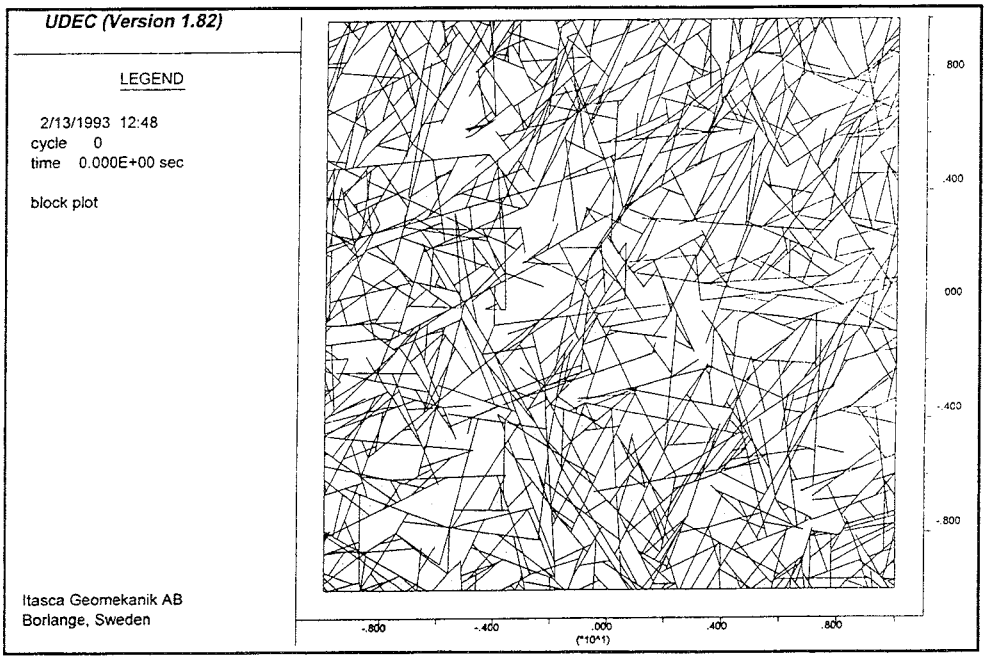

Fig. 1-3 *Joints within a 20 by 20 m block.*

Based on the above observations (i.e., too many blocks to be analyzed as a discontinuum, no dominating joint orientation and no geometric concentrations of joint orientations), it was decided to analyze the problem as a plane strain continuum using the continuum code *FLAC* (**F**ast **L**agranian **A**nalysis of **C**ontinua) /Itasca, 1992a/.

The *FLAC* grid was constructed to accommodate specified data acquisition in points and along lines as shown in Figure 1-4. Due to the vertical symmetry line (see section 2.1.2), the number of acquisition points was reduced as seen in Figure 1-4. The data to be collected and the locations of the points are listed in Table 1-1.

Table 1-1. Location and type of data acquisition points in the model.

	Type of data	**X**	**Y**	**Comments**
A	σx,σy,δx,δy,T(°C)	0	0	
B	-"-	-2.5	2.5	
C	-"-	0	5.0	
D	-"-	2.5	2.5	
E	-"-	-7.5	-7.5	
F	-"-	-7.5	7.5	
G	-"-	7.5	7.5	
H	-"-	7.5	-7.5	
I	-"-	0	-5.0	Not predefined
Tunnel periphery	Water flux			Water flux in m^3/s across the segments E-F, F-G etc. and into the tunnel.
Line E-F	-"-			
Line F-G	-"-			
Line G-H	-"-			
Line E-H	-"-			

Apart from the variables, listed in Table 1-1, the temperature was to be collected along two lines crossing the model vertically and horizontally through the center of the model (0,0). The lines are referred to as Line I and Line II. Also, nine (9) equally sized monitoring regions were predefined in which the porosity and the conductivity were to be recorded. These regions are not shown in Figure 1-4.

A high degree of detail was needed in the central part of the model, where the largest effect from the tunnel excavation and the heat flux from the borehole was expected. In order to keep the model size within reasonable limits, the zone size was increased farther out in the model.
The model consisted of 735 zones, ranging in size from 0.25 m^2 to 8 m^2.

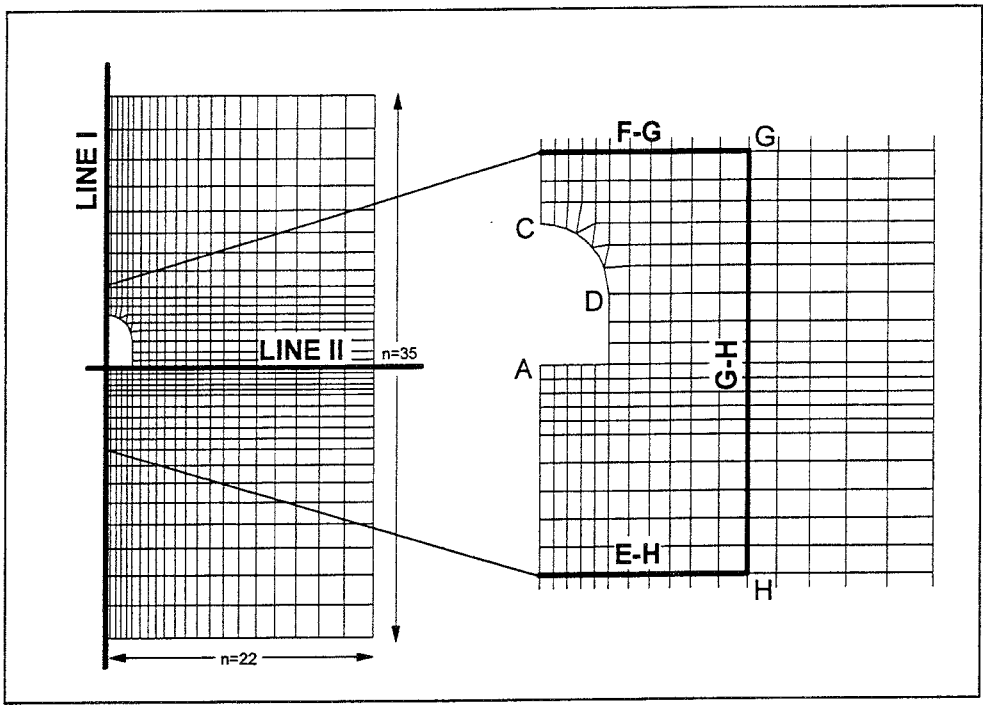

Fig. 1-4 *FLAC model geometry and data acquisition points and lines.*

2 MODELLING APPROACH

2.1 Determination of FLAC input parameters

2.1.1 Rock Mass Mechanical Properties

The mechanical parameters were given for the intact rock blocks and the joints explicitly as shown in Table 2-1. However, the modeling approach required continuum rock mass parameters to be determined.

Table 2-1. Mechanical properties for the intact rock and the joints.

Parameter	Value	Units
Intact Rock Block		
Young's Modulus, E	60	GPa
Poisson's ratio, υ	0.23	
Density, ρ	2670	kg/m^3
Uniaxial compressive strength, σ_c	200	MPa
Tensile strength, σ_T	10	MPa
Joints		
Normal stiffness, K_n	100	GPa/m
Shear stiffness, K_s	10	GPa/m
Cohesion, C	0.1	MPa
Friction angle, ϕ	30	°
Dilatancy angle, i	0	°
Tensile strength	0	MPa

Two different approaches were used to obtain continuum properties;

1 numerical "biaxial" test of a 10 m wide and 20 m high jointed block, using the code UDEC /Itasca, 1992b/ (The procedure and the results are described in Appendix D); and

2 Rock Mass Rating (RMR) /Bieniawski, 1979/, based on fracture observations in the 20 by 20 m block shown in Figure 1-2. (This is described in detail in Appendix E.)

The rock mass strength obtained from the biaxial compression test turned out to be very low, as can be seen in Table 2-2. Modeling the pure mechanical response (i.e., pore pressure=0) of the tunnel excavation using the results of the "biaxial test" resulted in more than one tunnel diameter of yielding around the tunnel. For comparison, it should be noted that the strength obtained from the uniaxial compression of the 1 m diameter and 2 m high Stripa Granite Core /Thorpe et al., 1980/ was greater than the strength values from the numerical biaxial test (see Table 2-2). Therefore, the RMR-rating approach was adopted. However, it is commonly felt that the RMR-ratings are not valid for the hard, crystalline Scandinavian type of rock. Accordingly, the total RMR was directly transformed to RMS (Rock Mass Strength) /Stille et al., 1982/, which gives strength parameters that correspond better to the hard crystalline rock type. As can be seen from Table 2-2, values of cohesion and friction angle obtained by using the RMR-RMS are more reasonable in comparison to results of the ultra large core of Stripa Granite. Therefore, the strength values from the RMR-RMS were used to describe the strength of the rock mass. The Young's modulus used was the average of the value from the RMR approach and a reduction based on the spacing (see Appendix E). The Poisson's ratio, n, was reduced the same amount as the Young's modulus. The strength envelopes resulting from the different approaches are shown in Figure 2-2.

Table 2-2. Continuum mechanical properties obtained with different assumptions.

Parameter	UDEC Biaxial Test	Properties Used	Ultra Large Core	Unit
Young's modulus, E	12	22	52.3	GPa
Poisson's ratio, υ	0.2	0.09	0.25	
Bulk modulus, K	6.7	9.1	34.8	GPa
Shear modulus, G	5.0	10.4	20.9	GPa
Density, ρ	2670			kg/m^3
Cohesion, c	0.1	2.5	1.5[1]	MPa
Friction angle, ϕ	32	45	45[2]	°
Tensile strength	0.1	2.5	1.5	MPa

[1] calculated cohesion, using a uniaxial compression strength of 7.5 MPa and assuming a friction angle of 45°.
[2] assumed

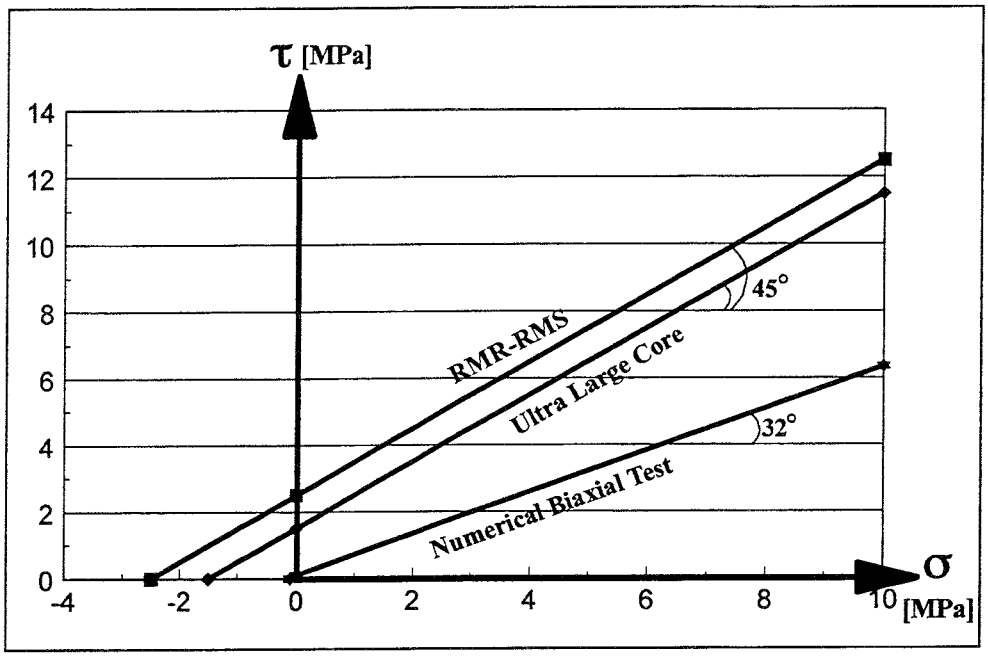

Fig. 2-1 *Strength envelope for different approaches.*

2.1.2 Rock Mass Hydraulic Properties

The calculated horizontal and vertical hydraulic conductivities for different levels of discretization of the model were given in the problem statement. The side lengths of the different "conductivity areas" varied from 5 to 50 m. A side length of 25 m (i.e., 4 different conductivity regions) was chosen for these analysis. However, since the difference in conductivity was low between the different regions, a vertical symmetry line was introduced through the tunnel and the borehole in order to reduce the problem size. The "permeability", *K*, required by *FLAC* is the proportionality constant in Darcy's law expressed in terms of pressure, rather than head. The *FLAC* permeability, K, was calculated using eq. (2-1).

$$K = \frac{k}{\rho_w g} \quad [\mathrm{m^3 s/kg}] \tag{2-1}$$

where k = conductivity [m/s],
ρ_w = water density = 1000 [kg/m^3], and
g = gravity = 9.81 [m/s^2].

The *FLAC* permeabilities, calculated using eq. (2-1) with the specified conductivities, and the symmetry line are shown in Figure 2-2.

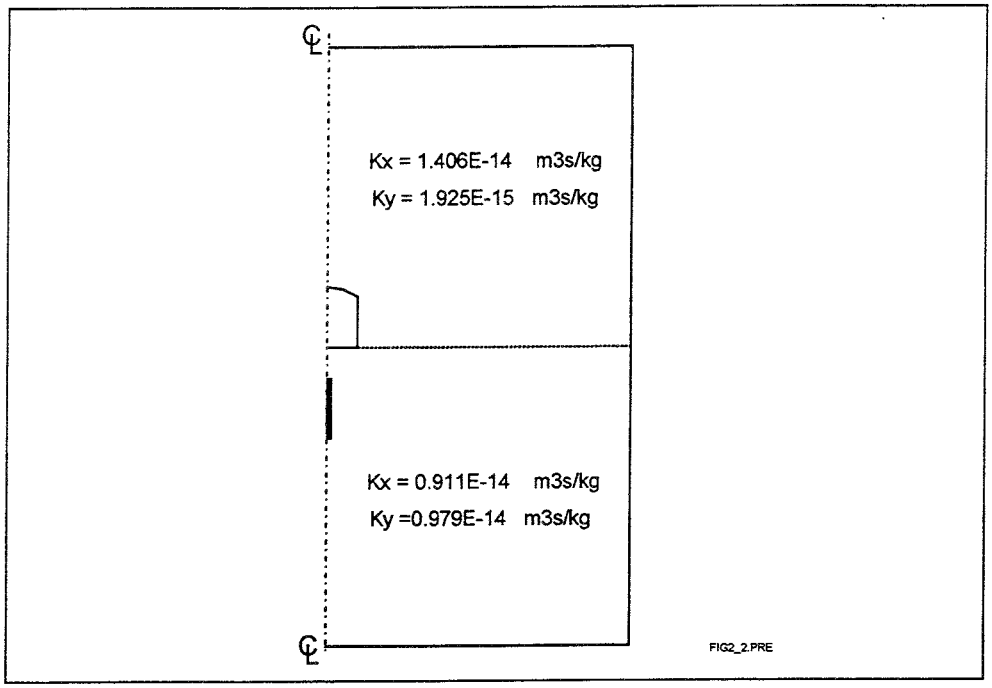

Fig. 2-2 *FLAC permeabilities for the two regions modeled.*

The given porosity, n=1e-4, was the porosity of the "solid", intact rock blocks. Since the rock mass was modeled as a continuum, the void space from the joints was added to the pore volume in an attempt to achieve an equivalent porosity. This was done as follows.

The conductivity, *k*, along one existing set of joints in a discontinuous volume, can be calculated using eq. (2-2).

$$k = \left(\frac{\rho_w g}{12\mu}\right)\frac{a^3}{S} \tag{2-2}$$

where ρ_w = water density = 1000 kg/m^3 (initially),
g = gravity = 9.81 m/s^2,
μ = dynamic viscosity = 1e-3 Ns/m^2 (initially),
a = joint aperture [m], and
S = joint spacing [m].

Plotting the distribution of apertures from the 6580 joints, provided an aperture of approximately 2.2e-6 m as the most frequent aperture (Figure 2-3). Knowing the conductivity and the aperture, an equivalent spacing in the x- and y-directions can be calculated as shown in eq. (2-3).

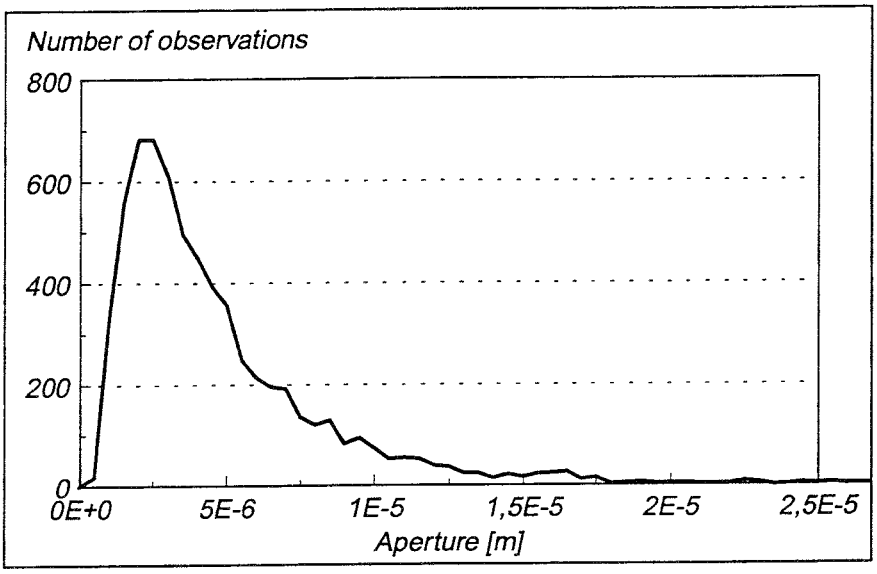

Fig. 2-3 *Joint aperture frequency.*

$$S_x = \left(\frac{\rho_w g}{12\,\mu}\right)\frac{a^3}{k_x} \qquad (2\text{-}3)$$

$$S_y = \left(\frac{\rho_w g}{12\,\mu}\right)\frac{a^3}{k_y}$$

where S_x = spacing between horizontal joints (assuming horizontal flow),
Sy = spacing between vertical joints (assuming vertical flow),
k_x = conductivity in a horizontal direction, and
k_y = conductivity in a vertical direction.

The void space (pore volume) from the joints was calculated using eq. (2-4)

$$V_{joints} = a\left(\frac{1}{S_x} + \frac{1}{S_y}\right) \qquad (2\text{-}4)$$

The calculated spacing and void space from joints are listed in Table 2-3.

Table 2-3. Equivalent joint spacing and pore volume from joints for different model regions.

model region	spacing (m)	pore volume (m^3)
upper right	Sx=6.3e-2 Sy=4.6e-2	0.83e-4
low right	Sx=9.7e-2 Sy=9.0e-2	0.47e-4

The total initial porosity was then simplified to be the sum of the porosity in the intact rock blocks and the void space from the joints — i.e., 1e-4 + 0.5E-4 and 1E-4 + 1e-4 for the two regions, respectively.

2.1.3 Rock Mass Thermal Properties

The thermal properties of the rock matrix, specified in the BMT3, are listed in Table 2-4.

Table 2-4. Thermal properties of the rock matrix as specified in the BMT3.

Parameter	Value	Unit
Thermal conductivity, λ	3	W/m°K
Spec. heat capacity, C_s	4200	J/kg°K
Therm. expansion coeff., a	9.e-6	1/°K

The values, specified in Table 2-4, were used as thermal properties for the continuum rock mass — i.e., no thermal influence from the joints were taken into account for.

2.1.4 Mechanical Influence on Rock Mass Hydraulic Properties

As the rock mass deforms, the hydraulic characteristics of the rock mass will change. In a discontinuous rock mass, this will mainly result from joint aperture changes as the normal effective stress changes.

It was assumed that the change in aperture was linearly related to the change in normal stress, according to eq. (2-5).

$$\Delta a_x = \frac{\Delta \sigma_y}{K_N}$$

$$\Delta a_y = \frac{\Delta \sigma_x}{K_N} \qquad (2\text{-}5)$$

The initial aperture of 2.2e-6 m was set to be the residual aperture — i.e., the aperture was not allowed to decrease below this value.

Substituting into eq. (2-2) the conductivity of the rock mass will be;

$$k_{xx} = \left(\frac{\rho_w\, g}{12\,\mu}\right) \frac{\left(a_0 + \frac{\sigma_{yy} - \sigma_{yy}^0}{K_N}\right)^3}{S_x}$$

$$k_{yy} = \left(\frac{\rho_w\, g}{12\,\mu}\right) \frac{\left(a_0 + \frac{\sigma_{xx} - \sigma_{xx}^0}{K_N}\right)^3}{S_y} \qquad (2\text{-}6)$$

Where a_0 = initial joint aperture

σ_{xx}^0 and

σ_{yy}^0 = initial stresses in the x- and y- directions,

K_N = normal stiffness of joints,

S_x and

S_y = joint spacing for flow in x and y direction

However, in order to avoid large conductivity contrasts, which would require significant computation, the change in conductivity was limited to 10 times the initial conductivity. This restriction was believed to have only a small effect on the overall flow rates.

2.1.5 Heat Source and Thermal Influence on Rock Mass Hydraulic Properties

The waste, stored in the borehole under the tunnel, serves as a heat generator, causing the rock mass temperature in the vicinity of the borehole to increase. The strength of the heat source was given for the assumption of an infinite, linear volumetric source — i.e., no assumption concerning the cross-sectional geometry of the borehole was made (e.g., square or circle). The total heat flux was reduced by half due to the symmetry plane used. The total flux, q, of the source was calculated using eq. (2-7).

$$q = \frac{1}{2} \cdot Q \cdot h \cdot D \cdot 1 = 587.5 \ \text{[W]} \qquad (2\text{-}7)$$

where D = diameter of source = 0.5 m,
h = height of source = 5 m, and
Q = heat flux per m^3 = initially 470 W/m^3.

The symmetry line made it possible to apply the heat source as a boundary flux with height 5 m and strength of

$$\frac{q}{5} = \frac{587.5}{5} = 117.5\ [\mathrm{W/m^2}]$$

The heat, Q, decayed as a function of time, t, given by

$$Q(t) = Q_0\ exp^{-\beta * t} \qquad (2\text{-}8)$$

where Q_0 = 0.47e3 [W/m^3],
β = 0.02 [1/year], and
t = time in year.

The decay history can be seen in Figure 2-4 together with the decay history for ten-year-old spent fuel, proposed by Peters, (1983).

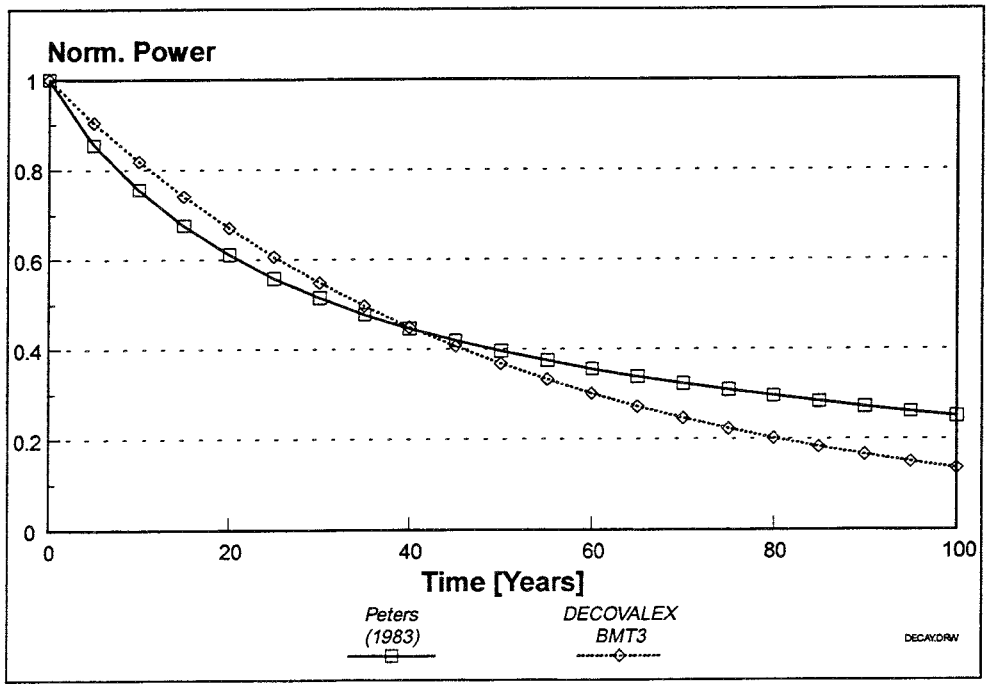

Fig. 2-4 *Heat flux decay with time for the BMT3 heat source and spent nuclear fuel after 10 years according to Peters, (1983).*

In a two dimensional *FLAC* calculation, the decay of the heat flux will result in a calculated maximum temperature of approximately 170°C in the center of the borehole after approximately 4.1 years, as can be seen in Figure 2-5.

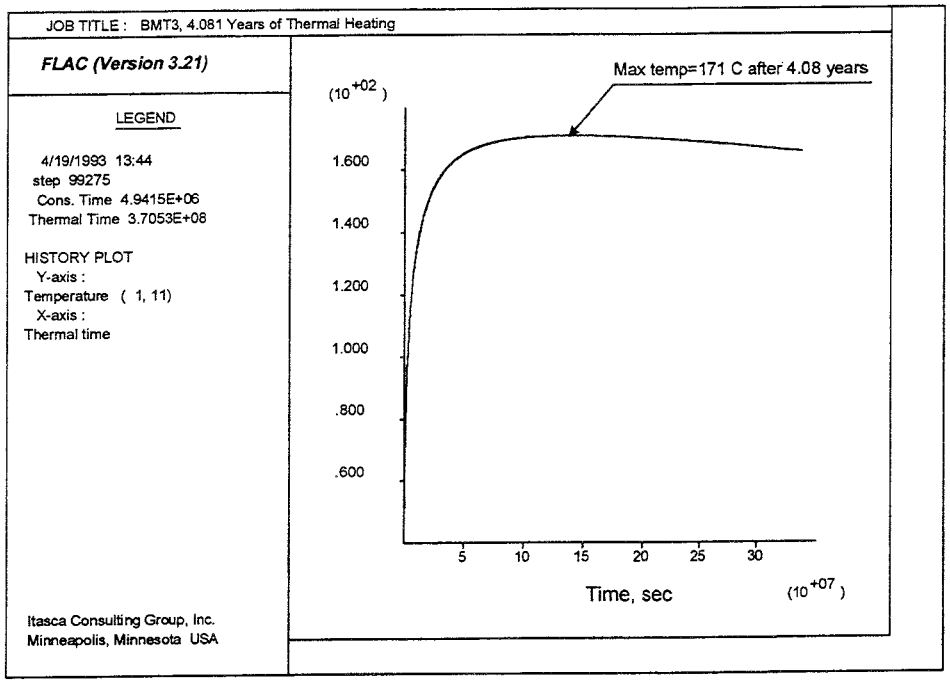

Fig. 2-5 *Calculated temperature history in the center of the borehole*

In the problem statement, the water density and the dynamic viscosity were supposed to be temperature dependent according to eqs. (2-9) and (2-10). Therefore, the conductivity of the rock mass will be temperature dependent.

$$\rho_w = \rho_w^0 [1 - \varepsilon(T - T^0)] \tag{2-9}$$

$$\mu = \frac{\mu^0}{[1 + \gamma(T - T^0)]} \tag{2-10}$$

where ρ_w^0 = initial density of water = 1000 kg/m^3,
T^0 = initial temperature = 27°C,
ε = 6e-4 1/°K,
μ^0 = initial dynamic viscosity = 1e-3 Ns/m^2, and
γ = 3.2e-2 1/°K

However, if eq. (2-2) is combined with eqs. (2-9) and (2-10), it is found that the density has no influence on the permeability, as shown in eq. (2-11):

$$K = \frac{\left(\frac{\rho_w^0 [1 - \varepsilon(T - T_0)]g}{\mu^0 / [1 + \gamma(T - T^0)]}\right)}{\rho_w^0 [1 - \varepsilon(T - T^0)]g} \left(\frac{a^3}{12S}\right) = \frac{[1 + \gamma(T - T^0)]}{\mu^0} \left(\frac{a^3}{12S}\right) \tag{2-11}$$

This means that the permeability used will be both stress- and temperature-dependent, as described in eq. (2-12):

$$K_{xx} = \frac{[1+\gamma(T-T^0)]\,[a^0+(\sigma_{yy}-\sigma_{yy}^0)/K_N]^3}{12\mu^0 S_x}$$

$$K_{yy} = \frac{[1+\gamma(T-T^0)]\,[a^0+(\sigma_{xx}-\sigma_{xx}^0)/K_N]^3}{12\mu^0 S_y} \qquad (2\text{-}12)$$

2.1.6 Properties of the Fluid

The properties of the fluid, specified in the BMT3, are listed in Table 2-5.

Table 2-5. Properties of the fluid as specified in the BMT3.

Parameter	Value	Unit
Initial density, ρ_w	1000	kg/m^3
Heat capacity, C_w	4200	J/kg°C

In *FLAC*, the fluid can not absorb or transport heat (see section 5), which means that the specific heat of the fluid was not used in the analyses. However, the temperature dependency of the water density, ρ_w, and the dynamic viscosity, μ, was modelled as specified. The water density varied with the temperature as described in eq. (2-9). The dynamic viscosity varied with the temperature as shown in eq. (2-10).

There was nothing specified in the BMT3 about the bulk modulus of the water and the amount of dissolved air in the water. However, by assuming that the content of dissolved air in the water was not more than one percent, a bulk modulus was calculated using eq. (2-13). A bulk modulus of the water of 2E8 Pa corresponding to 0.45% air content was used for the analysis.

$$K_f = \frac{K_a\,K_w}{K_a + x(K_w - K_a)} \qquad (2\text{-}13)$$

where K_f = bulk modulus of the fluid,
K_a = bulk modulus of the air, (average pore pressure of the system for isothermal expansion, 1 MPa),
K_w = bulk modulus of the water (2 GPa), and
x = proportion of air in the fluid.

2.2 BOUNDARY CONDITIONS

2.2.1 Mechanical Boundary Conditions

The mechanical boundary conditions specified in the problem were used. Roller boundaries were applied to the bottom and the two vertical sides of the model (see Figure 2-6). Roller boundaries prevent the boundary from moving in a normal direction. On the top boundary, a normal stress, corresponding to the overburden (475 m), was applied.

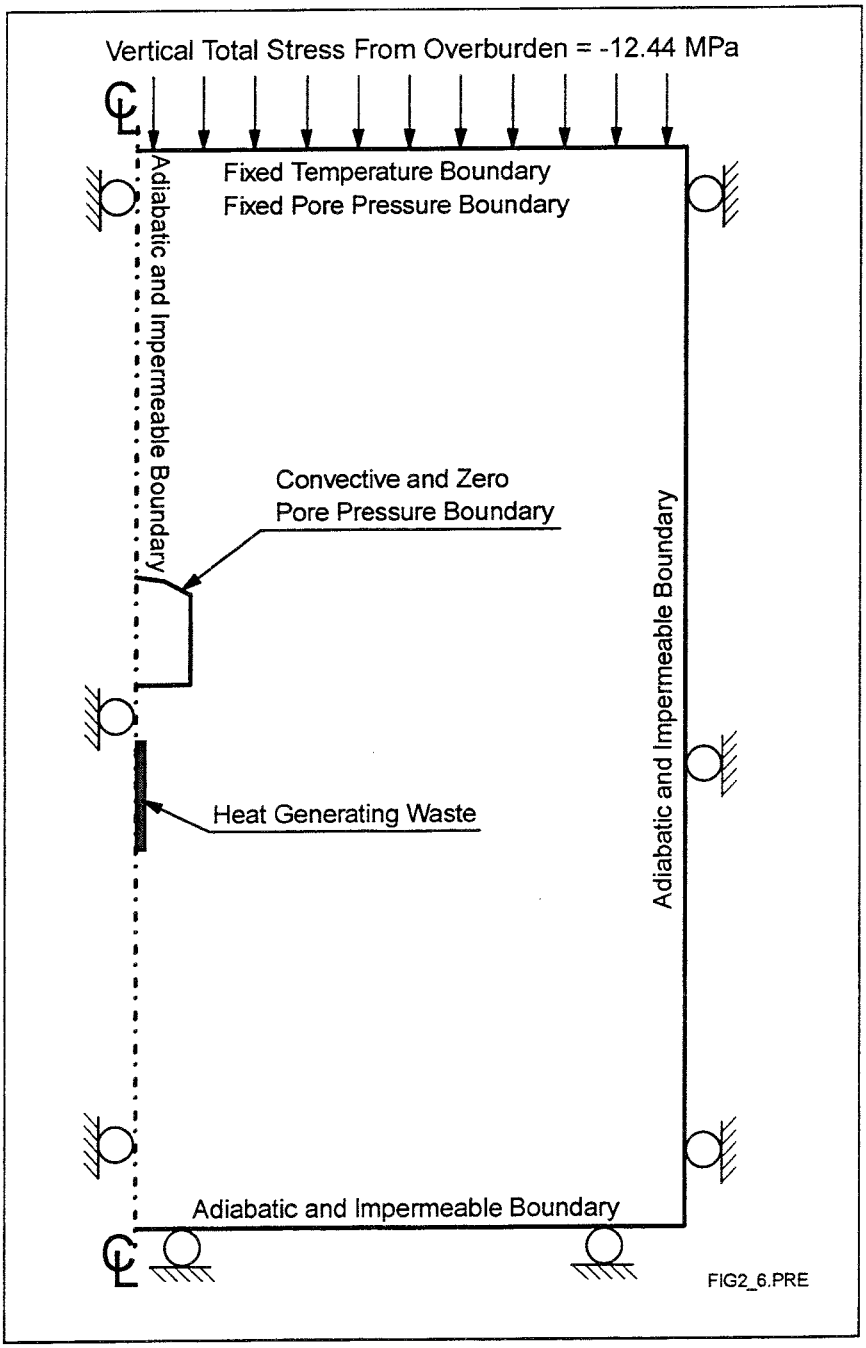

Fig. 2-6 *Boundary conditions of the BMT3 model.*

2.2.2 Thermal Boundary Conditions

The thermal boundary conditions specified in the problem were used. The bottom boundary and the two vertical boundaries were defined as adiabatic boundaries. The top boundary was given a constant temperature of 27°C. The tunnel wall was given a flux condition according to eq. (2-16) (Figure 2-7).

$$\phi_t = H(T_{wall} - T_0) \quad [\frac{W}{m^2}] \tag{2-16}$$

where ϕ_t = thermal flux into tunnel [W/m^2],
H = coefficient of surface heat transfer = 7 W/m^2°C ,
T_{wall}= wall temperature °C, and
T_0 = constant tunnel temperature = 27°C.

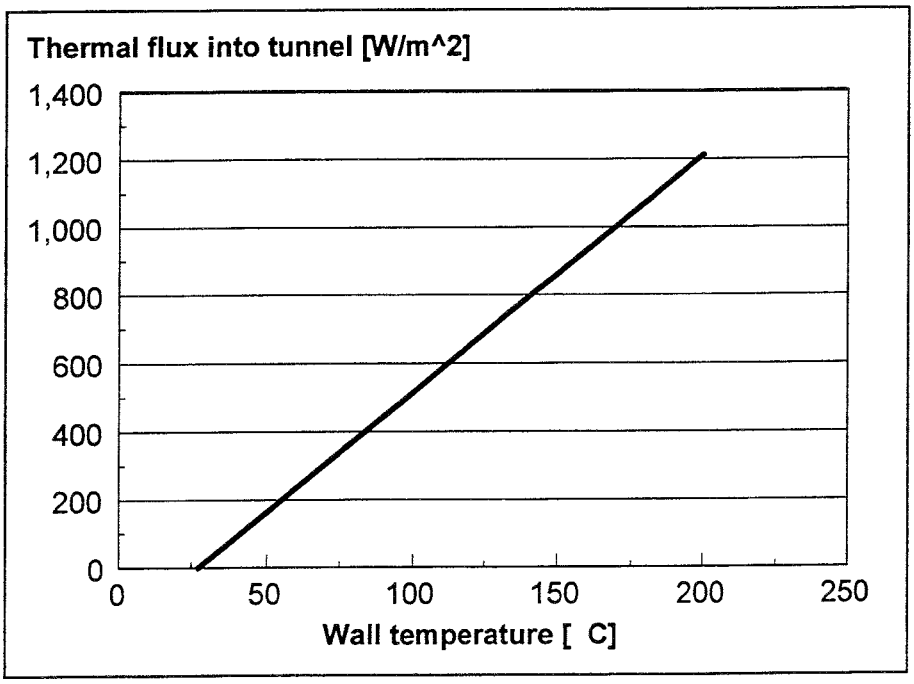

Fig. 2-7 *Thermal flux through tunnel wall as a function of tunnel wall temperature.*

2.2.3 Hydraulic Boundary Conditions

The hydraulic boundary conditions specified for the problem were used. At the top boundary, the pore pressure was fixed to a value (4.66 MPa) corresponding to a free water table at the ground surface. The bottom and the two vertical boundaries were impermeable, which implies that all inflow to the model had to occur through the top boundary. When the tunnel was excavated, the pore pressure at the tunnel surface was fixed to zero.

2.3 IN-SITU STRESSES AND PORE PRESSURES

The in-situ stresses acting in the model were applied as hydrostatic total stress corresponding to the weight of the overlying rock mass (eq. (2-17)).

$$\sigma_x = \sigma_y = \sigma_z = \rho g y \tag{2-17}$$

where ρ = rock mass density = 2670 kg/m^3,
g = gravity = 9.81 m/s^2, and
y = depth below ground surface [m].

The initial pore pressure was assumed to be hydrostatic from the ground surface and is governed by eq. (2-18).

$$p = \rho_w g y \tag{2-18}$$

where ρ_w = initial density of water = 1000 kg/m^3

Since the water table was supposed to be at the ground surface, the total stress and the pore pressure distribution are as shown in Figure 2-8.

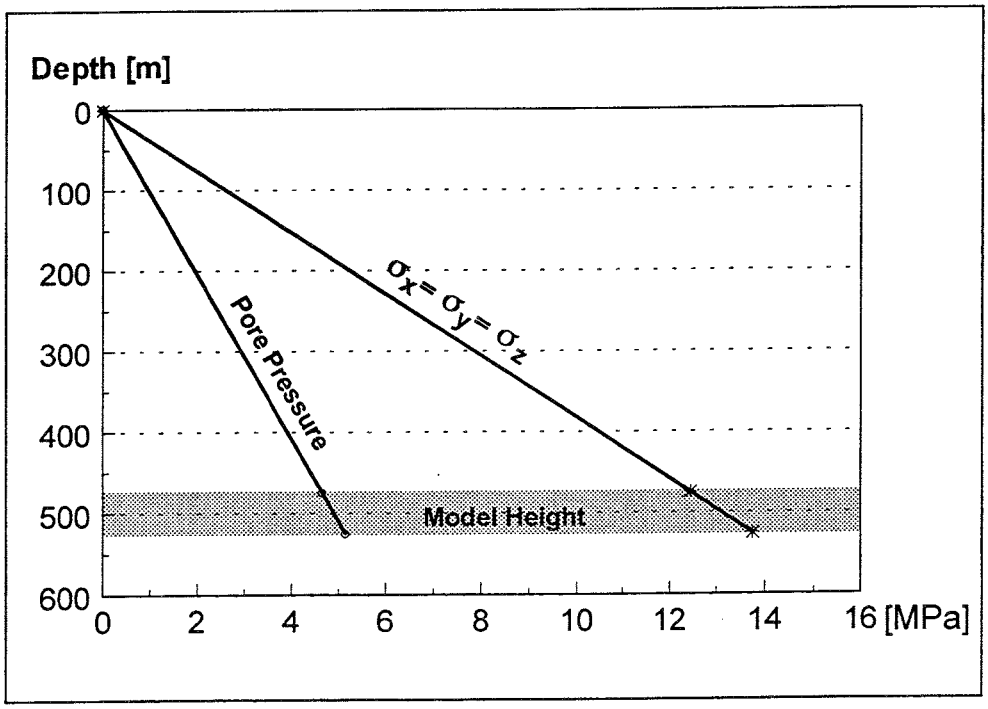

Fig. 2-8 *In-situ stresses and pore pressure distribution.*

3 RESULTS

3.1 Introduction

The analyses were conducted with *FLAC* Version 3.22, configured for Intel 387/487 coprocessors on a Gateway 486, 66 MHz. The coupled hydromechanical coupled analysis for 30 days of simulated time took approximately 60 hours. Due to practical reasons, all plots were extracted with Version 3.21. This does not change the results in any way.

The reader is kindly asked to note the following remarks for the result presentation.

1. In *FLAC*, compressional stresses are negative.

2. The flux over segments affected by the symmetry plane (i.e., into the tunnel, over the F-G and the H-E segments) are doubled in order to represent the total inflow into the tunnel and over the segments.

3.2 INITIAL STATE

Initially, all displacements are zero. There is no water flowing in the model and the permeability, stress and pore pressure distributions are those described earlier in this report as the initial state. However, for the comparison, the horizontal and vertical stresses in the monitoring points are listed in Table 3-1.

Table 3-1. In-Situ total stresses acting at monitoring points A-H.

Point	σ_x (MPa)	σ_y (MPa)
A	-13.08	-13.08
C	-12.95	-12.95
D	-13.02	-13.02
G	-12.88	-12.88
H	-13.28	-13.28

3.3 Tunnel Excavation (t=0)

The mechanical effect in the rock mass due to the excavation of the tunnel is more or less instantaneous if compared to the fluid response. Therefore, it is interesting to note the mechanical effects for future 1comparisons. The "instantaneous" mechanical response is represented by the mechanical equilibrium, established with the flow calculations set off, directly after the tunnel is excavated.

As can be seen from Figures 3-1 and 3-2, the vertical closure of the tunnel is slightly greater than the horizontal convergence --- i.e., around 4 mm. This is caused by the yielded zone under the tunnel which is larger than in the tunnel walls and in the roof, as shown in Figure 3-3.

For the comparison, the horizontal and vertical stresses and the displacements for the "instantaneous" mechanical response are listed in Tables 3-2 and 3-3.

Table 3-2. "Instantaneous" total stresses acting at monitoring points A-H.

Point	σ_x (MPa)	σ_y (MPa)
A	-10.7	-0.1
C	-19.7	-3.3
D	-3.8	-17.4
G	-12.4	-13.3
H	-13.2	-13.5

Table 3-3. "Instantaneous" displacements of monitoring points A-H.

Point	u_x (mm)	u_y (mm)
A	0	1.8
C	0	-2.2
D	-1.9	-0.8
G	-0.4	-0.7
H	-0.2	-0.1

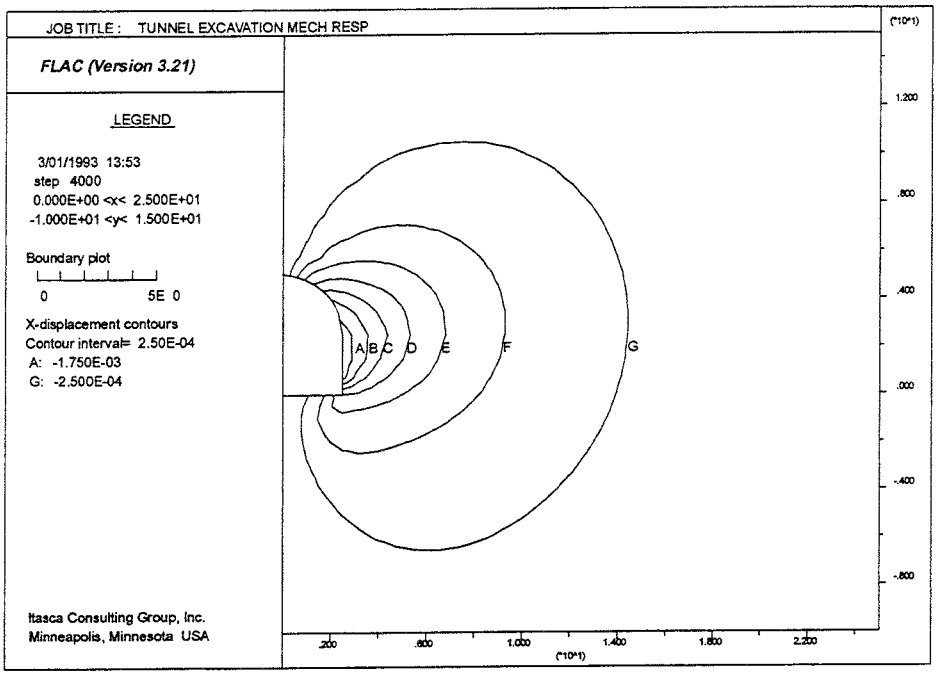

Fig. 3-1 *"Instantaneous" horizontal displacement contours from the mechanical response to tunnel excavation.*

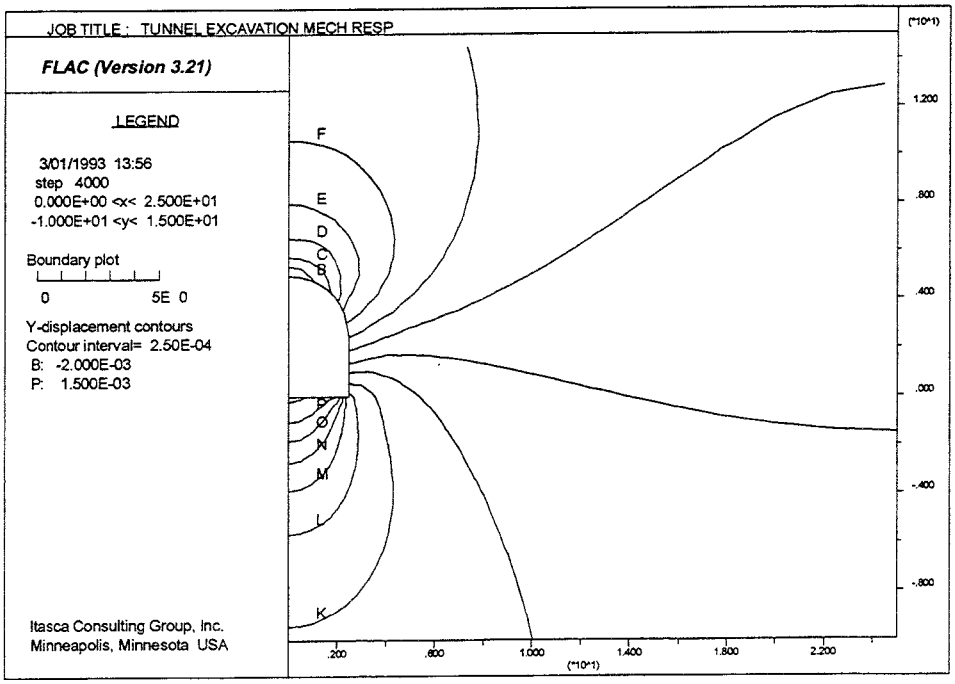

Fig. 3-2 *"Instantaneous" vertical displacement contours from the mechanical response to tunnel excavation.*

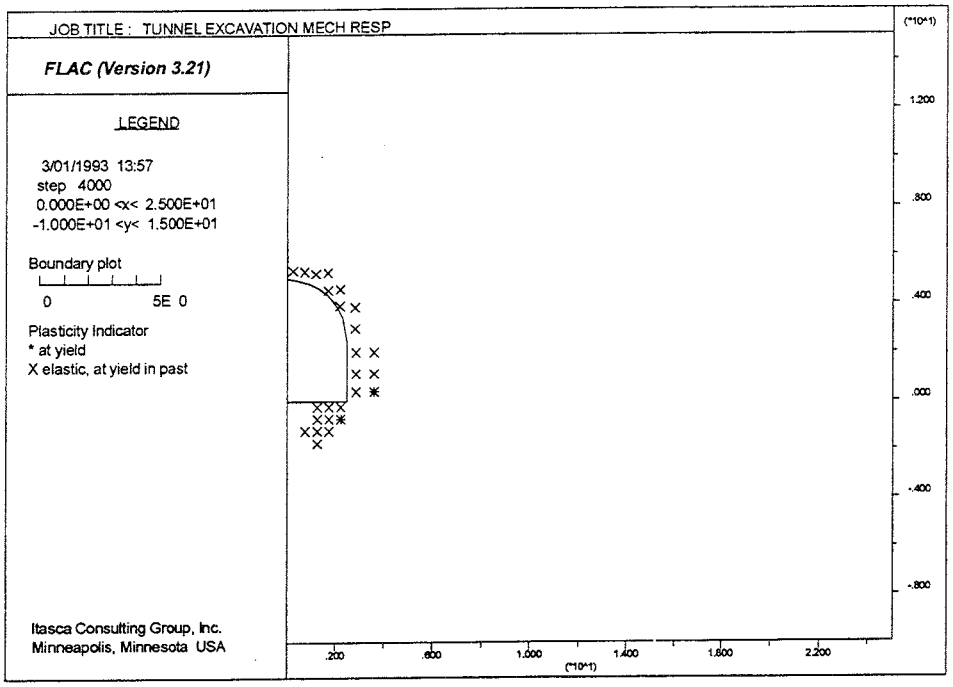

Fig. 3-3 *Yielded zones around tunnel due to "instantaneous" mechanical response to tunnel excavation.*

3.4 RESULTS AT ONE MONTH AFTER EXCAVATION

One month after the excavation of the tunnel, the model is close to its flow equilibrium state. The "qratio", which indicates the ratio between unbalanced flow and average flow in the model, is 1.8 % (see Figure 3-4).

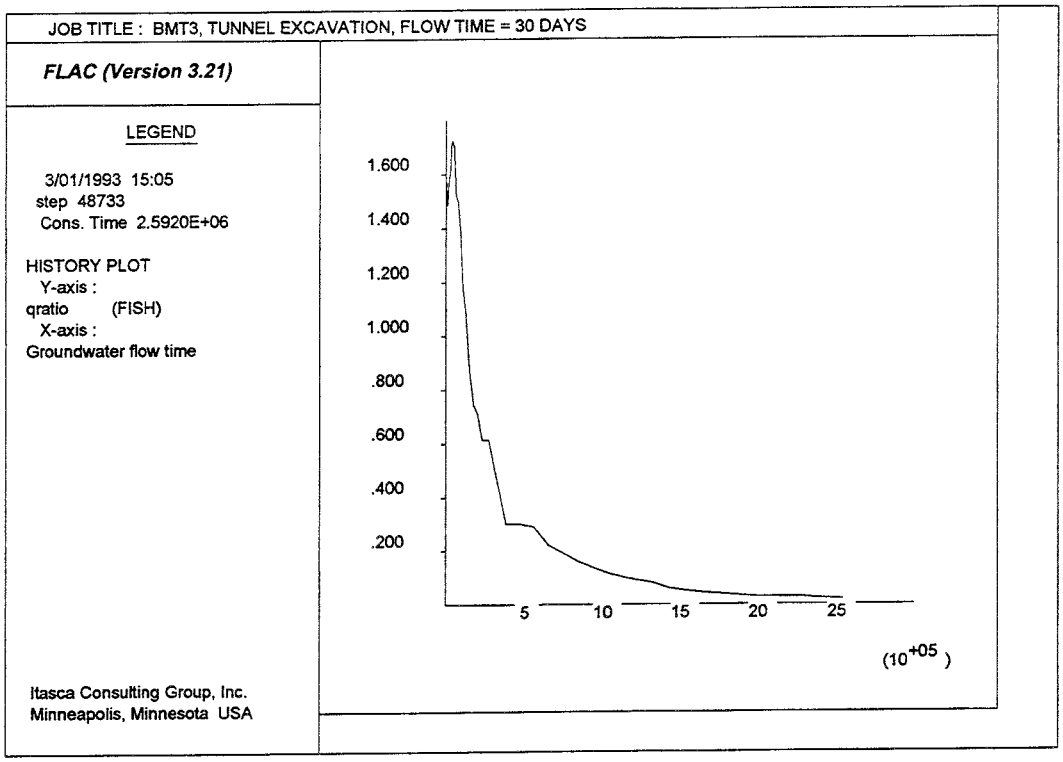

Fig. 3-4 *Ratio between unbalanced flow and average flow over the first 30 days (x-axis is time in seconds).*

The dominating activity throughout the model is the consolidation. The consolidation, which is a very slow process, is caused by the dissipation of water, which leaves the model through the tunnel. The flow situation is described with flow vectors and stream-lines in Figure 3-5

The water flux for the different segments are given in Table 3-4. Due to the use of a symmetry line, the listed fluxes into the tunnel and for segment F-G and E-H are multiplied by two.

Table 3-4. Water flux over segments after one month (values are corrected for the symmetry plane --- i.e., $Flux_{Tunnel}=2*Flux_{Tunnel}^{Sym}$).

Segment	Water flux (m^3/s)
Tunnel	23.6e-8
F-G	8.5e-8
G-H	5.8e-8
H-E	2.4e-8

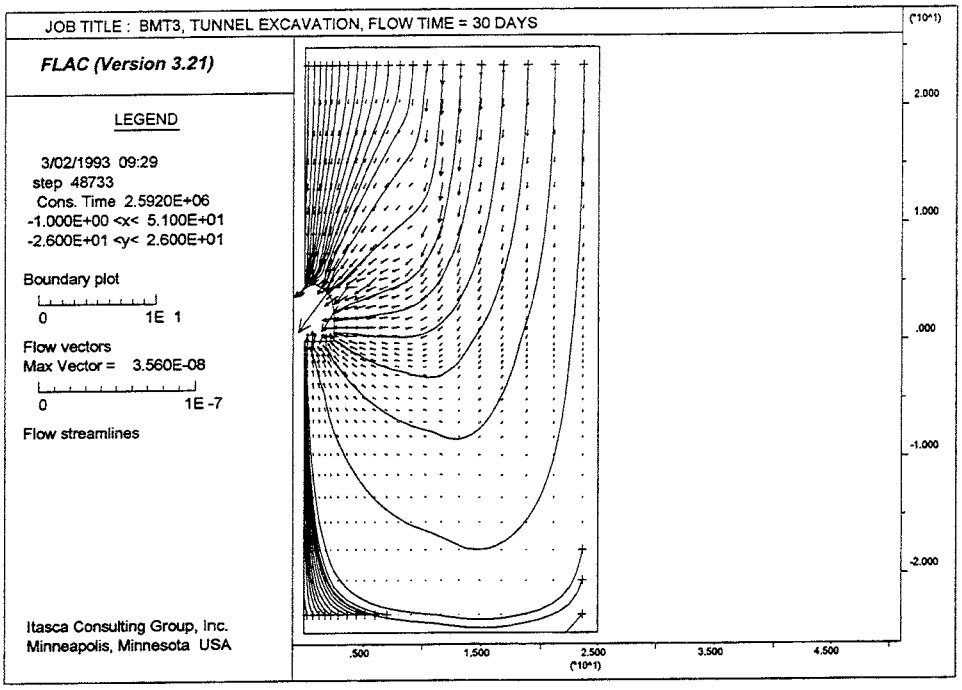

Fig. 3-5 *Water flow vectors and stream-lines after one month of flow.*

The pore pressure distribution and the permeability distribution can be found in Figures 3-6 through 3-8. Notice that the initial division of the model in two permeability regions causes a number of contour lines to appear at the sharp border between the regions.

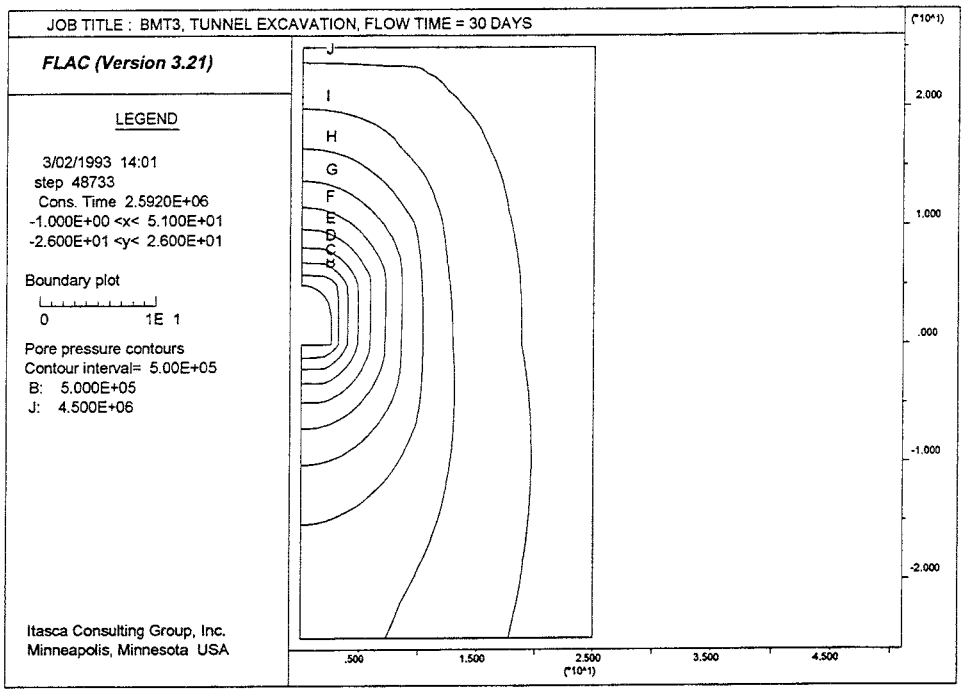

Fig. 3-6 *Pore pressure distribution after one month of flow.*

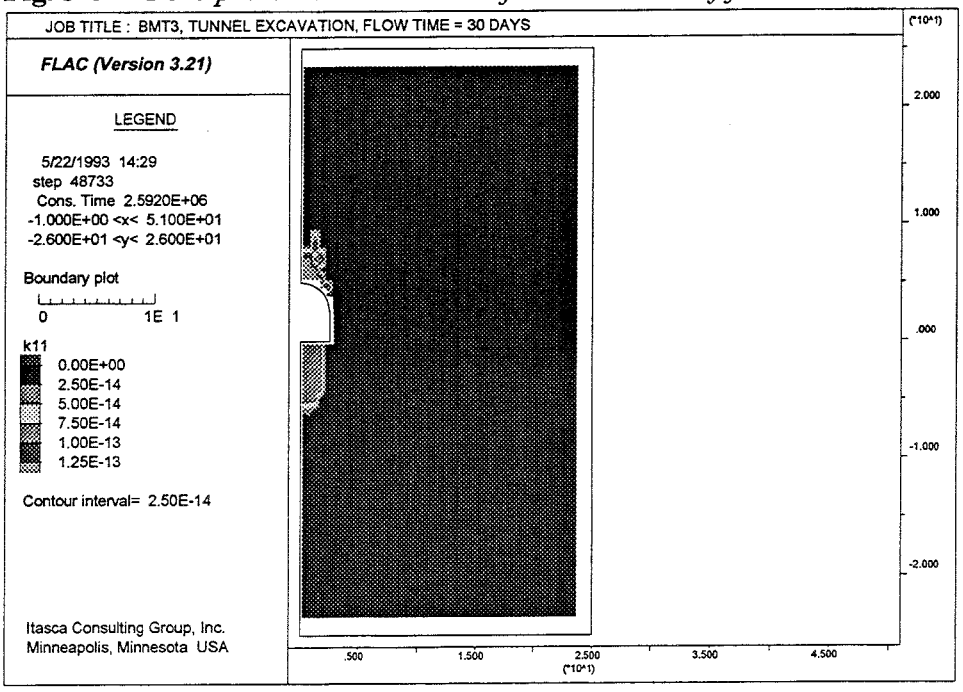

Fig. 3-7 *Distribution of horizontal permeability, K_{xx} (k11 in the legend), after one month of flow.*

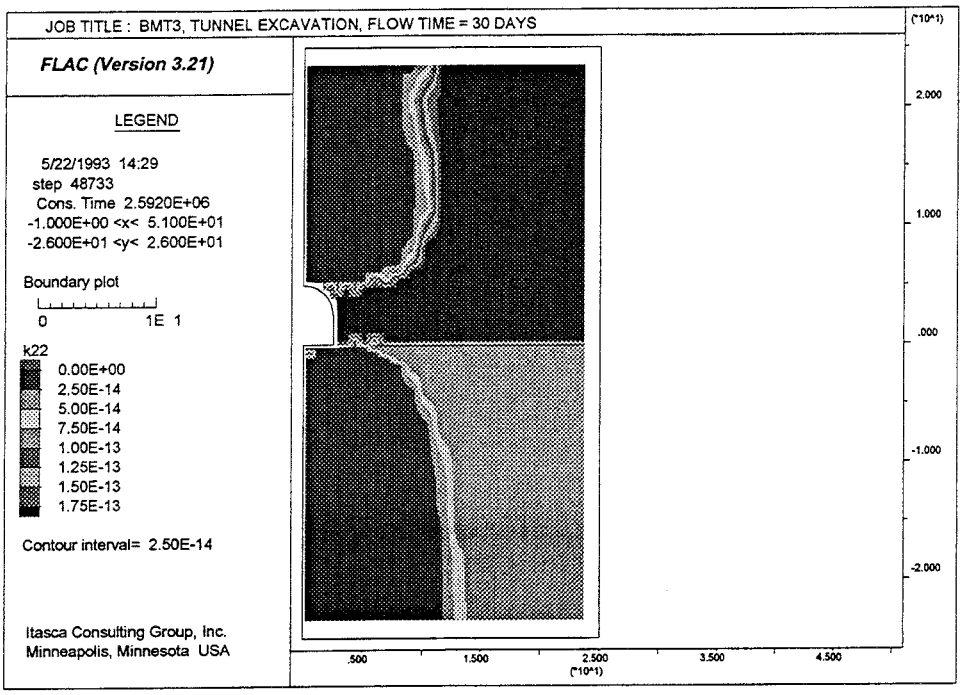

Fig. 3-8 *Distribution of vertical permeability, K_{yy} (k22 in the legend), after one month of flow.*

As seen in Figure 3-7, the horizontal permeability is increased below and above the tunnel due to the reduced vertical stress in those areas. Since the initial aperture was assumed to be residual (i.e., no further closure of the joints were allowed), no reduction of the horizontal permeability can be seen in the tunnel wall.

The vertical permeability, K_{yy}, is increased in a wedge-shaped area from the tunnel wall, upward and downward. This is due to the reduced horizontal stresses in these areas. Also in the yielded zone in the tunnel floor, an increase in the vertical permeability can be seen.

The stresses in the monitoring points are listed in Table 3-5. The overall horizontal and vertical stresses can be found in Figures 3-9 and 3-10. The total stresses normal to vertical and horizontal profile lines (i.e., lines I and II) can be seen in Figure 3-11.

Table 3-5. Total stresses acting at monitoring points A-H after one month.

Point	σ_x (MPa)	σ_y (MPa)
A	-9.2	-0.02
C	-18.8	-3.1
D	-3.9	-15.4
G	-11.4	-13.2
H	-12.0	-13.2

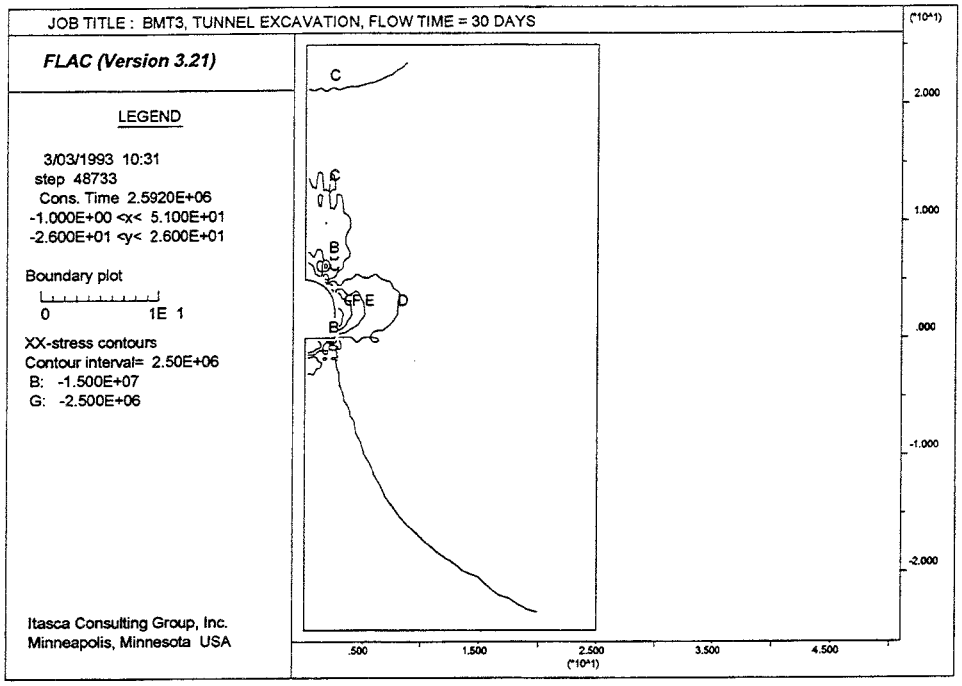

Fig. 3-9 *Horizontal total stress contours one month after excavation of the tunnel.*

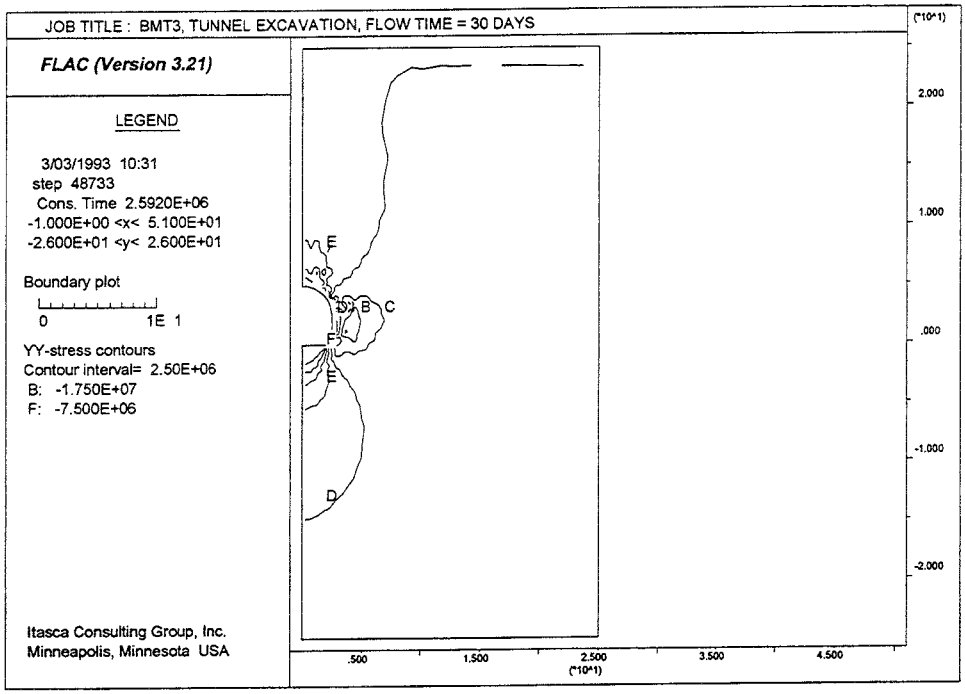

Fig. 3-10 *Vertical total stress contours one month after excavation of the tunnel.*

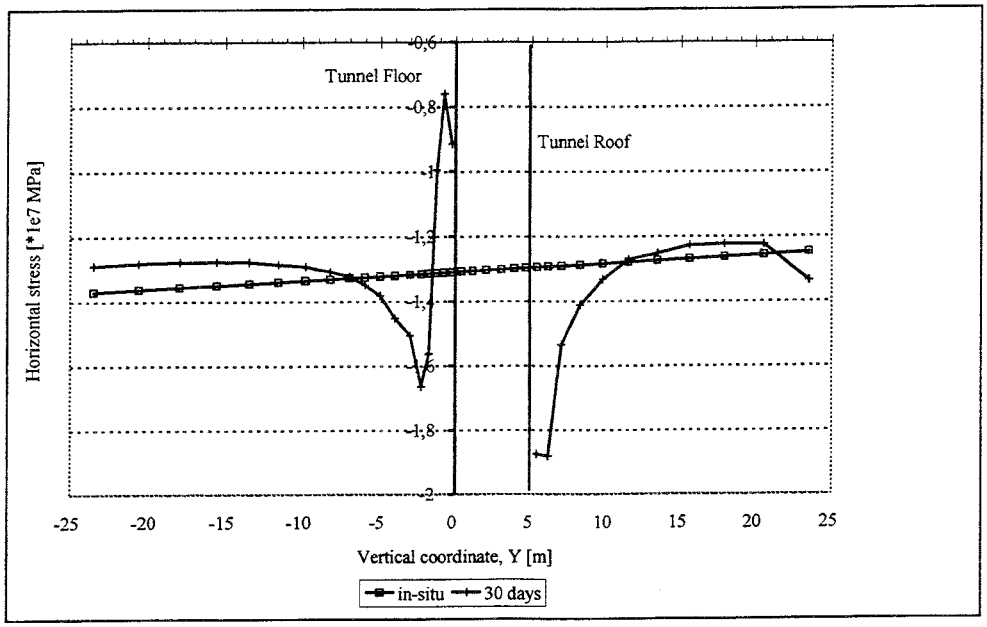

a)

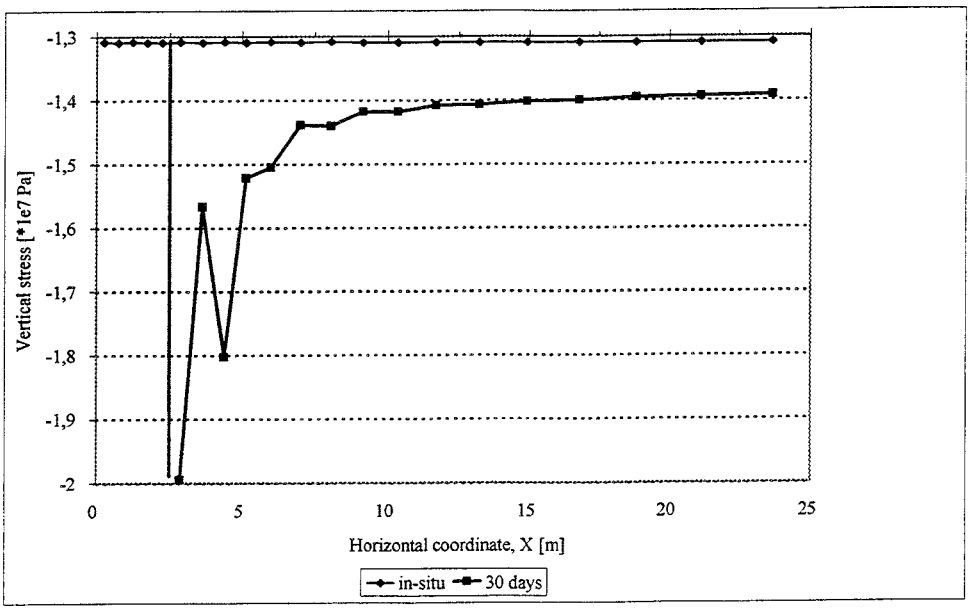

b)

Fig. 3-11 *(a) Horizontal and (b) vertical total stress (*1e7 Pa) along Line I and Line II, one month after excavation of the tunnel.*

The overall displacement field, which can be seen in Figures 3-12 and 3-13, is dominated by the vertical consolidation. Displacements at each monitoring point are listed in Table 3-6.

Table 3-6. Displacements of the monitoring points A-H after one month.

Point	u_x (mm)	u_y (mm)
A	0	+0.6
C	0	-3.9
D	-1.9	-2.4
G	-0.6	-2.5
H	-0.4	-0.8

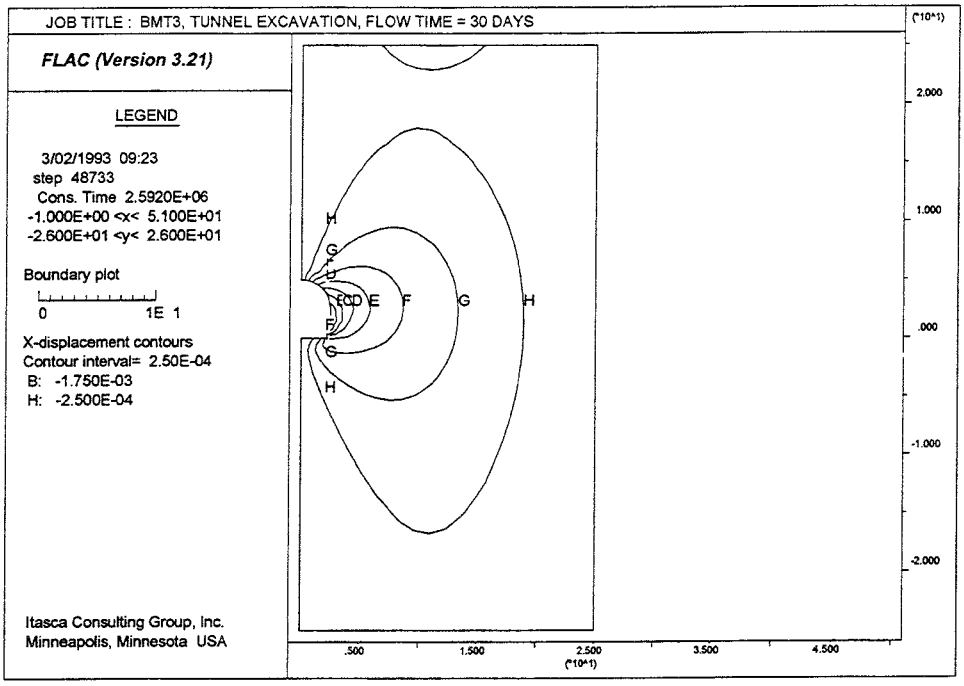

Fig. 3-12 *Horizontal displacement contours one month after excavation of the tunnel.*

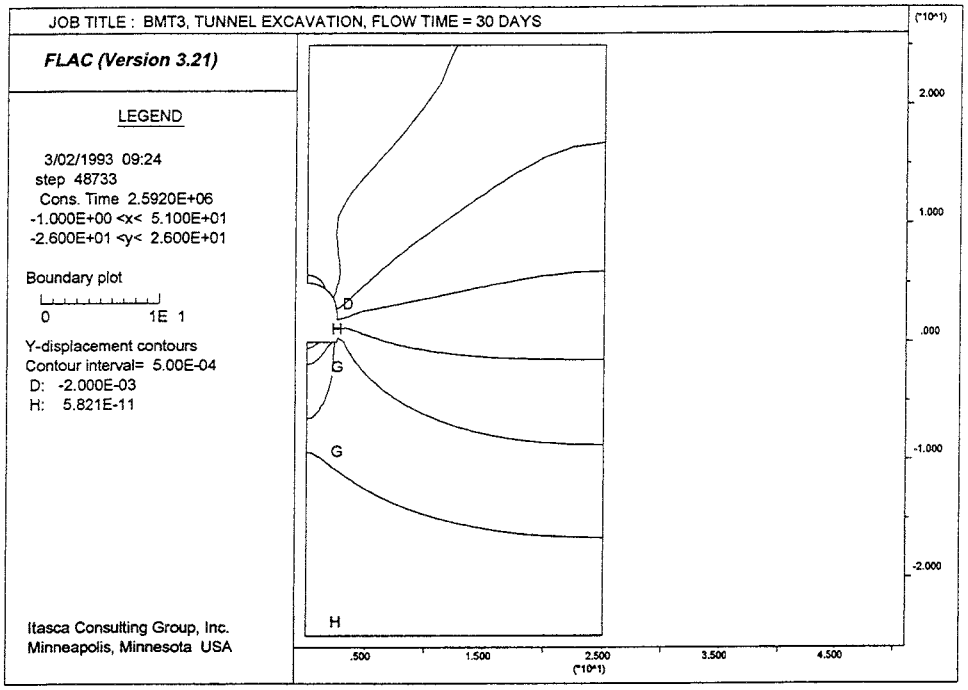

Fig. 3-13 *Vertical displacement contours one month after excavation of the tunnel.*

3.5 Results After 40 Days ("Steady State")

Approximately 40 days after the excavation of the tunnel, the flow has reached a quasi steady state, — i.e., the ratio between the unbalanced flow and the average flow in the model, qratio, is 1% as shown in Figure 3-14.

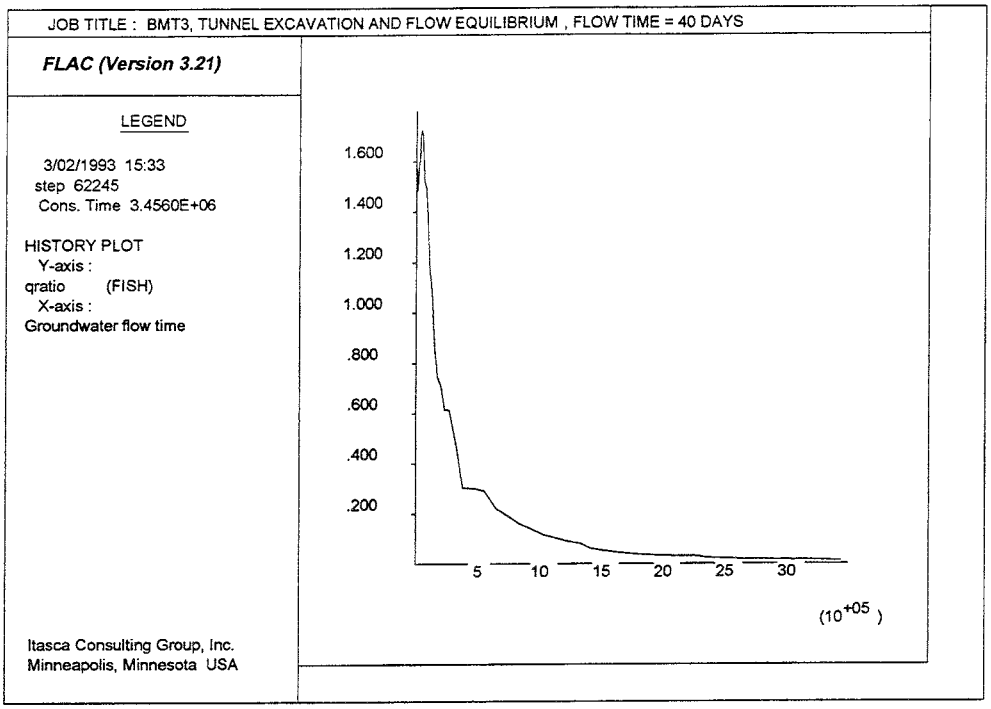

Fig. 3-14 *Ratio between unbalanced flow and average flow over the first 40 days of flow (x-axis is time in seconds).*

Only small changes in flow and displacements have occurred during the last 10 days of flow which, for the flow, can be seen in Table 3-7 and in Figure 3-15.

Table 3-7. Water flux over segments after 40 days of flow (values are corrected for the symmetry plane — i.e., $Flux_{Tunnel}=2*Flux_{Tunnel}^{Sym}$).

Segment	Water flux (m^3/s)
Tunnel	23.78e-8
F-G	8.54e-8
G-H	5.85e-8
H-E	2.36e-8

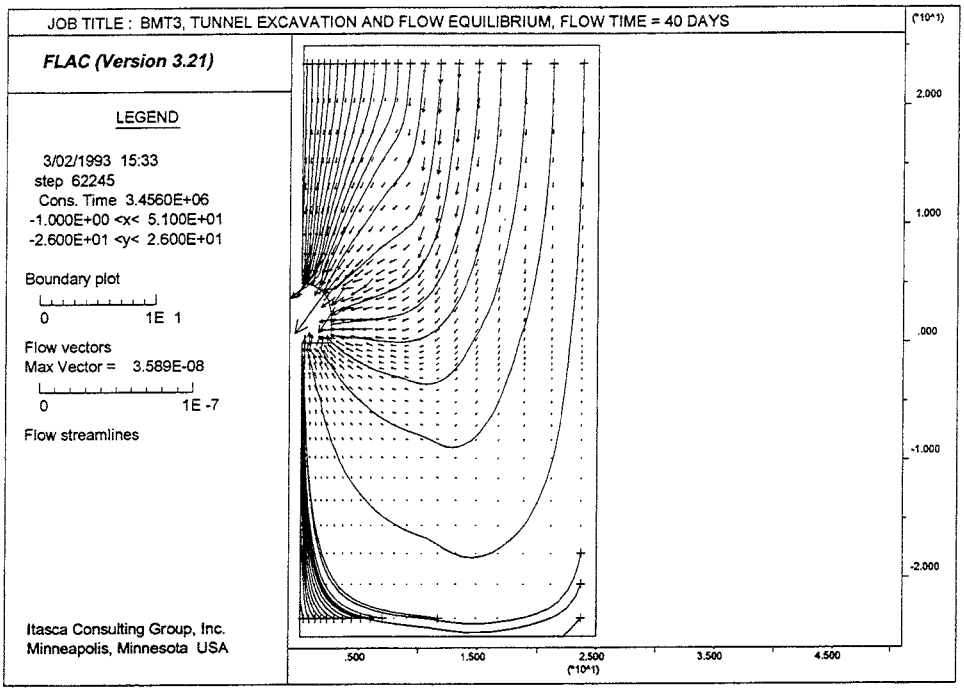

Fig. 3-15 *Water flow vectors and stream-lines after 40 days of flow.*

The pore pressure distribution is found in Figure 3-16. The distribution of the horizontal and the vertical permeabilities are shown in Figures 3-17 and 3-18.

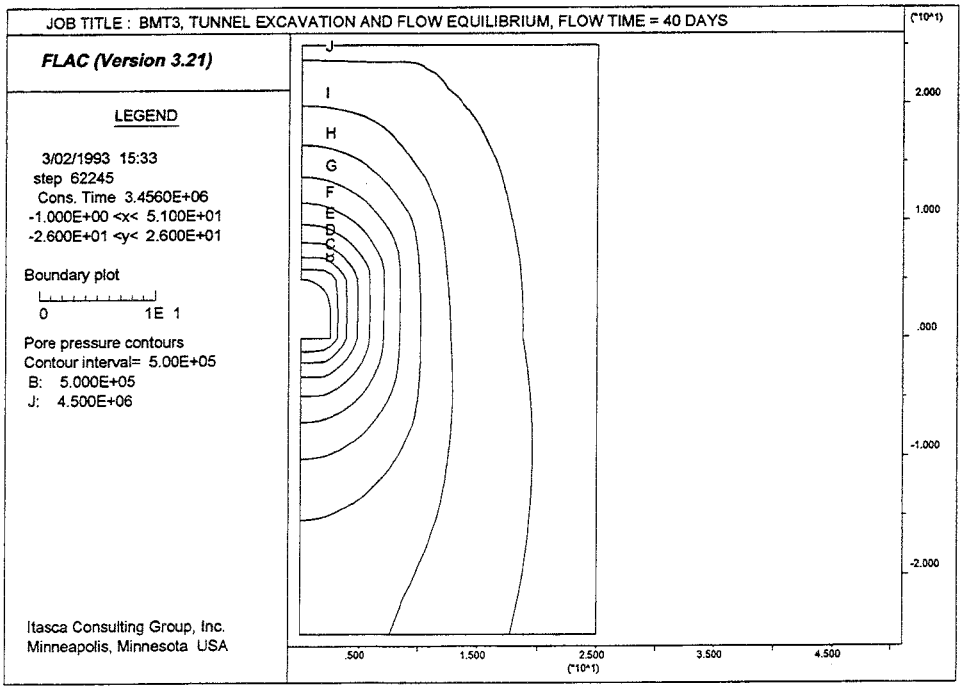

Fig. 3-16 *Pore pressure distribution after 40 days of flow.*

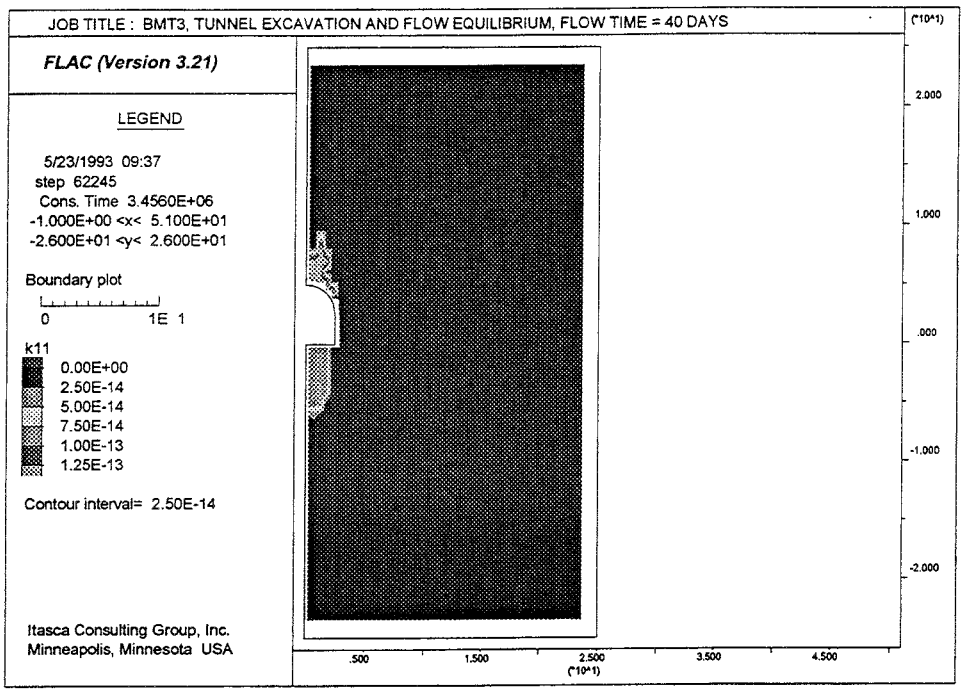

Fig. 3-17 *Distribution of horizontal permeability, K_{xx} (k11 in the legend), after 40 days of flow.*

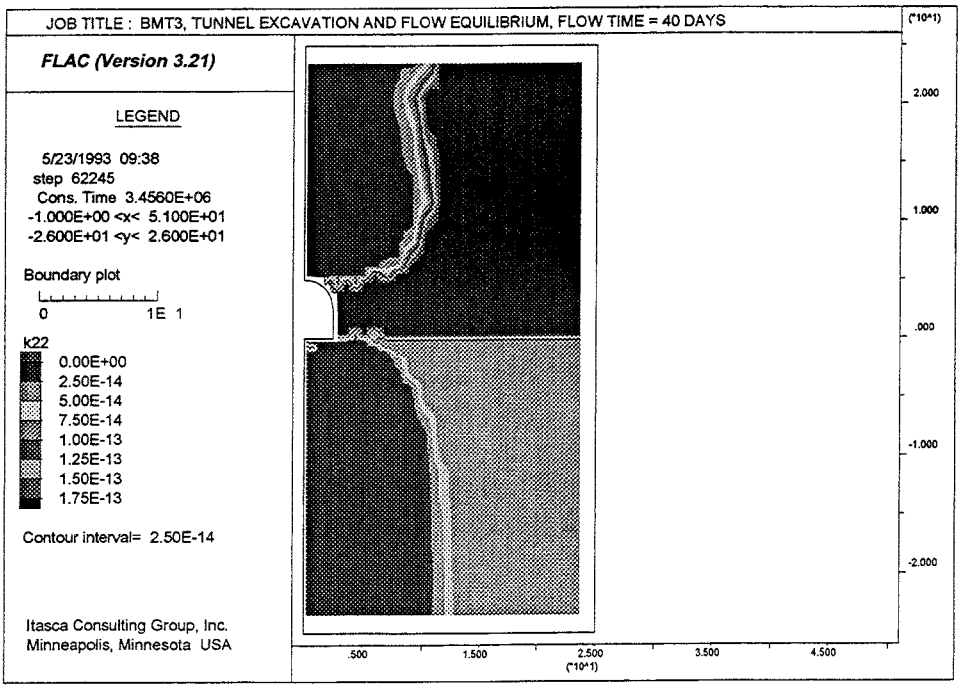

Fig. 3-18 *Distribution of vertical permeability, K_{yy} (k22 in the legend), after 40 days of flow.*

As can be seen from Figures 3-17 and 3-18, no obvious changes have occurred to the permeability fields compared to one month after excavation of tunnel. The horizontal permeability is still increased above and below the tunnel due to the reduced vertical stress in those areas. The vertical permeability has, as after one month, increased in a wedge shaped area from the tunnel wall upward and downward. Still, the assumption that the initial aperture was the residual aperture can be seen in the lack of decreased permeabillity areas.

The stresses acting at the monitoring points, are listed in Table 3-8, and the horizontal, σ_{xx}, and vertical, σ_{yy}, stress contours are shown in Figures 3-19 and 3-20. The stress normal to Line I and Line II are shown for the three phases t=0, t=30 days and t=40 days (equilibrium) in Figure 3-21.

Table 3-8. Total stresses acting in the monitoring points A-H, t=40 days

Point	σ_x (MPa)	σ_y (MPa)
A	-9.1	-0.02
C	-18.5	-3.0
D	-3.9	-15.3
G	-11.4	-13.2
H	-12.0	-13.2

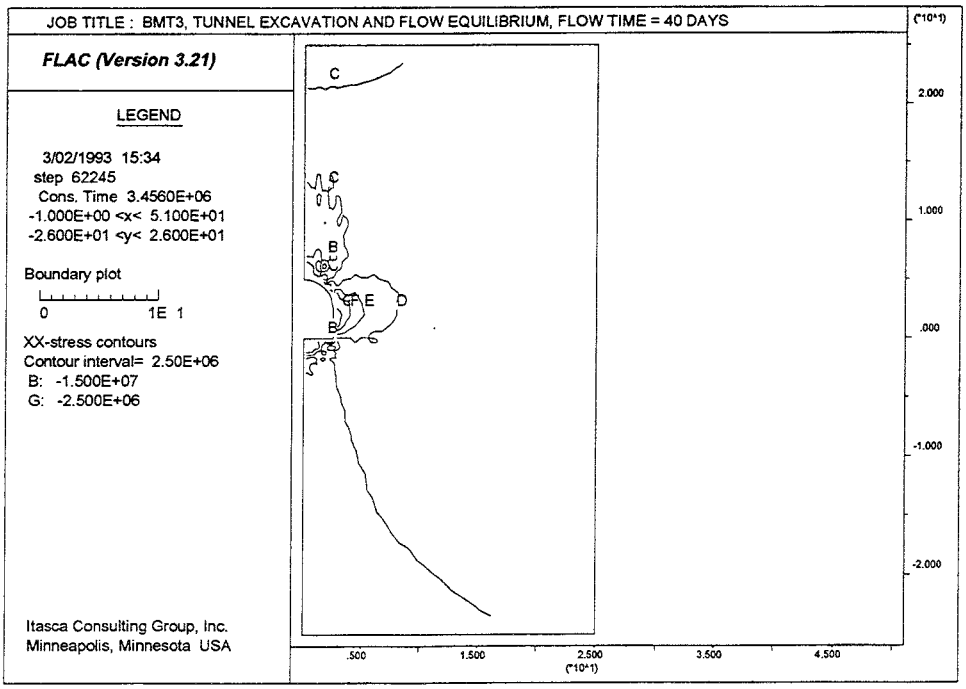

Fig. 3-19 *Horizontal total stress, σ_x, contours after 40 days of flow.*

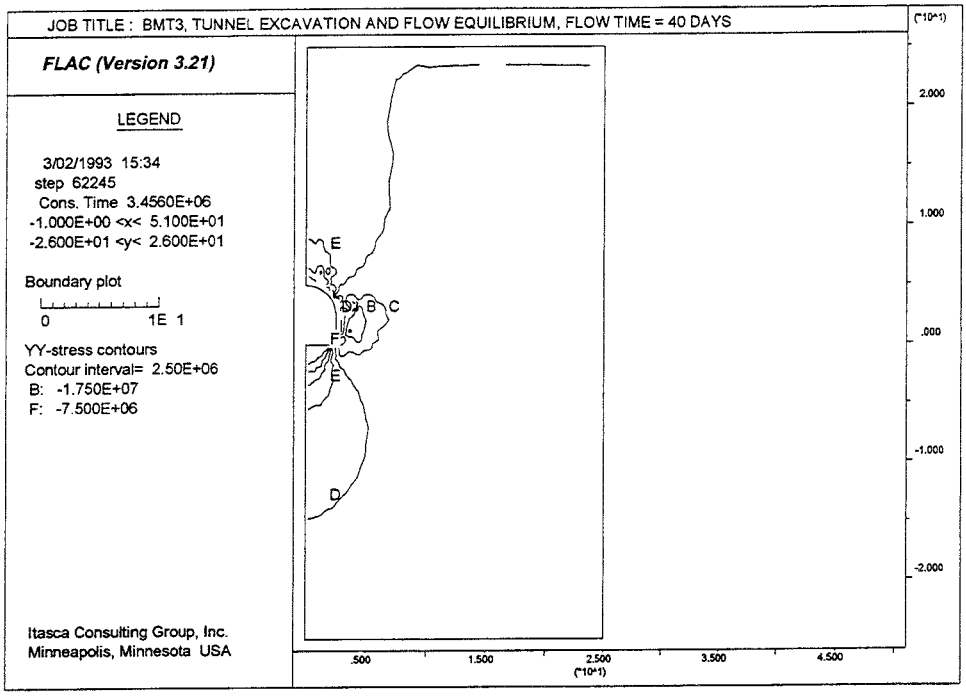

Fig. 3-20 *Vertical total stress, σ_y, contours after 40 days of flow.*

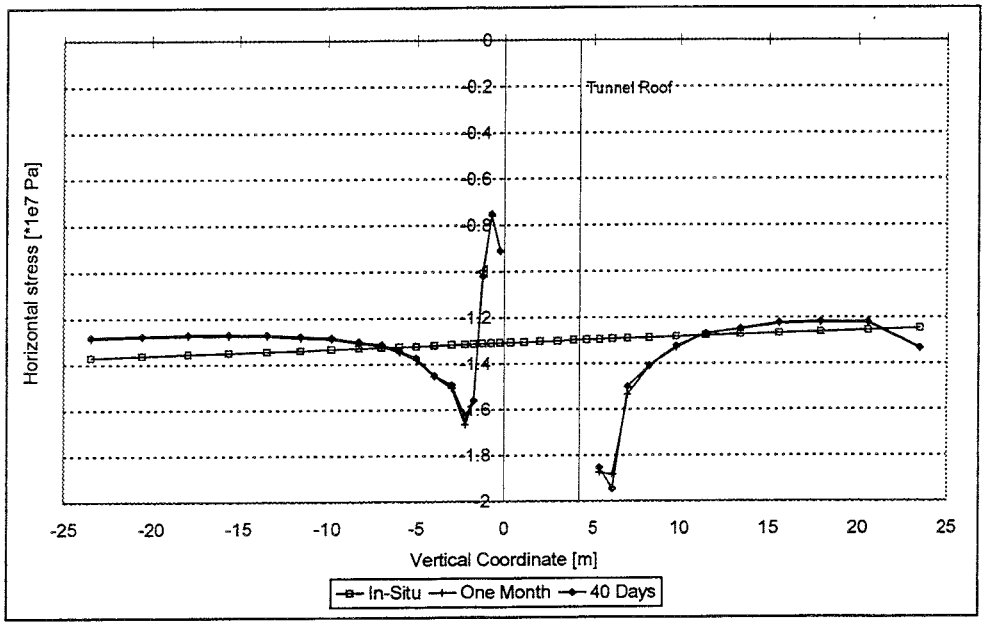

a)

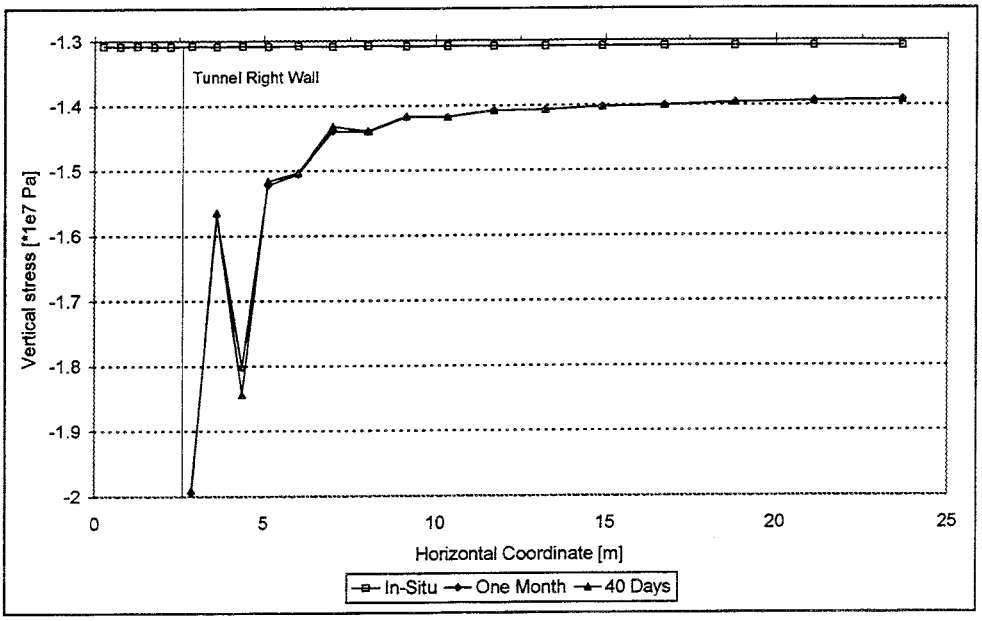

b)

Fig. 3-21 *(a) Horizontal and (b) vertical total stress (*1e7 Pa) along Line I and Line II after 40 days of flow.*

There are no major changes to the displacement field compared to the results after one month. The overall displacements are shown in Figures 3-22 and 3-23 and the displacements of the monitoring points are listed in Table 3-9.

Table 3-9. Displacements of the monitoring points A-H, t=40 Days.

Point	u_x (mm)	u_y (mm)
A	0	+0.6
C	0	-3.9
D	-1.9	-2.4
G	-0.6	-2.6
H	-0.4	-0.9

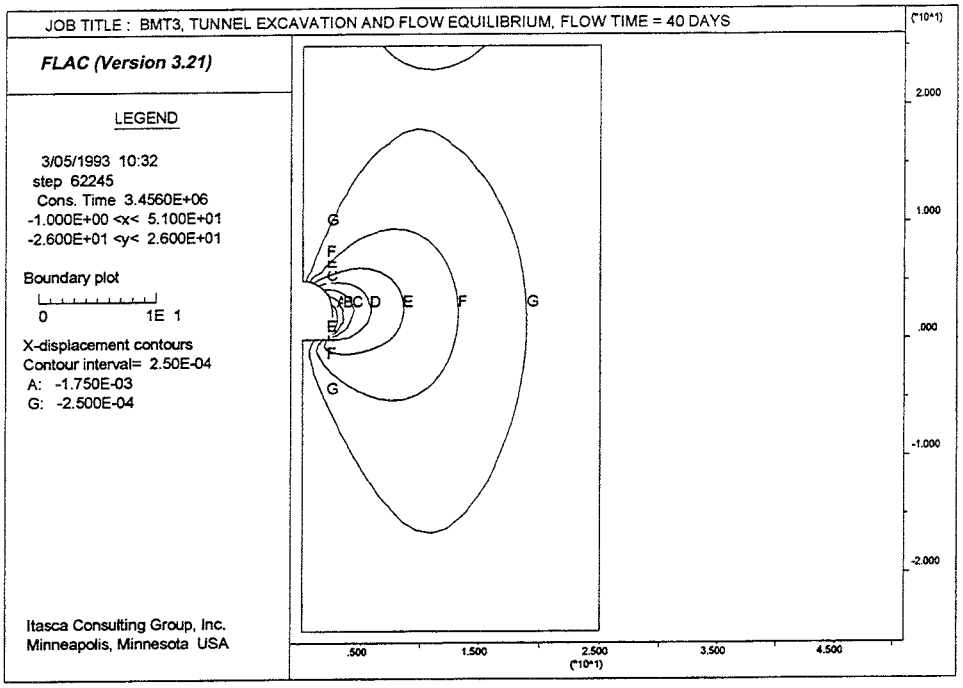

Fig. 3-22 *Horizontal displacement contours after 40 days of flow.*

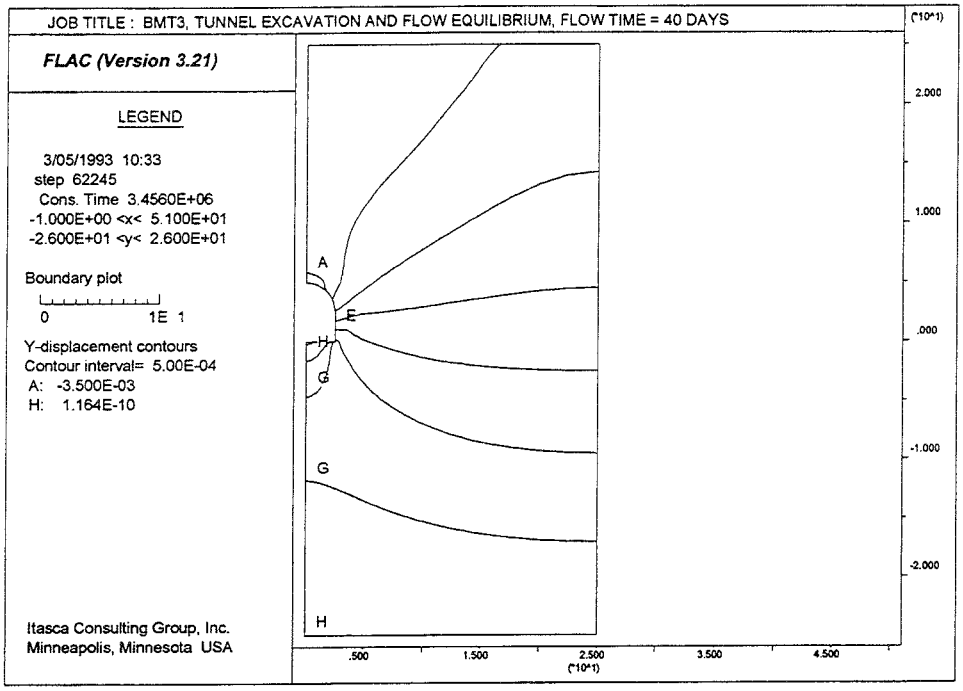

Fig. 3-23 *Vertical displacement contours after 40 days of flow.*

3.6 RESULTS AFTER ONE YEAR OF HEATING

The temperature has, after one year of thermal loading, increased to approximately 159°C in the center of the borehole. The contour of 100°C has reached approximately two meters out in the surrounding rock mass. The overall temperature field and the temperature along Lines I and II can be seen in Figures 3-24 and 3-35, respectively. Some minor temperature change was noted along the bottom boundary and along the lower part of the right, vertical boundary. The temperatures in the monitoring points A-H are listed in Table 3-13.

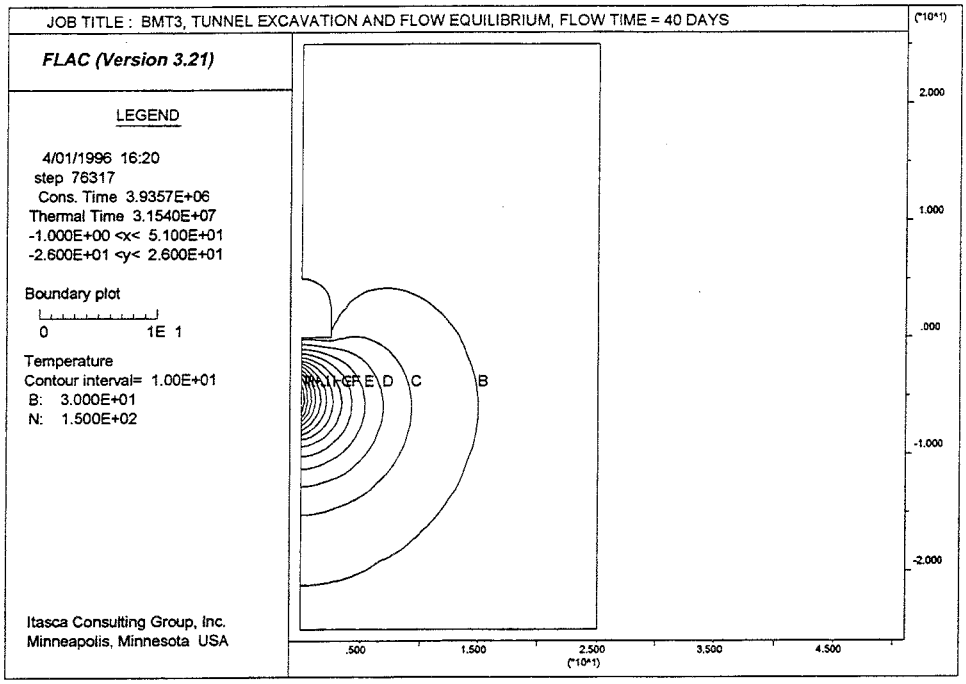

Fig. 3-24 *Temperature field after one year of thermal loading.*

The thermal load causes the permeability of the rock mass to change due to the induced stress and changed properties of the fluid (see sections 2.1.3 and 2.1.4). It can be seen from the water flux over the monitoring segments, listed in Table 3-10, that it has some effect on the flow.

Table 3-10. Water flux over segments after one year of thermal loading (values are corrected for the symmetry plane --- i.e., $Flux_{Tunnel} = 2*Flux_{Tunnel}^{Sym}$).

Segment	Water flux (m^3/s)
Tunnel	27.1e-8
F-G	9.2e-8
G-H	7.0e-8
H-E	2.8e-8

The flow pattern and the stream-lines are shown in Figure 3-25. The increase in flow in the upper part, 10 m out from the center line, that was seen during the establishment of steady-state flow, can still be seen. Apart from the increased inflow to the tunnel, most inflow now takes place in the floor of the tunnel instead of in the wall and in the ceiling. The total inflow in the tunnel is approximately 14% greater than for the steady- state flow after the excavation of the tunnel.

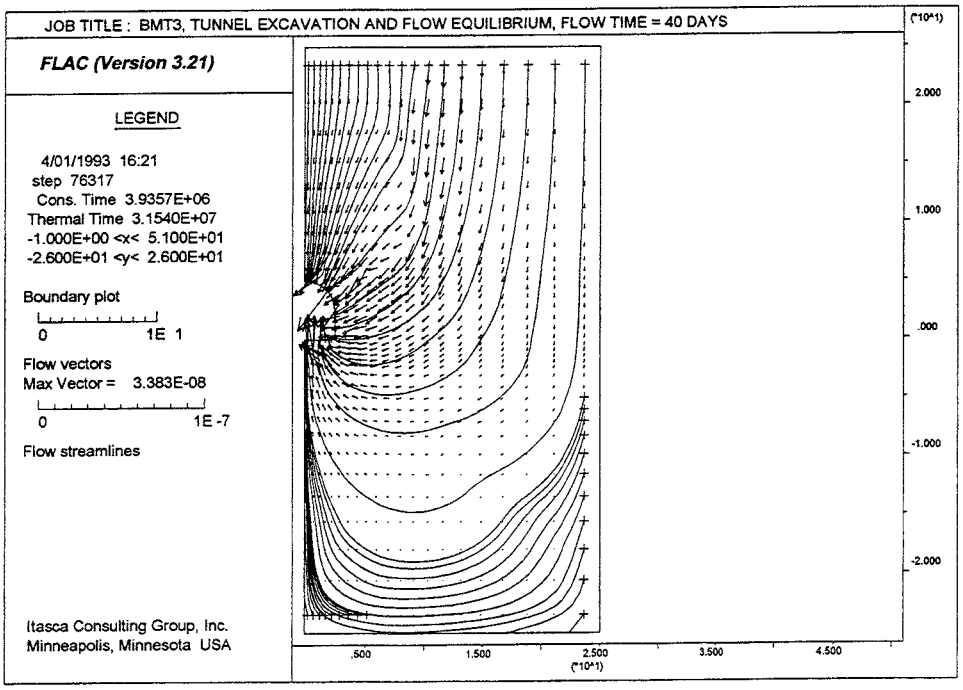

Fig. 3-25 *Water flow vectors and stream-lines after one year of thermal loading.*

The pore pressure distribution is shown in Figure 3-26. The distribution of the horizontal and vertical permeability are shown in Figures 3-27 and 3-28.

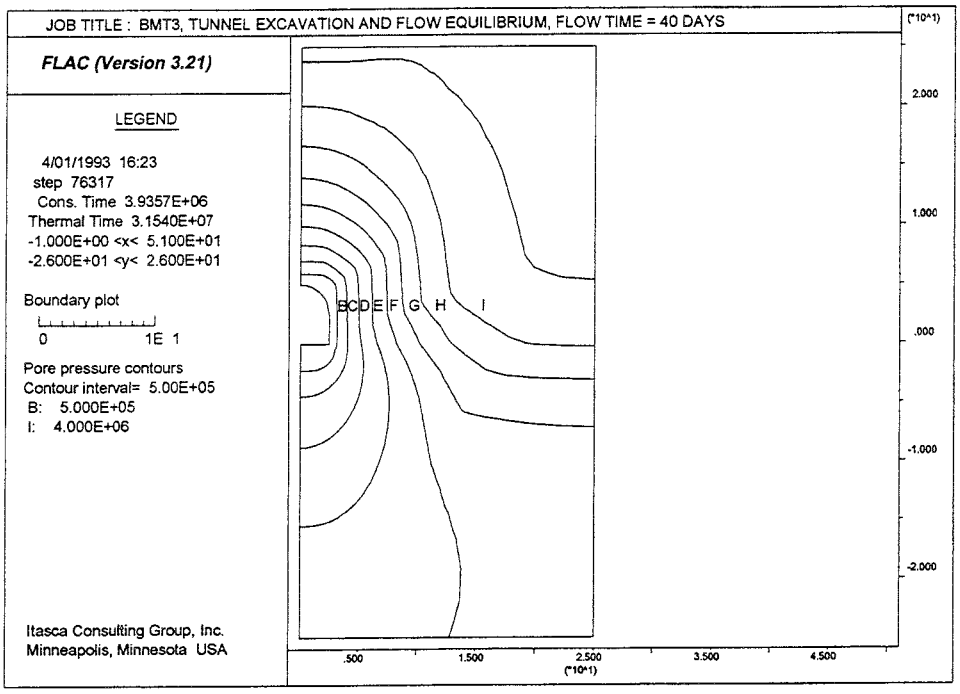

Fig. 3-26 *Pore pressure distribution after one year of thermal loading.*

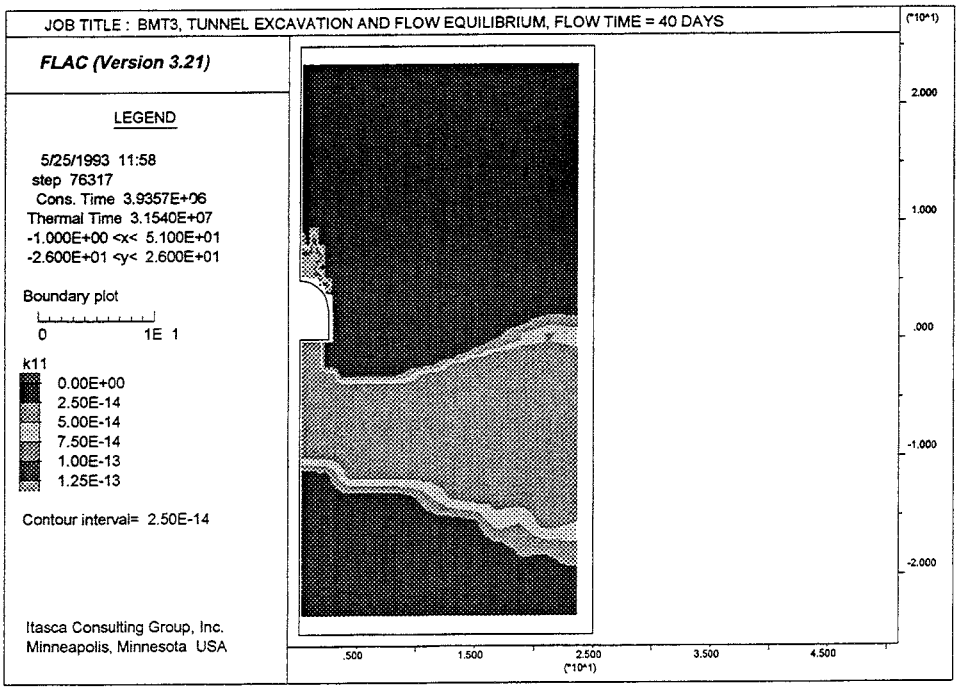

Fig. 3-27 *Distribution of horizontal permeability, K_{xx} (k11 in the legend), after one year of thermal loading.*

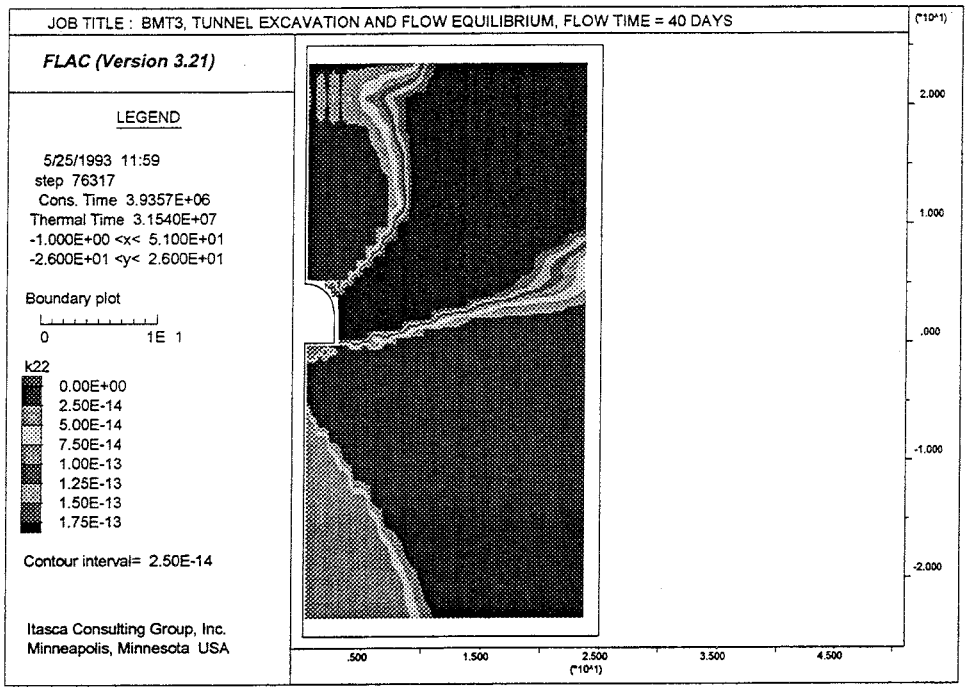

Fig. 3-28 *Distribution of vertical permeability, K_{yy} (k22 in the legend), after one year of thermal heating.*

The stresses acting at the monitoring points are listed in Table 3-11. The stresses normal to Line I and Line II can be found for the four phases t=0, t=30 days, t=40 days (equilibrium) and t=1 year in Figure 3-29 and the overall horizontal and vertical stresses can be found in Figures 3-30 and 3-31.

Table 3-11. Total stresses acting at the monitoring points A-H after one year of thermal loading.

Point	σ_x (MPa)	σ_y (MPa)
A	-2.9	-0.7
C	-15.8	-3.0
D	-3.0	-16.8
G	-10.6	-13.4
H	-12.9	-9.1

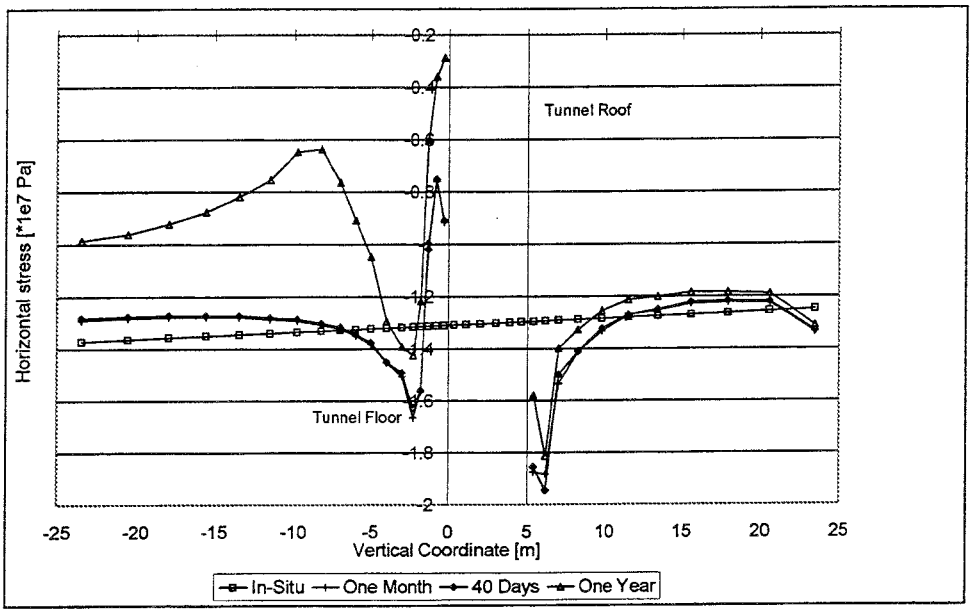

a)

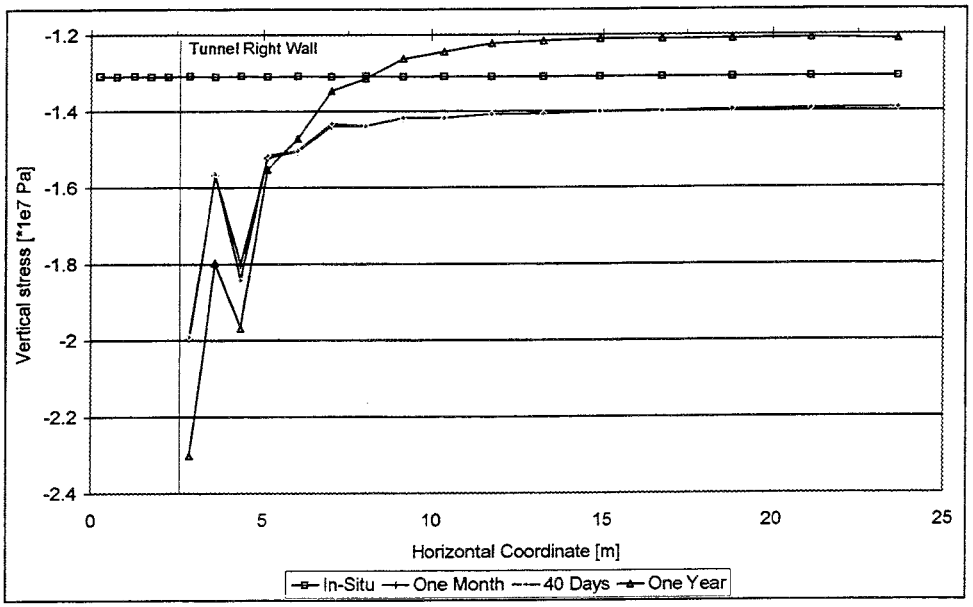

b)

Fig 3-29 *(a) Horizontal and (b) vertical total stress (*1e7 Pa) along Line I and Line II.*

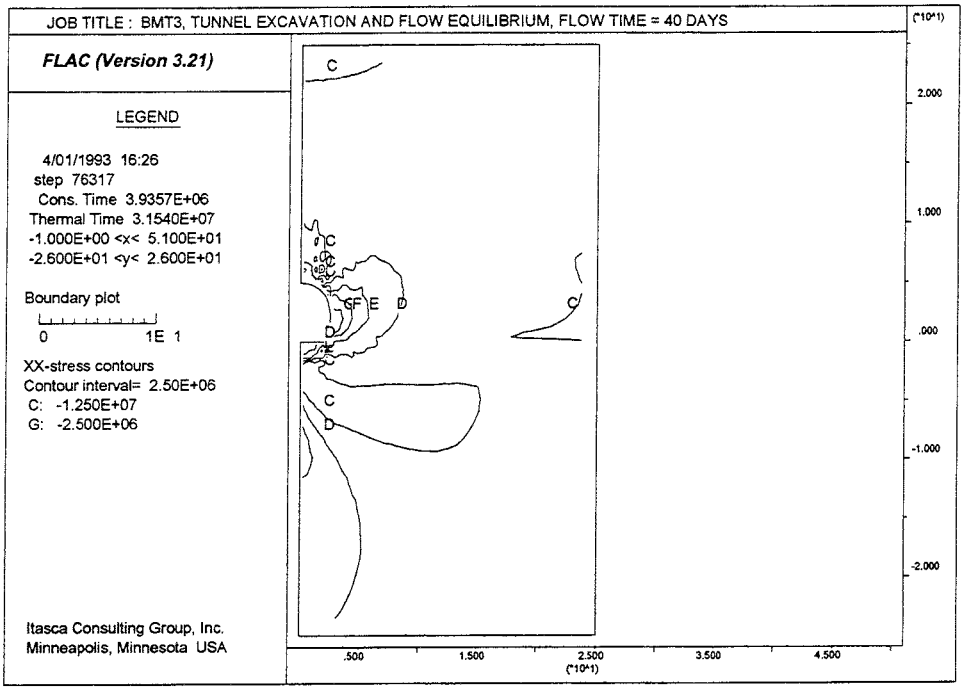

Fig. 3-30 *Horizontal stress, σ_x, contours after one year of thermal loading.*

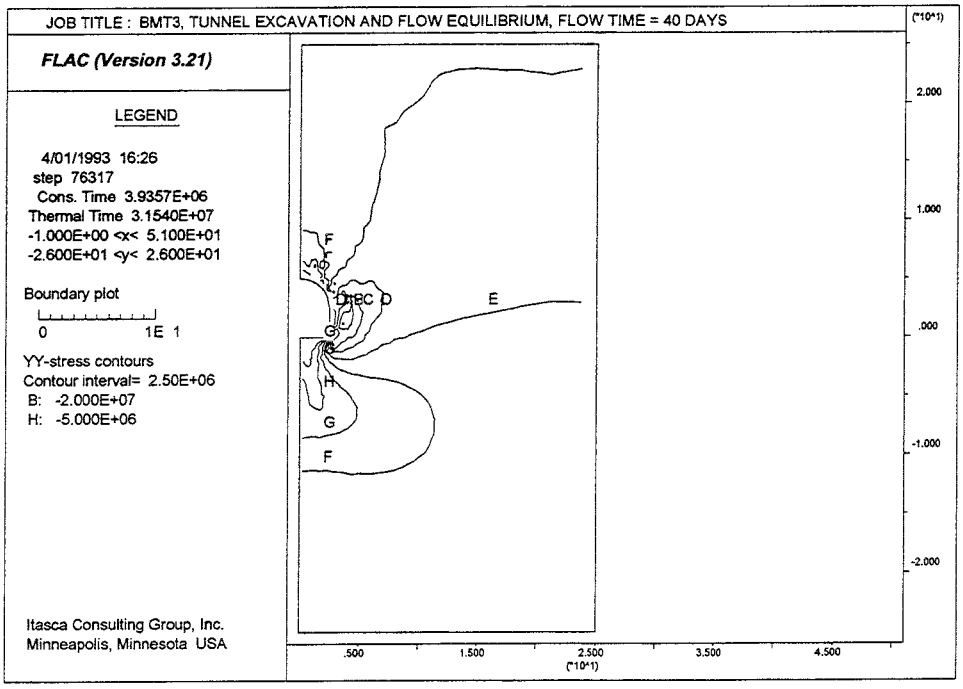

Fig. 3-31 *Vertical stress, σ_y, contours after one year of thermal loading.*

The displacement of the monitoring points can be seen in Table 3-12, and the horizontal and the vertical displacements are shown in Figures 3-32 and 3-33. The vertical convergence of the tunnel is now approximately 0.14%.

Table 3-12. Displacements of the monitoring points A-H after one year of thermal loading.

Point	u_x (mm)	u_y (mm)
A	0	5.4
C	0	-1.8
D	-1.3	0.04
G	-0.3	-0.3
H	0.9	0.1

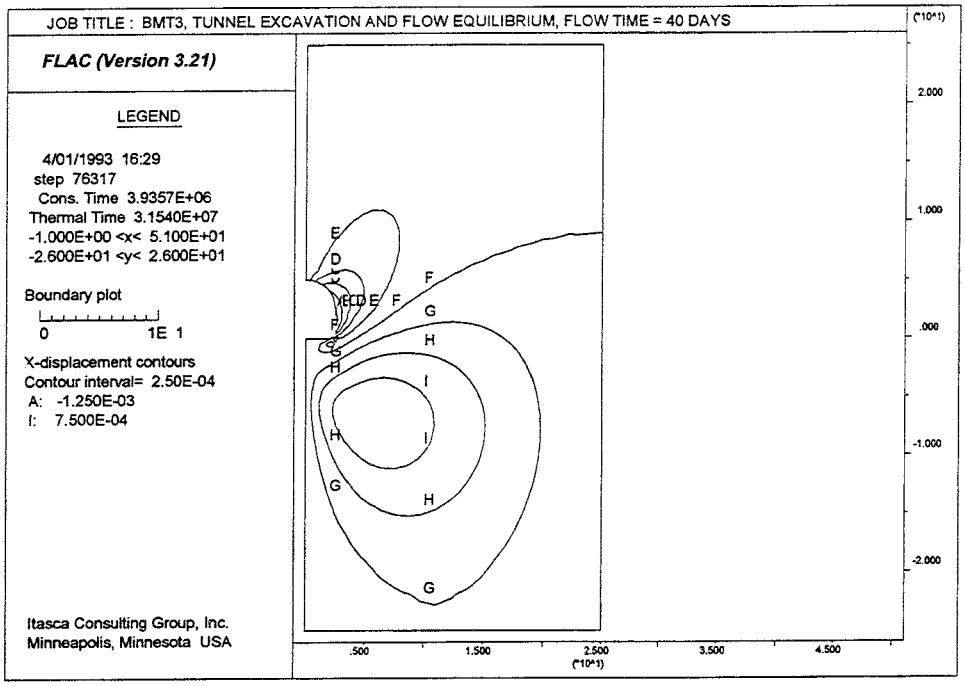

Fig. 3-32 *Horizontal displacement contours after one year of thermal loading.*

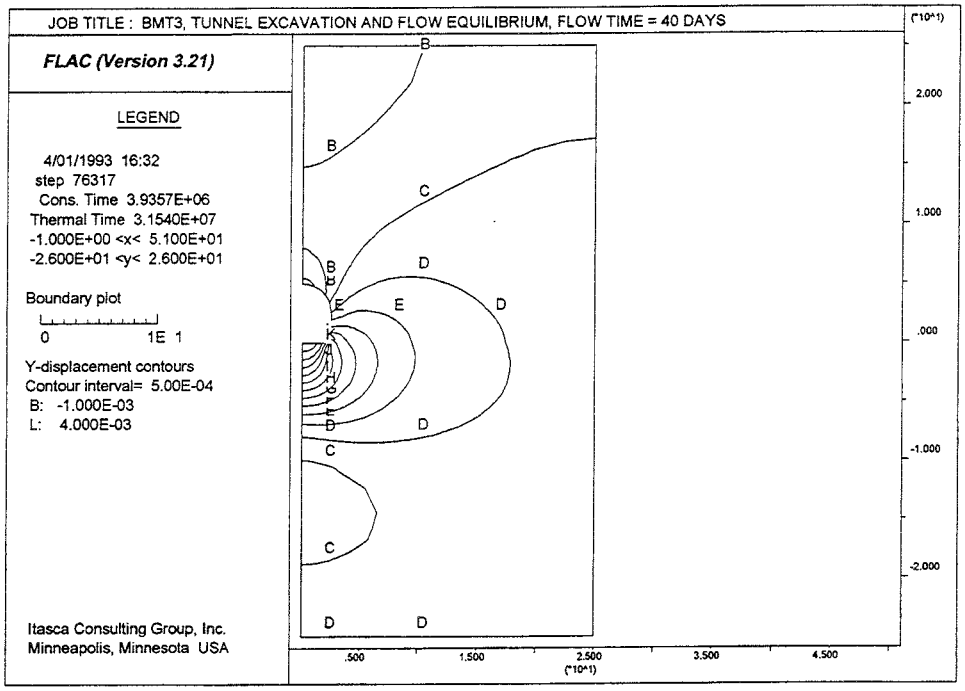

Fig. 3-33 *Vertical displacement contours after one year of thermal loading.*

3.7 RESULTS AT THE TIME OF MAXIMUM TEMPERATURE

The temperature has, after 4.081 years (1490 days) of thermal loading, increased to approximately 171°C, in the center of the borehole. This temperature is the highest that occurs in the model. The temperature at monitoring points A-H can be found in Table 3-13. The overall temperature field and the temperature along Lines I and II can be seen in Figures 3-34 and 3-35, respectively. As can be seen in Figure 3-34, the temperature field is affected by the convection to the tunnel. At this time, the upper boundary, which is defined with a fixed temperature restriction, starts to influence the temperature field. The temperature has increased to 35-40°C along the bottom and the right boundary. The 100°C contour has extended to a circle with a radius of approximately 3 m (contour I in Figure 3-34).

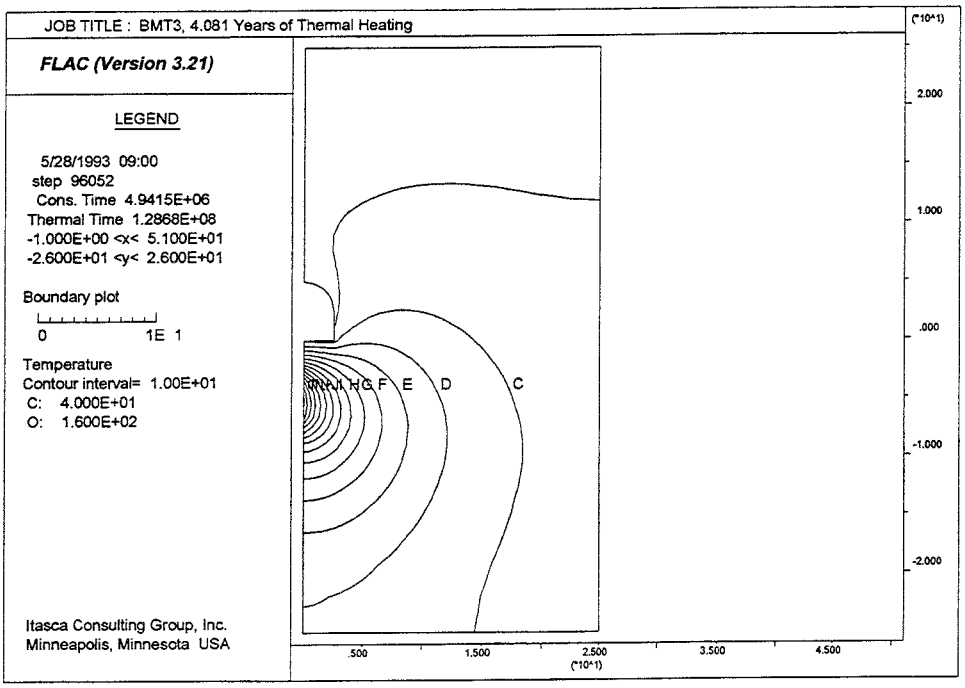

Fig. 3-34 *Temperature field after 4.08 years of thermal loading.*

Table 3-13. Temperature at monitoring points A-H after one year and 4.08 years of thermal loading.

	Temperature (°C)	
Point	**one year**	**4.08 years**
A	36.2	37.6
C	26.9	27.4
D	27.0	28.0
G	28.0	32.9
H	46.0	65.7

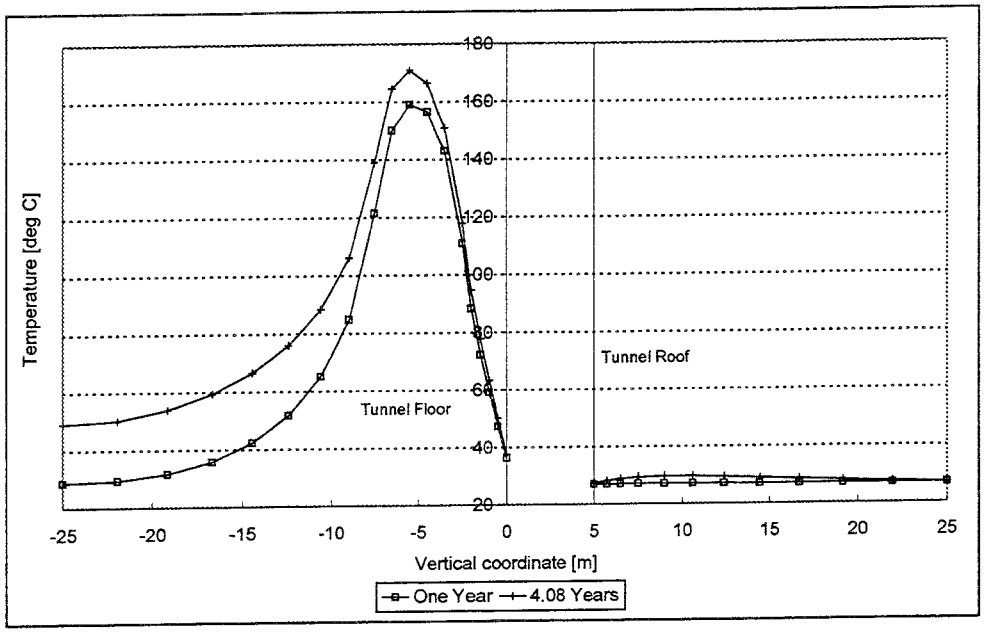

a)

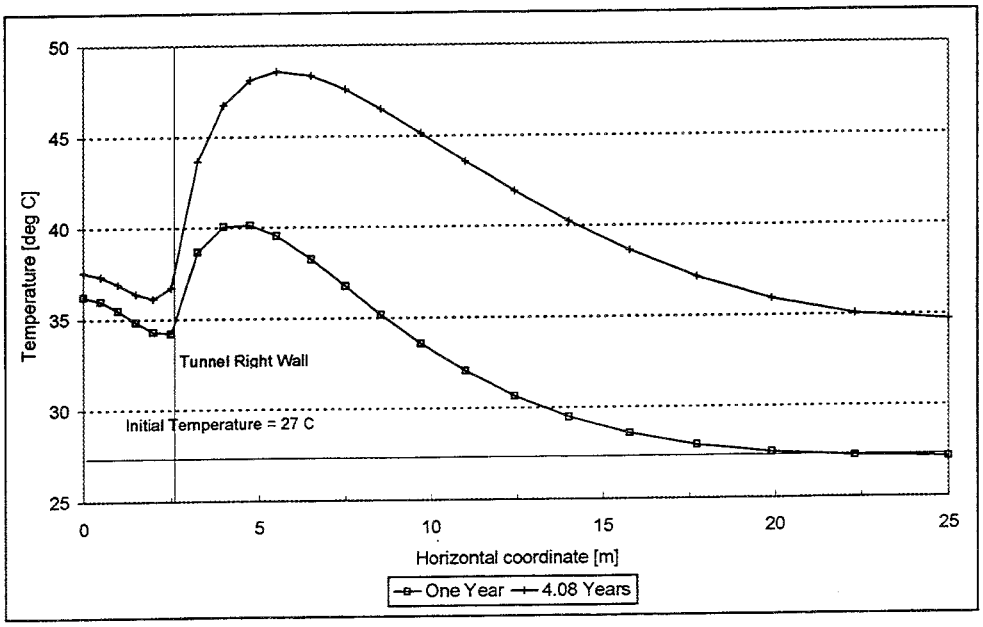

b)

Fig. 3-35 *Temperature distribution along (a) Line I and (b) Line II after 4.08 years of thermal loading.*

The water flux over the specified segments at the time of maximum temperature can be found in Table 3-14. The flow pattern and the stream lines are shown in Figure 3-36.

Table 3-14. Water flux over segments after 4.08 year of thermal loading (values are corrected for the symmetry plane — i.e., $Flux_{Tunnel} = 2*Flux_{Tunnel}^{Sym}$).

Segment	Water flux (m^3/s)
Tunnel	21.5e-8
F-G	9.6e-8
G-H	4.6e-8
H-E	1.8e-8

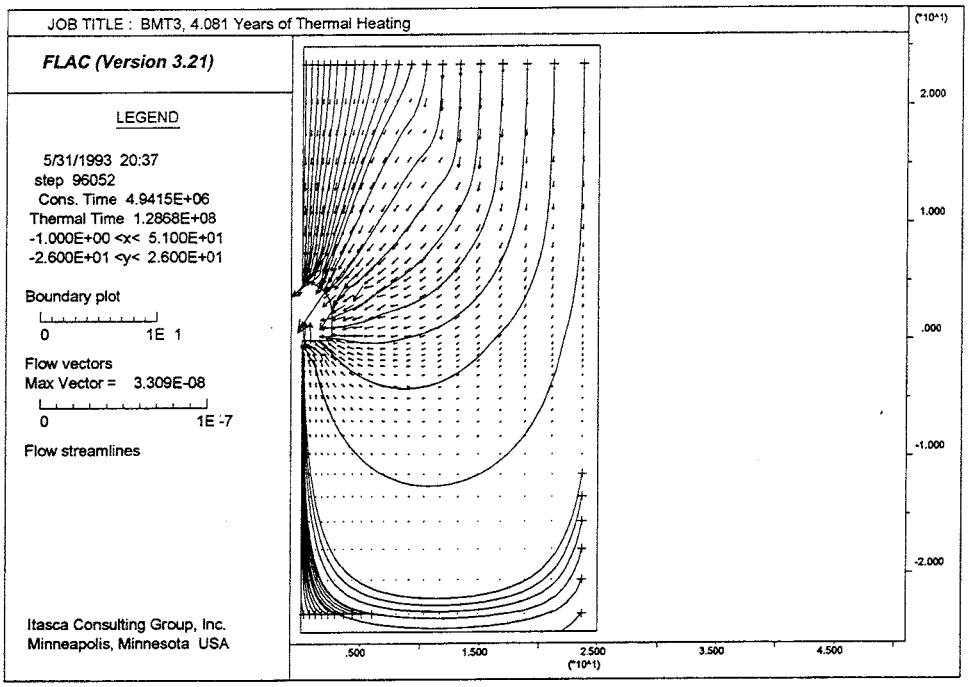

Fig. 3-36 *Water flow vectors and stream-lines after 4.08 years of thermal loading.*

The pore pressure distribution can be seen in Figure 3-37. The horizontal and vertical permeability distribution can be seen in Figures 3-38 and 3-39. The initial difference in permeability between the two model regions, causes a number of permeability contours to be drawn at the sharp border between the permeabilities.

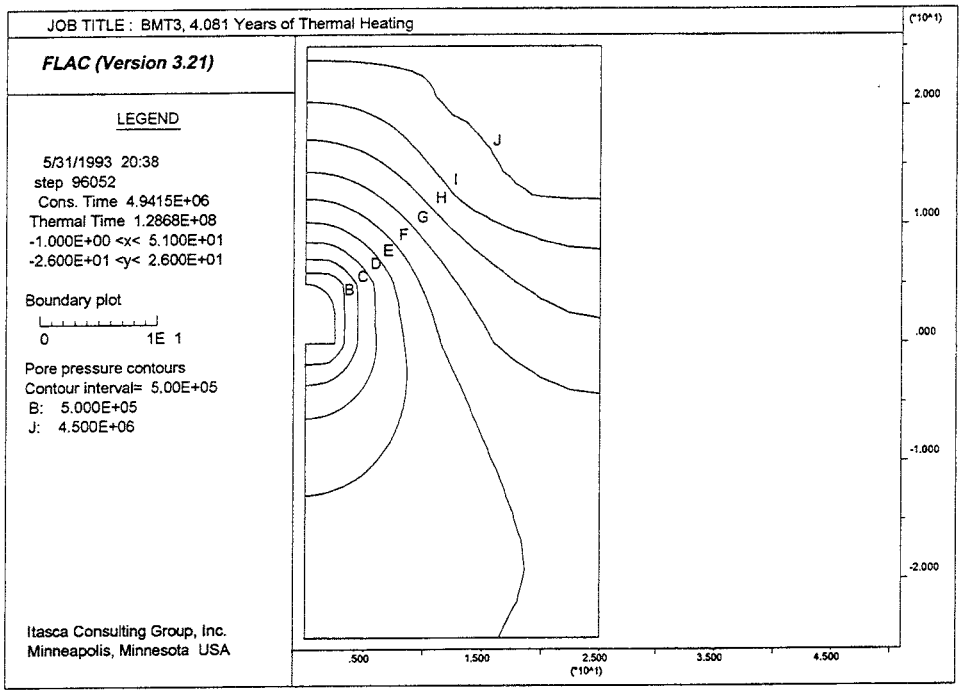

Fig 3-37 *Pore pressure distribution after 4.08 years of thermal loading.*

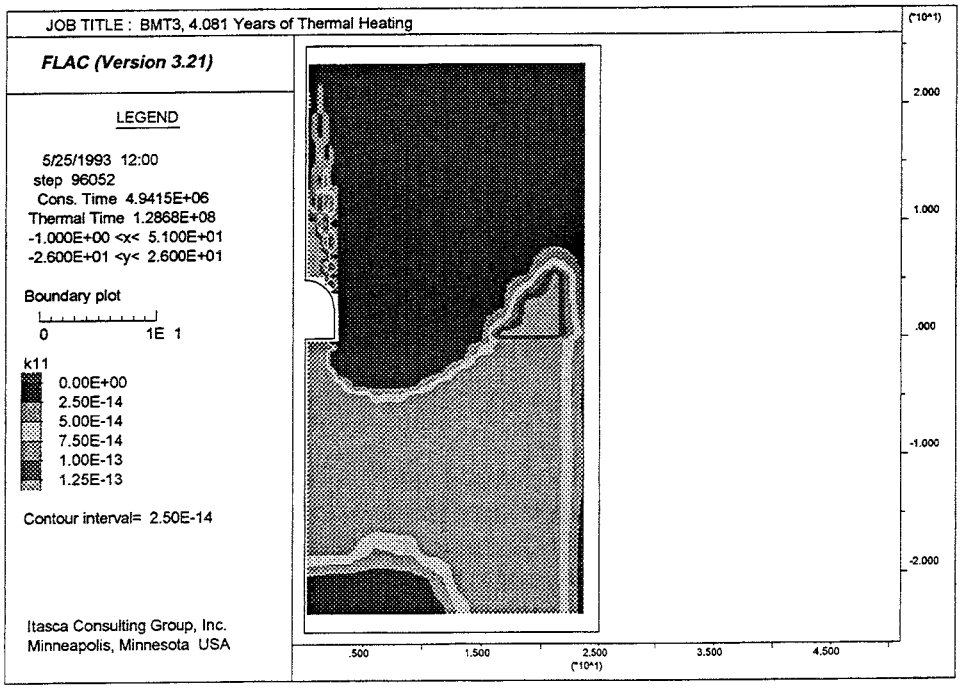

Fig. 3-38 *Distribution of horizontal permeability after 4.08 years of thermal loading.*

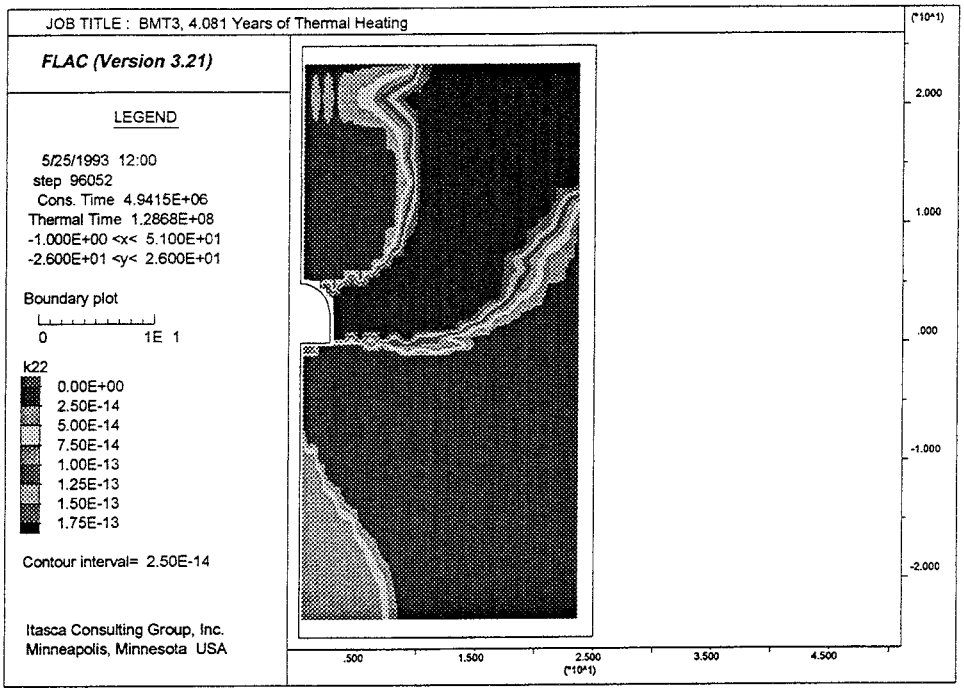

Fig. 3-39 *Distribution of vertical permeability after 4.08 years of thermal heating.*

The stresses, acting at the monitoring points are listed in Table 3-15. The stress normal to vertical and horizontal profiles can be found for the three phases t=0, t=30 days, t=40 days (equilibrium) and t=1 year and t=4.08 years in Figure 3-40. The overall horizontal and vertical stresses can be found in Figures 3-41 and 3-42.

Table 3-15. Total stresses acting at monitoring points A-H after 4.08 years of thermal loading.

Point	σ_x (mm)	σ_y (mm)
A	-6.1	-0.6
C	-18.0	-2.6
D	-3.2	-14.6
G	-10.5	-12.2
H	-12.2	-9.6

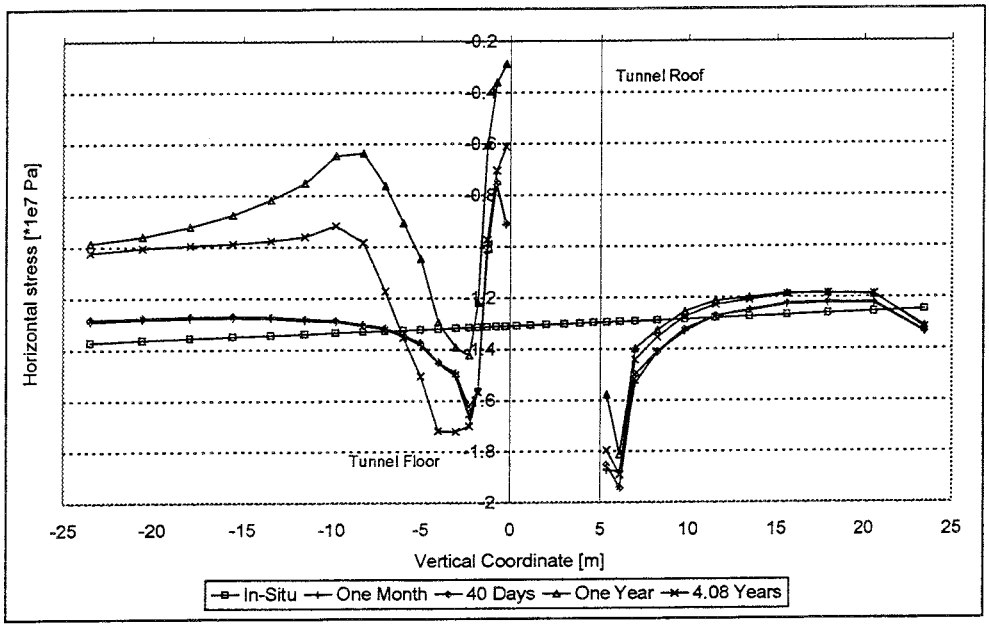

a)

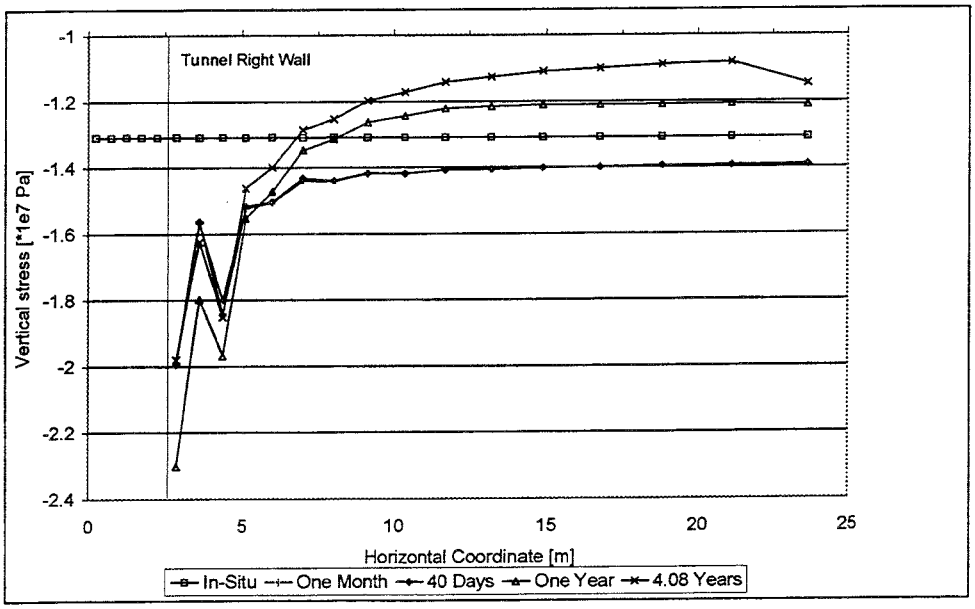

b)

Fig. 3-40 *(a) Horizontal and (b) vertical total stress (*1e7 Pa) along Line I and Line II after 4.08 years of thermal loading.*

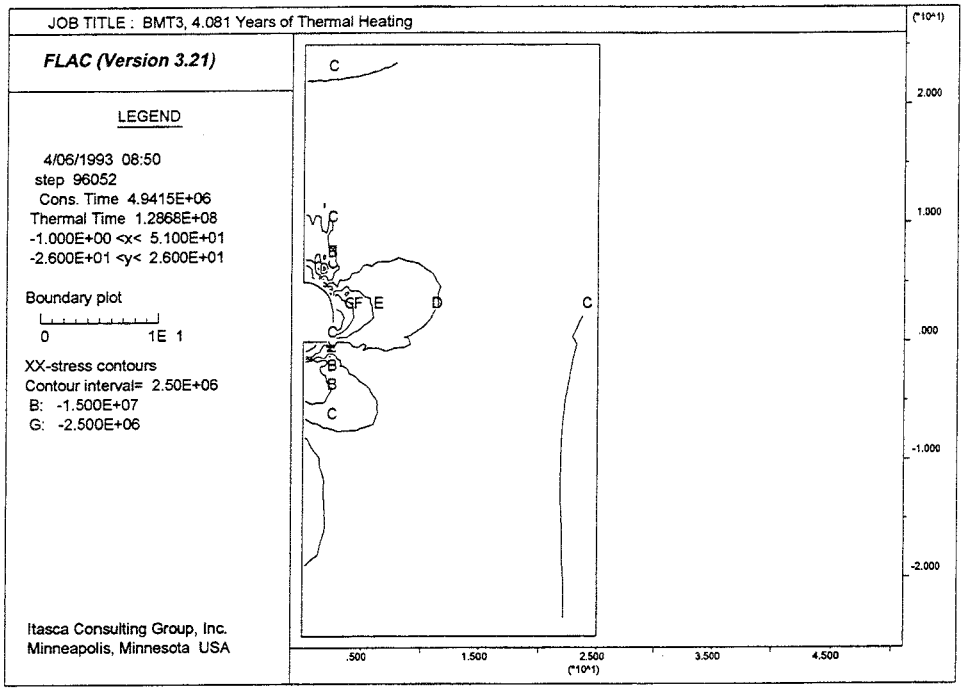

Fig. 3-41 *Horizontal stress, σ_x, contours after 4.08 years of thermal loading.*

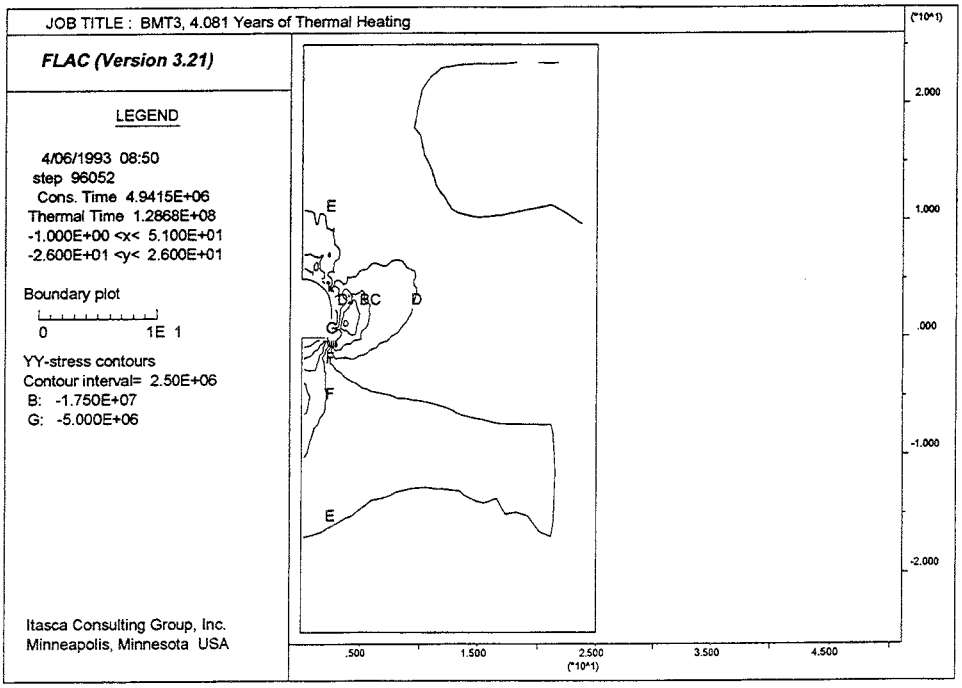

Fig. 3-42 *Vertical stress, σ_y, contours after 4.08 years of thermal loading.*

At this time, the vertical convergence of the tunnel is approximately 0.13 %. The displacement of the monitoring points can be seen in Table 3-16, and the horizontal and the vertical displacements are shown in Figures 3-42 and 3-43.

Table 3-16. Displacements of the monitoring points A-H after 4.08 years of thermal loading.

Point	u_x (mm)	u_y (mm)
A	0	6.0
C	0	-0.4
D	-1.8	1.1
G	-0.5	1.1
H	0.4	1.3

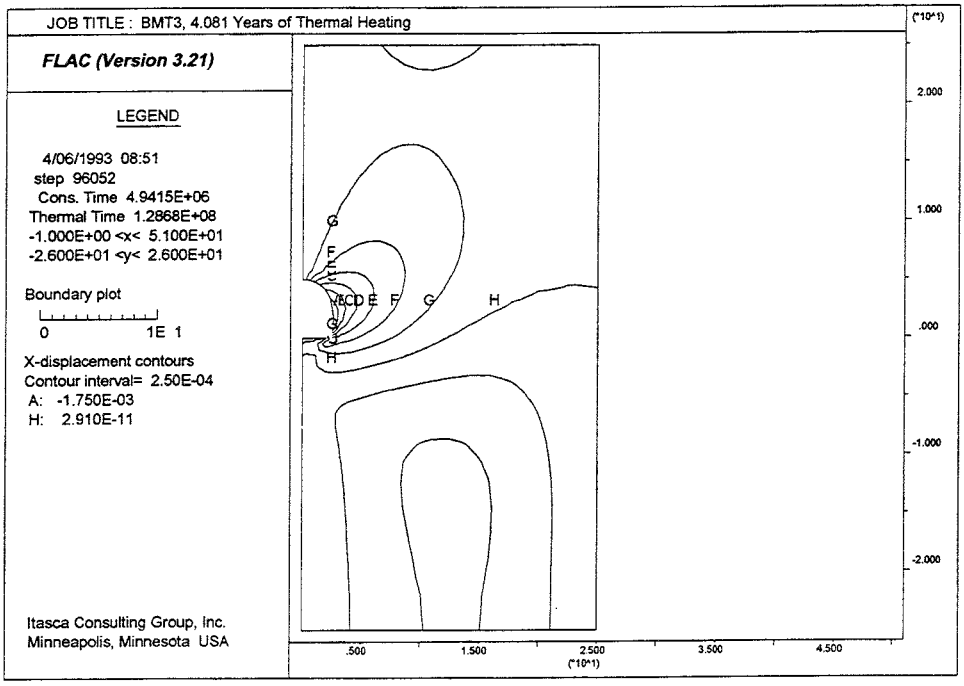

Fig 3-43 *Horizontal displacement contours after 4.08 years of thermal loading.*

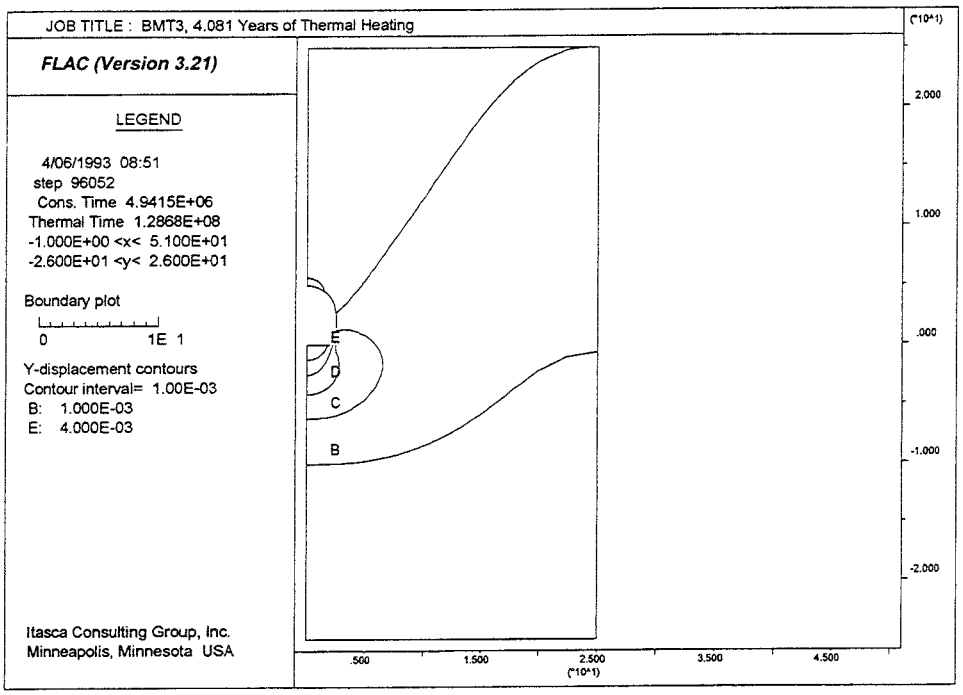

Fig. 3-44 *Vertical displacement contours after 4.08 years of thermal loading.*

4 COMMENTS ON GIVEN SPECIFICATIONS

The thermal source was described as a 0.5 m diameter borehole located between 2.5 and 7.5 m below the tunnel floor. in order to apply the correct heat strength acting on the plane of analysis, the spacing between the boreholes in the direction perpendicular to the plane of analysis has to be known. However, it was suggested, by the problem specification, that the given volumetric strength of the source should be applied as a unlimited linear, volumetric source with the width equal to the diameter of the borehole and the height equal to the height of the borehole.

The following comparison concerns the case in which the spacing between the boreholes is 1 m, — i.e., for each "plane of analysis", one borehole is active.

The difference in total thermal strength acting over the one unit wide plane of analysis is proportional to the difference in volume.

$$V_{borehole} = h\pi r^2 = 5\pi 0.25^2 = 0.982\ m^2$$

$$V_{linear} = 1h2r = 2.5\ m^2$$

where h = source height, and
r = radius of the borehole.

This means that a linear source, which was supplied in this study, will be more than 2.5 times stronger than the borehole shaped source.

The boundary conditions specified require that the tunnel analyzed is part of a system of parallel tunnels, all equipped with a borehole and a thermal source, since the boundaries will work as symmetry planes. The upper boundary, however, at which fluid flux is allowed and the temperature is fixed, will govern the behavior of the model: first because the only inflow to the model. In order to avoid this kind of boundary influence, the model size could have been larger. However, that would imply larger problem size, possibly requiring even further simplifications in order to obtain results in a reasonable time.

The strength properties given for the joints were apparently too low since the continuum property output from the numerical discontinuum biaxial compressional test resulted in very large plasticity zones around the tunnel (more than one tunnel diameter).

5 DISCUSSION OF THE RESULTS

1 The continuum approach was adopted because of the large numbers of joints and the lack of dominating joint orientations. A possible division of orientations in different joint areas or apertures was not investigated. However, such a division would not influence the hydraulic situation since the hydraulic conductivities in the x- and y-directions was given in the problem definition.

2 The use of a symmetry line reduced the number of different conductivity areas from four to two. However, the differences in conductivity between the different sides of the symmetry line were very small and should not result in any major differences in flow rate or paths.

3 At the start of this problem, FLAC was modified to allow both ground water calculations and thermal calculations in the same analysis. The coupling between the thermal and the hydraulic logic was done with FISH, the built-in programming language. The pore pressure was increased, zone by zone, proportionally to the average stress increase induced by the thermal load. This procedure was repeated after every thermal load step. The reason for using a different approach for the hydro-thermal coupling was that FLAC interpreted the volumetric strain from the thermal expansion as an increased pore volume, which gave a reduced pore pressure and counter-intuitive flow vectors. If the code had an automatic numerical coupling between the flow and the thermal part, the pore pressure would have been adjusted in smaller increments. However, since the flow is equilibrated in a shorter time than the heat is built up, the discrepancy should be small.

4 The maximum change in permeability, due to induced stress changes, was limited to 10 times the initial permeability. This was done in order to avoid very large permeabilities and permeability contrasts in the model. An increase in permeability will result in a decreased timestep, which causes the calculation to take longer. The final flow situation, however, is not expected to be much different even if the permeability were to change without limitation.

5 Transportation of thermal energy with water is not presently possible in FLAC. In this problem, not much energy would be distributed with the water flow since the hydraulic conductivity of the rock material was low (approximately 1E-9 m/s).

6 The thermal loading in this problem is probably too high to be considered relevant, resulting in temperatures far beyond the boiling temperature for water. The SKB/KBS concept for final storage of spent nuclear fuel, KBS-3, uses approximately 0.8 kW initial strength for cylindrical sources with 6 m spacing. The strength per meter tunnel would then be 0.8/6=0.133 kW/m, compared to the 1.175 kW/m used in the BMT3 problem. Consequently, the maximum increases in temperatures are 65° and 144°, respectively.

7 The hydrostatic in-situ stress given in this problem must be considered as rare and optimum from a mechanical point of view. Also, no considerations have been taken of the third dimension of possible flow paths and stress influences.

6 RECOMMENDATIONS

The following are recommendations for DECOVALEX regarding the BMT3 problem.

- In future analyses, the thermal loadings should be within possible strengths for repositories. In modelling the present Swedish design, KBS-3 /SKB-KBS, 1983/, this means the strength should at least be low enough to keep the temperature below the boiling point of water.
- In connection with the strength of the source, the far-field boundaries should be located distant enough not to influence the temperature field over the time period to be investigated.
- It is recommended that the differences between using a continuous "step-by-step" coupling of the thermal-hydraulic logic and the more "instantaneous" pore pressure change that was applied after each thermal loading period should be further investigated.
- The water bulk modulus and the amount of dissolved air in the water should be specified in order to complete the description of the problem.
- It is recommended that the result from FLAC and UDEC be compared to see where and when the different approaches can be used.
- Permeability tensors should be determined rather than permeabilities in x- and y-directions.

7 ACKNOWLEDGMENTS

I would like to extend my thanks to Dr. Loren Lorig and Pedro Varona of Itasca, Minneapolis, for their support and guidance during this project.

8 REFERENCES

Bieniawski, Z.T., 1979. The Geomechanics Classification in Rock Engineering Applications, Int. Congress of Rock Mechanics, Montreaux, Vol 2, 1979.

Cundall, P. and M. Board, 1988. A Microcomputer Program for Modelling Large-strain Plasticity Problems. p. 2101-2108, Numerical Methods in Geomechanics (Innsbruck 1988), Swoboda (ed.). 1988 Balkema, Rotterdam, ISBN 90 6191 809 X.

DECOVALEX, 1992. DECOVALEX-Bench-Mark Test 3, DECOVALEX Doc 92/112, Stockholm 1992.

Deere, D., 1964. Technical Description of Rock Cores For Engineering Purposes. Rock Mechanics and Engineering Geology. Vol 1, No 1, 1964.

Itasca Consulting Group, Inc., 1992a. FLAC Version 3.2, Vol I-III. Minneapolis, ICG, 1992.

Itasca Consulting Group, Inc., 1992b. UDEC Version 1.8, Vol I-III. Minneapolis, ICG, 1992.

Peters, PR.R., 1983. Thermal Response to Emplacement of Nuclear Waste in Long, Horizontal Boreholes. SAND82-2497, April 1983.

Priest, S.D., and J.A. Hudson, 1976. Discontinuity Spacings in Rock. Int. J. Rock Mech. Min. Sci. & Geomech. Abstr. 13, 135-148.

SKB-KBS, 1983. Final Storage of Spent Nuclear Fuel - KBS3, Parts I-IV. SKB-KBS. May 1983.

Stille, H., T. Groth, and A. Fredriksson, 1982. FEM-analys av Bergmekaniska Problem Med JOBFEM. BEFO Report No. 307:1/82. Stockholm 1982. (In Swedish)

Thorpe, R., D.J. Watkins, W.E. Ralph, R. Hsu, and S. Flexser, 1980. Strength and Permeability Tests on Ultra-Large Stripa Granite Core. Technical Information Report No. 31, LBL-11203, SAC-31, UC-70. Lawrence Berkely Laboratory, University of California, 1980.

Appendix A MATHEMATICAL BACKGROUND OF FLAC

In FLAC, the dynamic equations of motion are included in the formulation in order to find a static solution to a problem. In the finite difference method, every derivative in the set of governing equations is replaced directly by an algebraic expression written in terms of the field variables (e.g., stress or displacement) at discrete points in space; these variables are undefined anywhere else.

FLAC embodies an explicit, time-marching solutions scheme: the right-hand sides of all equations consist of known values, because the timestep is chosen to be small enough that information cannot physically propagate from one element to the next within the timestep. One reason for doing this is to ensure that the numerical scheme is stable when the physical system being modeled is unstable. The general calculation sequence embodied in FLAC is illustrated in Fig. 1. This procedure first invokes the equations of motion to derive new velocities and displacements from stresses and forces. Then, strain rates are derived from velocities, and new stresses from strain rates.

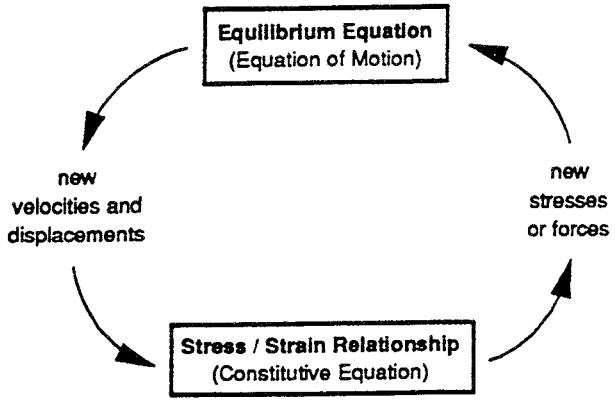

Fig. 1 Basic explicit calculation cycle

The calculation cycle of FLAC consists of the following operations:

1. For all zones, derive:

   - strain increment from known nodal velocities
   - new stresses from strain increments using constitutive model

2. For all nodes, derive:

   - nodal forces from known stresses in surrounding zones
   - updated velocities from forces, using law of motion
   - updated coordinates

Each FLAC quadrilateral is modelled as two pairs of constant-stress triangles:

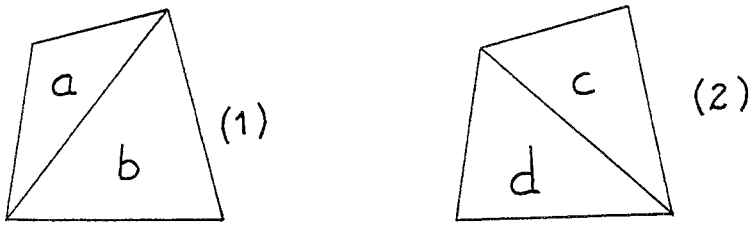

Each triangle maintains its stress components independently of the other triangles --- i.e., twelve stress components are stored for each quadrilateral (in plane-strain mode). The forces exerted on each node are taken to be the mean of those exerted by the quadrilaterals (1) and (2). The overlay scheme thereby ensures symmetry where symmetry should exist.

The difference equations for a generic triangle are derived from the generalized form of Gauss' divergence theorem:

$$\int_s n_i \, f \, ds = \int_A \frac{\partial f}{\partial x_i} \, dA \tag{1}$$

where $\int_s$ is the integral around the boundary of a closed area,

$\int_A$ is the integral within the area,

n_i is the unit vector normal to the surface,

x_i is a position vector, and

f is a scalar, vector or tensor.

Defining the average value of the gradient over the areas as

$$< \frac{\partial f}{\partial x_i} > = \frac{1}{A} \int_A \frac{\partial f}{\partial x_i} dA \tag{2}$$

we obtain

$$< \frac{\partial f}{\partial x_i} > = \frac{1}{A} \int_s n_i \, f \, ds \tag{3}$$

If the closed area is a triangle and f varies linearly along each side, we obtain the finite difference formula:

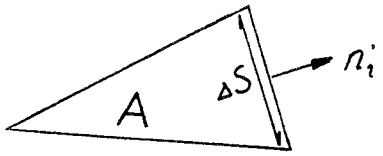

$$< \frac{\partial f}{\partial x_i} > = \frac{1}{A} \sum_s <f> n_i \Delta s \tag{4}$$

where the summation is over 3 sides, and <f> is the average value of f over the side.

This formula, suggested by Wilkins (1969), enables strain increments, Δe_{ij}, to be written in terms of nodal velocities for a zone by substituting the velocity vector for f:

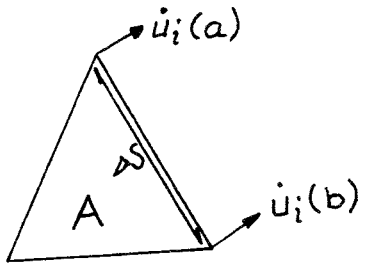

$$\frac{\partial \dot{u}_i}{\partial x_j} + \frac{1}{2A} \sum_s (\dot{u}_i^{(a)} + \dot{u}_i^{(b)}) \, n_j \, \Delta s \tag{5}$$

$$\Delta e_{ij} = \frac{1}{2} \left[\frac{\partial \dot{u}_i}{\partial x_j} + \frac{\partial \dot{u}_j}{\partial x_i} \right] \Delta t \tag{6}$$

where Δt is the timestep.

The volumetric strain is then averaged over each pair of triangles, according to the mixed discretization scheme of Marti and Cundall (1982):

$$\Delta e_m = \frac{\Delta e_{11}^{(a)} + \Delta e_{22}^{(a)} + \Delta e_{11}^{(b)} + \Delta e_{22}^{(b)}}{2} \tag{7}$$

$$\Delta e_d^{(a)} = \Delta e_{11}^{(a)} - \Delta e_{22}^{(a)} \tag{8}$$

$$\Delta e_{11}^{(a)} := \frac{\Delta e_m + \Delta e_d^{(a)}}{2} \tag{9}$$

$$\Delta e_{22}^{(a)} := \frac{\Delta e_m + \Delta e_d^{(a)}}{2} \tag{10}$$

and similarly for the strains in (b) and for the triangle-pair (c)-(d). At this stage, new zone stresses are computed by means of a specified constitutive model:

$$\sigma_{ij} := M\,(\sigma_{ij},\ \Delta e_{ij},\ S_1,\ S_2\ \ldots\ldots) \tag{11}$$

where M( ) is the constitutive model, and
S_i are state variables.

Mixed discretization is again invoked to equalize the isotropic stress between the two triangles in a pair:

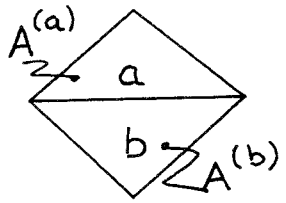

$$\sigma_0^{(a)} = \sigma_0^{(b)} := \left[\frac{\sigma_0^{(a)} A^{(a)} + \sigma_0^{(b)} A^{(b)}}{A^{(a)} + A^{(b)}}\right] \tag{12}$$

This equation only has an effect for constitutive laws that involve shear-induced dilatation.

In the explicit method, eq. (8) is evaluated once per zone timestep. No iterations are necessary because information cannot physically propagate from one zone to the next within one timestep.

The net force on a node is calculated from the summation of forces imposed by the zones surrounding the node. The force that one triangle contributes to the node is found from the stress vector acting on the edges of the triangle:

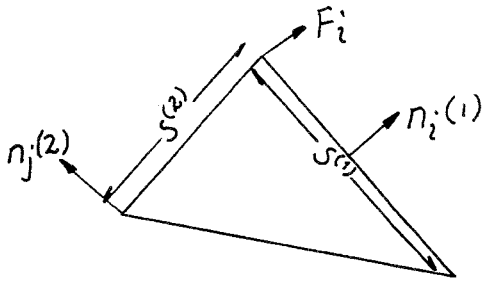

$$F_i = \frac{\sigma_{ij}^{(1)} \left[n_j^{(1)} S^{(1)} + n_j^{(2)} S^{(2)} \right]}{2} \tag{13}$$

At equilibrium, or in steady-state flow, the net force ΣF_i on a node is zero; otherwise, the node is accelerated. The acceleration is integrated numerically to obtain velocities:

$$\dot{u}_i := \dot{u}_i + \left[\sum F_i - \alpha \left| \sum F_i \right| \, sgn(\dot{u}_i) \right] \frac{\Delta t}{m} + g_i \Delta t \tag{14}$$

where m = inertial mass of the node (see below),
g_i = gravitational acceleration, and
α = damping factor.

Because FLAC is intended to model quasi-static problems, the inertial mass can be treated as a relaxation factor and set for optimum convergence. For a single mass-spring system, the critical timestep is

$$\Delta t_c = 2 \sqrt{\frac{m}{k}} \tag{15}$$

where k is the spring stiffness.

Assuming that optimum convergence is obtained when Δt_c is the same for all nodes, the inertial mass is set equal to the sum of the stiffnesses connected to the node (includes zone stiffness, structural; connections, and interface connections).

The term containing α in eq. (14) is a form of damping that vanishes when the net force on a node is zero --- i.e., it imposes no body forces on material in steady-state flow. This is advantageous when modeling plastic flow, but the solution tend to be under-damped for realistic values of α (e.g., 0.8)

Equation (14) may be integrated again to update coordinates in large strain mode :

$$x_i := x_i + \dot{u}_i \Delta t \tag{16}$$

The solution of solid body, heat transfer or fluid flow problems in FLAC invokes the equations of motion and constitutive relations, Fourier's Law for conductive heat transfer, and Darcy's Law for fluid flow in a porous solid, as well as boundary conditions.

REFERENCES

Cundall, P. and M. Board, (1988). A Microcomputer Program for Modelling Large-strain Plasticity Problems. p. 2101-2108, Numerical Methods in Geomechanics (Innsbruck 1988), Swoboda (ed.). 1988 Balkema, Rotterdam, ISBN 90 6191 809 X.

Itasca Consulting Group, Inc., (1992a). FLAC Version 3.2, Vol I-III. Minneapolis, ICG, 1992.

Marti, J. and P. A. Cundall, (1982). Mixed discretization procedure for accurate modelling of plastic collapse, Int. J. for Num. & Anal. Meth. in Geomech. 6:129-139.

Wilkins, M. L., (1969). Calculation of elastic-plastic flow. Report UCRL-7322, Lawrence Radiation Laboratory, Livermore.

Appendix B GROUNDWATER FLOW AND CONSOLIDATION

FLAC models the flow of groundwater through a permeable solid, such as soil. The flow modeling may be done by itself, independently of the usual mechanical calculation of FLAC or it may done in parallel with the mechanical modeling, so as to capture the effects of fluid/solid interaction. One type of fluid/solid interaction is "consolidation," in which the slow dissipation of pore pressure causes displacements to occur in the soil. This type of behavior involves two mechanical effects. First, changes in pore pressure cause changes in effective stress, which affect the response of the solid --- for example, a reduction in effective stress may induce plastic yield. Second, the fluid in a zone reacts to mechanical volume changes by a change in pore pressure, since the fluid is quite stiff.

The code handles both fully-saturated flow as well as flow in which a phreatic surface develops. The groundwater equations in FLAC are expressed in terms of pressure rather than head, although the latter is more common in soil mechanics. It seems more consistent to work in terms of pressure, since FLAC models the coupling between solid and fluid --- the interaction between the two phases is critically dependent on the relative magnitude of pressure and stress, not of head and stress. Further, a system may contain two disconnected but similar regions, separated by a vertical distance. The pressures in the two regions will be similar, but the heads will differ, although there is no difference in the physics. Finally, the numerical value of hydraulic conductivity (defined in terms of head) is dependent on the acceleration of gravity. This is unsatisfactory because a material "constant" should not depend on its position in the universe. A permeability defined in terms of pressure is not so dependent.

Darcy's law for an anisotropic porous medium is

$$V_i = K_{ij} \frac{\partial P}{\partial x_j} \tag{1}$$

where V_i is the specific discharge vector (units of velocity),
P is the pressure, and
K_{ij} is a "permeability" tensor

Each quadrilateral element is divided into triangles in two different ways. The specific discharge vector can be derived for a generic triangle, using the formula (2):

$$V_i \propto \frac{K_{ij}}{A} \sum P n_j s \tag{2}$$

where $\sum$ is the summation over the three sides of the triangle.

The general expression of the flowrate is

$$Q = V_i n_i s \tag{3}$$

For example, the flowrate into node (a) is

$$Q^{(a)} = [-V_1(x_2^{(b)} - x_2^{(c)}) + V_2(x_1^{(b)} - x_1^{(c)})]/2 \tag{4}$$

The factor of 2 accounts for the fact that the node only captures half the flow crossing a neighboring edge (since the other half goes to the other node of the edge).

The flow imbalance, $\sum Q$, at a node causes a change in pore pressure at a saturated node as follows:

$$\frac{\partial P}{\partial t} = -\frac{K_w}{nV}\sum Q \tag{5}$$

where nV is the pore volume associated with the node (n is the porosity and V is the total volume). The term $\sum Q$ includes contributions from the four surrounding zones and any sources that are specified by the user (e.g., inflow from a well).

In finite difference form, eq. (5) becomes

$$P := P - \frac{K_w(\sum Q\Delta t + \Delta V_{mech})}{nV} \tag{6}$$

where ΔV_{mech} is the equivalent nodal volume increase arising from mechanical deformations of the grid. The term nV is computed as the sum of the contributions from all triangular sub-zones connected to the node.

There are two aspects of numerical stability associated with the pore-fluid scheme. First, an explicit solution of the fluid flow equations requires that the timestep is less than a critical value; second, the bulk modulus of the fluid increases the mechanical stiffness of a saturated zone. The effect of increased mechanical stiffness is incorporated into the density-scaling scheme already in FLAC ; the apparent mechanical bulk modulus of a zone is modified by the presence of fluid as follows:

$$K := K + \frac{K_w}{n} \tag{7}$$

where n is the porosity of the zone.

The explicit fluid timestep can be derived by imagining that one node at the center of four zones is given a pressure of P_0. The excess nodal flow gives rise to an increment in pressure ΔP, according to eq. (6):

$$\Delta P + \frac{K_w Q \Delta t}{nV} \tag{8}$$

Porosity, n, is a dimensionless number defined as the ratio of void volume to total volume of an element. It is related to the void ratio, e, by:

$$n = \frac{e}{1 + e} \tag{9}$$

For low values of n, the stiffness may become very large in comparison with the stiffness of the solid material, causing the FLAC solution to take a long time to converge.

The "permeability", K, required by FLAC is the proportionality constant in Darcy's law, expressed in terms of pressure, rather than head:

$$q = K\frac{dP}{dx} \tag{10}$$

where q is the specific discharge (in units of velocity [m/sec]), and dP is the pressure gradient (e.g., Pa/m).

The more usual expression of Darcy's law is

$$q = k\frac{dh}{dx} \tag{11}$$

where h is the head (e.g., in m), and
k is the hydraulic conductivity (e.g., in m/sec).

Since $P = g\rho_w h$ (where g is the gravitational acceleration and ρ_w is the mass density of water),

$$K = \frac{k}{g\rho_w} \tag{12}$$

If there is a variation of permeability across the grid, the timestep will be dominated by the largest permeability. In problems in which the steady state is required (but not the transient behavior), it may be beneficial to limit the variations in permeability to improve convergence speed. For example, there will probably be little difference in the final state between systems where there is a 20:1 variation in permeability, compared to a 200:1 variation.

By default, FLAC will do a coupled flow and mechanical calculation if the grid is configured for flow and if the fluid bulk modulus and permeability are set to realistic values. The relative time scales associated with consolidation and mechanical loading should be appreciated. Mechanical effects occur almost instantaneously --- in the order of seconds or fractions of seconds. However, fluid flow is a long-term process: the dissipation associated with consolidation takes place over hours, days or weeks.

As discussed earlier, FLAC is an explicit code, which means that it takes "timesteps" to solve a problem. Thus, although mechanical effects take place almost instantaneously (e.g., pore pressures are generated when a load is applied), FLAC takes a finite (and sometimes large) number of steps to reach mechanical equilibrium. However, there is no true time period associated with these steps; they are merely an internal mechanism for the code to attain equilibrium. An alternative way to think of these mechanical steps is to imagine that each step represents a microsecond or less of time, so that, even if many steps are taken, almost no time elapses. Each fluid step does correspond to a real period of time.

FLAC uses an explicit solution scheme by default. However, this leads to quite a small timestep. When conditions are changing rapidly, this is usually appropriate but, for slowly changing conditions, an implicit solution scheme is provided. If the implicit option is selected, an iterative method is used to obtain the solution within each timestep.

REFERENCES

Itasca Consulting Group, Inc., (1992a). FLAC Version 3.2, Vol I-III. Minneapolis, ICG, 1992.

Appendix C THERMAL-MECHANICAL OPTION

FLAC has the capability to solve both transient and steady-state thermal and thermal-mechanical problems. Both implicit and explicit solution methods are available.

The thermal option in FLAC allows simulation of transient heat conduction in materials and the development of thermally-induced displacements and stresses. This option has the following specific features.

1. There are three material models for the thermal behavior of the material --- isotropic conduction, anisotropic conduction, and a temperature-dependent conductivity model.

2. As in the standard version of FLAC different zones may have different models and properties.

3. Any of the mechanical models may be used with any of the thermal models.

4. Several different thermal boundary conditions may be prescribed.

5. Heat sources may be inserted into the material either as line sources or as volume sources. These sources may be made to decay exponentially with time.

6. Both explicit and implicit solution algorithms are available.

The basic equation of conductive heat transfer is Fourier's law, which can be written as

$$Q_i = -k_{ij}\frac{\partial T}{\partial x_j} \qquad (1)$$

where Q_i = flux in the i-direction (W/m^2),
k_{ij} = thermal conductivity tensor (W/m K), and
T = temperature.

Also, for any mass, the change in temperature can be written as

$$\frac{\partial T}{\partial t} = \frac{Q_{net}}{C_p M} \tag{2}$$

where Q_{net} = heat flow into the mass (W),
C_p = specific heat (J/kg K), and
M = mass (kg).

These two equations are the basis of the thermal version of FLAC.

Temperature changes cause stress changes according to the equation

$$\Delta\sigma_{ij} = -\delta_{ij} 3K\alpha\Delta T \tag{3}$$

where $\Delta\sigma_{ij}$ = change in stress,
δ_{ij}= Kronecker delta (δ_{ij}=1 for i=j and 0 for i # j),
K = bulk modulus,
α = linear thermal expansion coefficient, and
ΔT= temperature change.

The mechanical changes can also cause temperature changes as energy is dissipated in the system. This coupling is not modeled in FLAC because the heat produced is usually negligible.

The Diffusion Equation,

$$\frac{\partial T}{\partial t} = \frac{1}{C_p \rho}\left[k_x \frac{\partial^2 T}{\partial x^2} + k_y \frac{\partial^2 T}{\partial y^2} \right] \tag{4}$$

can be rewritten as:

$$\rho C_p \frac{\partial T}{\partial t} = k_x \frac{\partial^2 T}{\partial x^2} + k_y \frac{\partial^2 T}{\partial y^2} \tag{5}$$

For a finite difference grid consisting of rectangular zones which are Δx wide by Δy in height (Fig. 1), an energy balance may be performed[1].

---

[1]The formulation in FLAC is based upon triangular elements, so the expressions actually are written in terms of the contributions from sides of the triangles rather than rectangles. The formulation is analogous to that for the groundwater flow logic described in Appendix B.

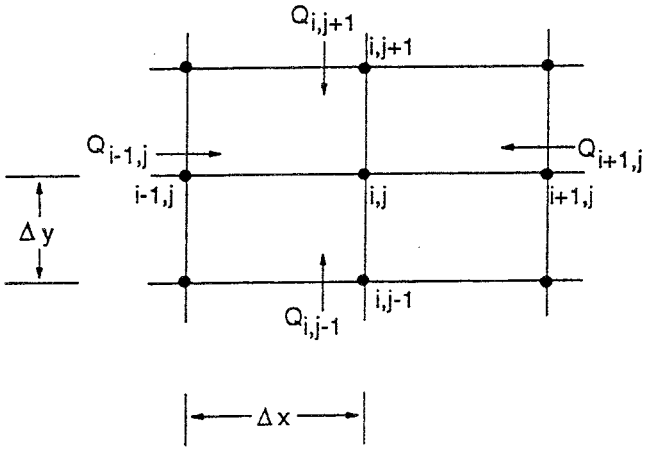

Fig. 1 Nomenclature for determination of energy balance for a typical interior gridpoint.

The heat transfer may be coupled to thermal stress calculations at any time during a transient simulation. The coupling occurs in one direction only --- i.e., the temperature may result in stress changes, but mechanical changes in the body resulting from force application do not result in temperature change. This restriction is not believed to be of great significance here since the energy changes for quasi-static mechanical problems is usually negligible. The stress change in a triangular zone is given by:

$$\Delta\sigma_{ij} = -\delta_{ij} 3K\alpha\Delta T \tag{6}$$

The above assumes a constant temperature in each triangular zone which is interpolated from the surrounding gridpoints. This stress is added to the zone stress state prior to application of the constitutive law.

REFERENCES

Itasca Consulting Group, Inc., (1992a). FLAC Version 3.2, Vol I-III. Minneapolis, ICG, 1992.

Appendix D NUMERICAL BIAXIAL TEST

In order to obtain mechanical properties for the continuum analysis, a biaxial test was conducted using a discontinuum code, UDEC /Itasca, 1992/. In the distinct element method, a rock mass is represented as an assemblage of discrete blocks which interact through corner and edge contacts. Joints are viewed as interfaces between distinct bodies --- i.e., the discontinuity is treated as a boundary condition rather than a special element in the model. The method utilizes an explicit timestepping (dynamic) algorithm which allows large displacements and rotations and general non-linear constitutive behavior for both the matrix and discontinuities.

Since UDEC is specifically designed to simulate the predominant features of fractured rock masses, including complex joint structures, non-linear, inelastic joint behavior and elasto-plastic behavior of intact rock, it was thought to be appropriate to do the test with UDEC.

The biaxial test was performed as a strain-controlled test with three different confining pressures --- namely 0, 1 and 2 MPa. The strain control was obtained by applying a compressional velocity (i.e., displacement) to the both short end boundaries while the long boundaries were stress controlled with the confining stress.

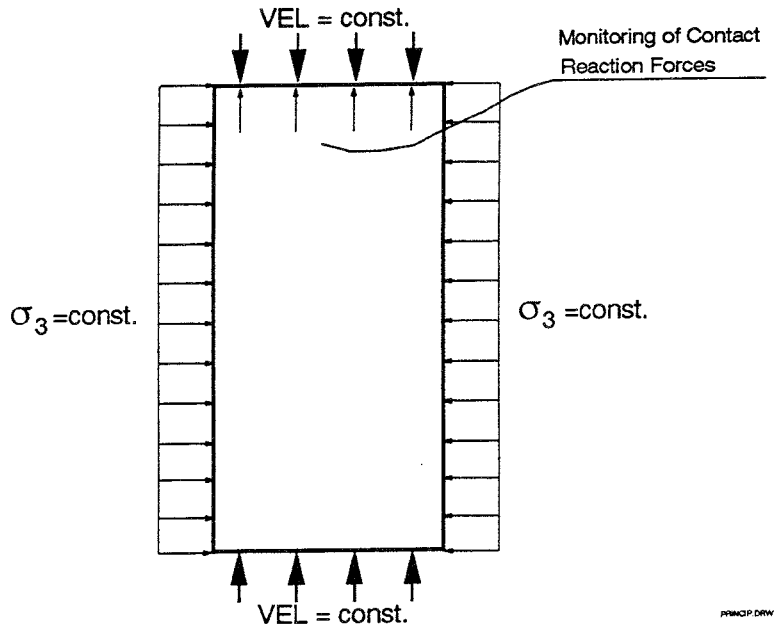

Fig. 1 Boundary conditions used and principle for contact force monitoring for the numerical biaxial test.

The test model, generated from the joint data in the problem specification is shown in Fig. 2.

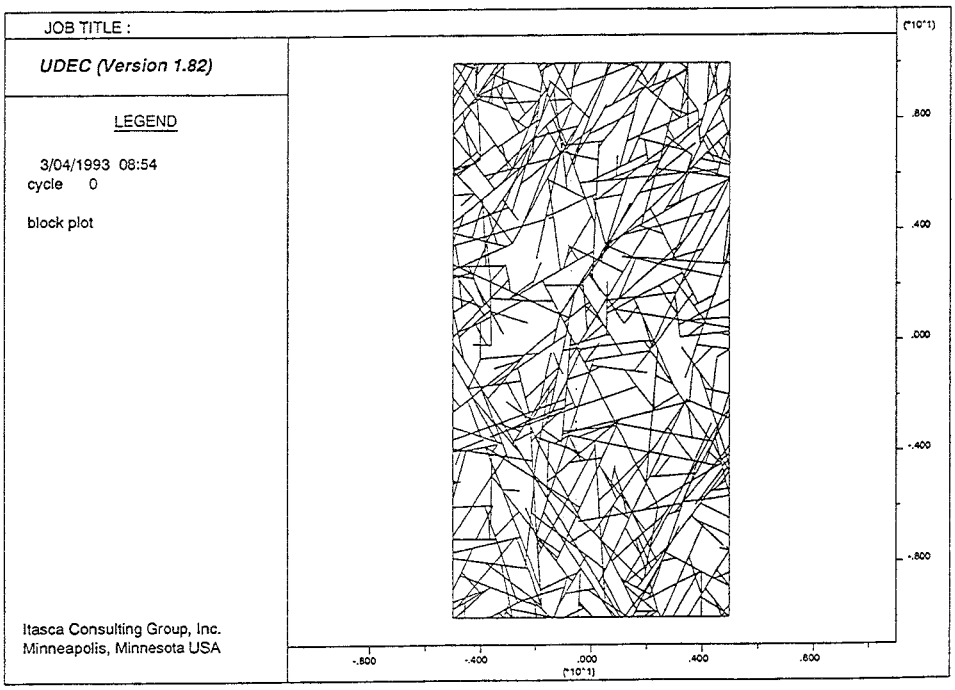

Fig. 2 UDEC model for biaxial compression test.

During compression of the block, the contact stress at the upper and lower boundary were recorded as well as the vertical and the horizontal deformation of the model.

The intact block material in the test block was modelled with a Mohr-Coulomb shear failure criterion. Since only the uniaxial compressive strength of the intact block material was given, a cohesion, C, and a friction angle, ϕ, of the intact material were calculated using eq. (1).

$$\sigma_c = \frac{2C\cos\phi}{1-\sin\phi} \qquad (1)$$

For the calculation, a friction angle of 60 ° was assumed as a typical Stripa value. The cohesion then became 26.8 MPa. Also, a tension cut-off at 10 MPa was used. The joints were modelled with a Coulomb slip criterion.

The results from the analyzes are presented in Figs. 3 and 4 and in Table 1.

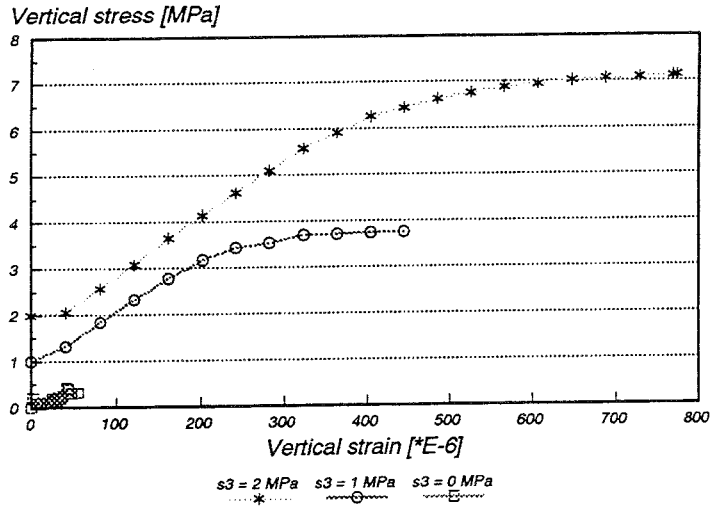

Fig. 3 σ-ε diagram from numerical biaxial test.

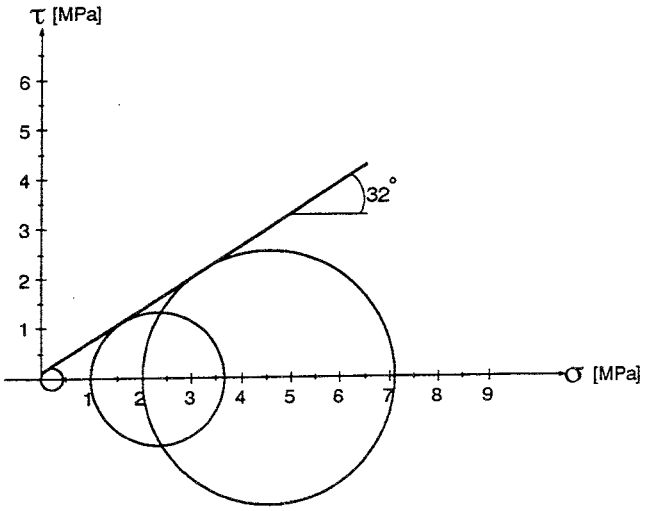

Fig. 4 Mohr-diagram from numerical biaxial test.

Table 1 Mechanical properties for the equivalent rock mass.

Parameter	**Value**	**Units**
Young's Modulus, E	12	GPa
Poisson's ratio, υ	0.2	-
Bulk Modulus, K	6.67	GPa
Shear Modulus, G	5.00	GPa
Density, ρ	2670	kg/m^3
Cohesion, C	0.1	MPa
Friction angle, ϕ	32	°
Tensile strength, σ_T	0.1	MPa

Appendix E Rock Mass Rating (RMR)

A 20 by 20 m jointed area was used for estimating an average joint spacing, S. For that purpose, nine horizontal and nine vertical scan lines were uniformly distributed with 2 m spacing, along which all intersecting joints were counted. The average number of joints along the horizontal scan-lines turned out to be 2.87 joints/m and along the vertical lines 2.65 joints/m. Due to the small difference, a mean value of 2.76 joints/ m was used. This would, according to the empirical relation between spacing and RQD by Deere (1964), give a RQD-value of 88% and, according to the analytical expression by Priest & Hudson (1976),

$$RQD = 100 \cdot e^{-0.1\lambda}(0.1\lambda+1)$$

where λ is the average number of discontinuities per meter), 97%. The RQD was therefore assumed to be 90%.

The different RMR aspects were given the following points (Fig. 1);

A1	A2	A3	A4	A5	B	TOT
12p	15p	10p	20p	10p	-5p	62p

This would lead to a rock mass stiffness Erm = 2RMR-100=24GPa according to Bieniawski (1979), Erm=20 GPa according to Serafim & Periera (1983) and to Erm = 22.6 GPa using the spacing, S, and the joint normal stiffness, K_N, in eq. (1)

$$E_{rm} = \frac{1}{\frac{1}{E_{lab}} + \frac{1}{K_N \cdot S}} \qquad (1)$$

By using an average of Young's modulus of 22 GPa, the Poisson's ratio for the rock mass, ν_{rm} was reduced proportionally to the reduction of the Young's modulus, to ν_{rm} =0.09.

It has been found that the strength parameters, in the form of cohesion and friction angle, obtained from the RMR-system, are not applicable to the Scandinavian, crystalline rock type. Therefore, the RMR-rating was assumed equal to the RMS system /Stille et al., 1982/ --- i.e., RMR=62 was assumed to be equal to RMS=62. This assumption gives a cohesion of 2.5 MPa and a friction angle of 45°. These properties would give an uniaxial compressive strength of

$$\sigma_c = \frac{2C \cdot \cos\phi}{1-\sin\phi} = 12.1 MPa$$

The calculated uniaxial compressive strength corresponds to some degree to the value obtained by Thorpe et al. (1980) from the ultra-large stripa granite core which gave an uniaxial strength of the sample of 7.4 MPa.

However, the Young's modulus was measured to be 52.3 GPa compared to 22 GPa calculated here.

A. CLASSIFICATION PARAMETERS AND THEIR RATINGS

PARAMETER			RANGES OF VALUES						
1	Strength of intact rock material	Point-load strength index	> 10 MPa	4 - 10 MPa	2 - 4 MPa	1 - 2 MPa	For this low range - uniaxial compressive test is preferred		
		Uniaxial compressive strength	>250 MPa	100 - 250 MPa	50 - 100 MPa	25 - 50 MPa	5-25 MPa	1-5 MPa	< 1 MPa
	Rating		15	12	7	4	2	1	0
2	Drill core quality RQD		90% - 100%	75% - 90%	50% - 75%	25% - 50%	< 25%		
	Rating		20	17	13	8	3		
3	Spacing of discontinuities		>2 m	0,6 - 2 m	200 - 600 mm	60 -200 mm	<60 mm		
	Rating		20	15	10	8	5		
4	Condition of discontinuities		Very rough surfaces. Not continuous No seperation Unweathered wall rock.	Slightly rough surfaces. Separation < 1 mm Slightly weathered walls	Slightly rough surfaces. Separation < 1 mm Highly weathered walls	Slickensided surfaces OR Gouge < 5 mm thick OR Separation 1-5 mm. Continuous	Soft gouge > 5 mm thick OR Separation > 5 mm. Continous		
	Rating		30	25	20	10	0		
5	Ground water	Inflow per 10 m tunnel length	None	<10 litres/min	10-25 litres/min	25 - 125 litres/min	> 125		
		Ratio joint water pressure / major principal stress	0	0,0-0,1	0,1-0,2	0,2-0,5	>0,5		
		General conditions	Completely dry	Damp	Wet	Dripping	Flowing		
	Rating		15	10	7	4	0		

B. RATING ADJUSTMENT FOR JOINT ORIENTATIONS

Strike and dip orientations of joints		Very favourable	Favourable	Fair	Unfavourable	Very unfavourable
Ratings	Tunnels	0	-2	-5	-10	-12
	Foundations	0	-2	-7	-15	-25
	Slopes	0	-5	-25	-50	-60

C. ROCK MASS CLASSES DETERMINED FROM TOTAL RATINGS

Rating	100 ← 81	80 ← 61	60 ← 41	40 ← 21	< 20
Class No.	I	II	III	IV	V
Description	Very good rock	Good rock	Fair rock	Poor rock	Very poor rock

D. MEANING OF ROCK MASS CLASSES

Class No	I	II	III	IV	V
Average stand-up time	10 years for 15 m span	6 months for 8 m span	1 week for 5 m span	10 hours for 2,5 m span	30 minutes for 1 m span
Cohesion of the rock mass	> 400 kPa	300 - 400 kPa	200 - 300 kPa	100 - 200 kPa	< 100 kPa
Friction angle of the rock mass	> 45°	35° - 45°	25° - 35°	15° - 25°	< 15°

The Effect of Discontinuity Strike and Dip Orientations in Tunneling.

Strike perpendicular to tunnel axis				Strike parallel to tunnel axis		Dip 0° - 20° irrespective of strike
Drive with dip		Drive against dip				
Dip 45°-90°	Dip 20°-45°	Dip 45°-90°	Dip 20°-45°	Dip 45°-90°	Dip 20°-45°	
Very favourable	Favourable	Fair	Unfavourable	Very unfavourable	Fair	Unfavourable

Fig 1. Rock mass classification according to Bieniawski (1979).

REFERENCES

Bieniawski, Z.T., (1979). The Geomechanics Classification in Rock Engineering Applications. Int. Congress of Rock Mechanics, Montreaux Vol 2, 1979.

Deere, D.V., (1964), Technical Description or Rock Cores for Engineering Purposes. Rock Mech. Engng Geol., 1, 17-22.

Priest, S. D. and J.A. Hudson, (1976), Discontinuity spacings in Rock , Int. J. Rock Mech. Min. Sci. & Geomech. Abstr 13, 135-148.

Serafim, J. L., and J. P. Periera, (1983), Consideration of the Geomechanics Classification of Bieniawski. In Procedings of the International Symposium on Engineering Geology and Underground Construction, (Lisbon 1983), pp.1133-44.

Stille, H., T. Groth, A. Fredriksson, (1982). FEM-analys av Bergmekaniska Problem Med JOBFEM. BEFO Report No. 307:1/82. Stockholm 1982. (In Swedish)

Appendix F FLAC Input Data

```
**********************************************************
**   SYM7.DAT    1993.02.16
**   DECOVALEX BMT3, HYDRO-MECHANICAL-THERMAL
**   SIMUL OF TUNNEL EXCAV WITH FLOW EQUILIBRIUM
**   AND THERMAL HEATING FROM NUCLEAR WASTE
**   CANISTER
**
**   FLAC Version 3.22,  2-19-93
**   EFFECTIVE STRESS AND THERMALLY DEPENDENT
**   PERMEABILITY
**   MAX PERMEABILITY CHANGE = 10 TIMES
**********************************************************

SET LOG ON
CONFIG GW EXTRA 15 THERMAL

GR 21,35
MODEL MOHR TH_I

GEN 0,-25 0,-7.5 2.5,-7.5 2.5,-25 RATIO=1,0.9 I=1,6 J=1,9
GEN 0,-7.5 0,-2.5 2.5,-2.5 2.5,-7.5 RATIO=1,1 I=1,6 J=9,14
GEN 0,-2.5 0,0 2.5,0 2.5,-2.5 RATIO=1,1 I=1,6 J=14,19
GEN 0,0 0,7.5 2.5,7.5 2.5,0 RATIO=1,1 I=1,6 J=19,28
GEN 0,7.5 0,25 2.5,25 2.5,7.5 RATIO=1,1.11 I=1,6 J=28,36
GEN 2.5,7.5 2.5,25 5.5,25 5.5,7.5 RATIO=1,1.11 I=6,10 J=28,36
GEN 5.5,7.5 5.5,25 7.5,25 7.5,7.5 RATIO=1,1.11 I=10,12 J=28,36
GEN 7.5,7.5 7.5,25 25,25 25,7.5 RATIO=1.11,1.11 I=12,22 J=28,36
GEN 7.5,0 7.5,7.5 25,7.5 25,0 RATIO=1.11,1 I=12,22 J=19,28
GEN 7.5,-2.5 7.5,0 25,0 25,-2.5 RATIO=1.11,1 I=12,22 J=14,19
GEN 7.5,-7.5 7.5,-2.5 25,-2.5 25,-7.5 RAT=1.11,1 I=12,22 J=9,14
GEN 7.5,-25 7.5,-7.5 25,-7.5 25,-25 RATIO=1.11,0.9 I=12,22 J=1,9
GEN 5.5,-25 5.5,-7.5 7.5,-7.5 7.5,-25 RATIO=1,0.9 I=10,12 J=1,9
GEN 2.5,-25 2.5,-7.5 5.5,-7.5 5.5,-25 RATIO=1,0.9 I=6,10 J=1,9
GEN 2.5,-7.5 2.5,-2.5 5.5,-2.5 5.5,-7.5 RATIO=1,1 I=6,10 J=9,14
GEN 2.5,-2.5 2.5,0 5.5,0 5.5,-2.5 RATIO=1,1 I=6,10 J=14,19
GEN 2.5,0 2.5,7.5 5.5,7.5 5.5,0 RATIO=1,1 I=6,10 J=19,28
GEN 5.5,0 5.5,7.5 7.5,7.5 7.5,0 RATIO=1,1 I=10,12 J=19,28
GEN 5.5,-2.5 5.5,0 7.5,0 7.5,-2.5 RATIO=1,1 I=10,12 J=14,19
GEN S        S        S       S   RATIO=1,1 I=10,12 J=9,14

INI Y=0.75 J=20
INI Y=1.5  J=21
INI Y=2.5  J=22
INI Y=3.5  J=23
INI Y=4.25 J=24
INI Y=5.0  J=25
INI Y=5.75 J=26
INI Y=6.5  J=27

*---------GENERATE TUNNEL SHAPE-------------------------

GEN LINE -2.5,0  2.5,0
GEN LINE -2.5,0 -2.5,2.5
GEN LINE  2.5,0  2.5,2.5
GEN ARC 0,2.5 2.5,2.5 180


*---------SET KINEMATIC BOUNDARY CONDITIONS-------

FIX X I=1
FIX X I=22
FIX Y J=1
```

```
*---------EQUIVALENT ROCK MASS PROPERTIES----------

*---------Mechanical properties

PROP BULK 9E9
PROP SHEAR=10.4E9
PROP DENS=2670.
PROP COHESION=2.5E6
PROP FRICTION=45
PROP TENS=2.5E6

*---------Thermal properties

PROP SPEC_HEAT=900.
PROP CONDUCT=3.
PROP THEXP=9.0E-6

*---------Hydraulic properties

* Lower square
PROP POROSITY=2.0E-4 J=1,18 *Including void space from struct
PROP K11=9.10722E-15 I=1,22 J=1,18  *
PROP K22=9.79449E-15 I=1,22 J=1,18  *
*Upper square
PROP POROSITY=1.5E-4 J=19,35  *Including void space from struct
PROP K11=1.40650E-14 I=1,22 J=19,35 *          -"-
PROP K22=1.92480E-14 I=1,22 J=19,35 *          -"-

*---------Properties of the fluid

WATER DENS=1000 BULK=2.0E8 TENS=1E10


*---------IN-SITU STRESS AND BOUNDARY LOADS-------

INI SYY=-13.7512E6 VAR 0,1.3096E6
INI SXX=-13.7512E6 VAR 0,1.3096E6
INI SZZ=-13.7512E6 VAR 0,1.3096E6

APPLY SYY=-12.44E6 J=36

SET GRAVITY 9.81


*---------SET THE INITIAL TEMP. TO 27 DEG CELCIUS-

INI TEMP=27.0


*---------SET INITIAL PORE PRESSURE---------------

INI PP=5.15E6 VAR 0,-.4905E6
FIX PP J=36


*---------DEFINE HISTORIES------------------------

HIS NSTEP=20
HIS UNBAL
HIS GWTIME
HIS THTIME

HIS YVEL I=1 J=25  *C
HIS YVEL I=1 J=36  *Upper boundary
HIS XVEL I=6 J=22  *D
```

```
HIS XDIS YDIS I=1 J=19    *A
HIS XDIS YDIS I=1 J=25    *C
HIS XDIS YDIS I=6 J=22    *D
HIS XDIS YDIS I=12 J=28   *G
HIS XDIS YDIS I=12 J=9    *H

HIS SXX SYY I=1 J=19    *A
HIS SXX SYY I=1 J=25    *C
HIS SXX SYY I=6 J=22    *D
HIS SXX SYY I=12 J=28   *G
HIS SXX SYY I=12 J=9    *H

HIS TEMP I=1 J=19    *A
HIS TEMP I=1 J=25    *C
HIS TEMP I=6 J=22    *D
HIS TEMP I=12 J=28   *G
HIS TEMP I=12 J=9    *H

HIS TEMP I=1 J=11    *MAX TEMP

HIS PP I=8 J=21
HIS PP I=18 J=2


*---------CONSOLIDATE-----------------------------

SET THERMAL OFF
SET FLOW OFF
STEP 1000
TIT
CONSOLIDATION
SAVE CONSOL.SAV

RE CONSOL.SAV

***    INITIATE STRESS AND HYDRAULIC IN-SITU VALUES AS
***    EXTRA FISH VARIABLES

DEF TEMP_INI
;LOWER RIGHT SQUARE
  LOOP I (1,IZONES)
     LOOP J (1,18)
       TEMPZ =  0.25*(TEMP(I,J)+TEMP(I,J+1)+TEMP(I+1,J)+TEMP(I+1,J+1))
       EX_1(I,J) = TEMPZ
       EX_2(I,J) = SXX(I,J)+PP(I,J)
       EX_3(I,J) = SYY(I,J)+PP(I,J)
       EX_4(I,J) = 9.7432E-2      ; EQ SPACING FOR HORIZ. FLOW
       EX_5(I,J) = 9.0595E-2      ;    -------"------------ VERTICAL
       EX_6(I,J) = 2.2E-6         ;INITIAL APERTURE
       EX_7(I,J) = POROSITY(I,J)
       EX_8(I,J) = K11(I,J)
       EX_9(I,J) = K22(I,J)
    END_LOOP
  END_LOOP
;
;UPPER RIGHT SQUARE
  LOOP I (1,IZONES)
     LOOP J (19,JZONES)
       TEMPZ = 0.25*(TEMP(I,J)+TEMP(I,J+1)+TEMP(I+1,J)+TEMP(I+1,J+1))
       EX_1(I,J) = TEMPZ
       EX_2(I,J) = SXX(I,J)+PP(I,J)
       EX_3(I,J) = SYY(I,J)+PP(I,J)
       EX_4(I,J) = 6.309E-2       ; EQ SPACING FOR HORIZ. FLOW
       EX_5(I,J) = 4.610E-2       ;    -------"------------ VERTICAL
       EX_6(I,J) = 2.2E-6         ;INITIAL APERTURE
       EX_7(I,J) = POROSITY(I,J)
       EX_8(I,J) = K11(I,J)
```

```
        EX_9(I,J) = K22(I,J)
      END_LOOP
   END_LOOP
END
;
TEMP_INI
;

INI SAT 1
FIX SAT

*--EXCAVATE TUNNEL AND STEP TO MECH-FLOW EQUILIB

M NULL REG 1,23
INI PP=0.0 MARK I=1,7 J=18,26
FIX PP MARK I=1,7 J=18,26
SET FLOW OFF
INI XDIS=0
INI YDIS=0
TIT
TUNNEL EXCAVATION AND FLOW EQUILIBRIUM
HIS NSTEP 250
STEP 3000
SAVE MECH.SAV

*--------DEF ZONE INFLOW RECORDING FISH FUNCTION

DEF INFLOWZ
 SUM=0.0
   LOOP I (1,IZONES)
      SUM=SUM-YFLOW(I,35)*(X(I+1,35)-X(I,35))
   END_LOOP
 INFLOWZ=SUM
END

*--------DEF ZONE OUTFLOW RECORDING FISH FUNCTION

DEF OUTFLOWZ
 SUM1=0.0
 SUM2=0.0
 SUM3=0.0
   LOOP I (1,12)
      SUM1=SUM1-YFLOW(I,28)*(X(I+1,28)-X(I,28))
   END_LOOP
   LOOP J (9,28)
      SUM2=SUM2-XFLOW(12,J)*(Y(12,J+1)-Y(12,J))
   END_LOOP
   LOOP I (1,12)
      SUM3=SUM3+YFLOW(I,9)*(X(I+1,9)-X(I,9))
   END_LOOP
 OUTFLOWZ=SUM1+SUM2+SUM3
END

*--------DEF FUNCTION TO RECORD FLOW BALANCE---
DEF QRATIO
INFLOW=0.0
OUTFLOW=0.0
LOOP I (1,IGP)
  LOOP J (1,JGP)
    IF AND(FLAGS(I,J),512)=512 THEN
       IF GFLOW(I,J)>0.0 THEN
         INFLOW=INFLOW+GFLOW(I,J)
        ELSE
         OUTFLOW=OUTFLOW-GFLOW(I,J)
      END_IF
    END_IF
  END_LOOP
```

```
END_LOOP
QBALANCE=INFLOW-OUTFLOW
IF (INFLOW+OUTFLOW)#0.0 THEN
QRATIO=2.0*ABS(QBALANCE)/(INFLOW+OUTFLOW)
END_IF
END


*--------FLOW HISTORIES-----------

HIST QRATIO
HIST INFLOW
HIST OUTFLOW
HIST INFLOWZ
HIS OUTFLOWZ

*--------DEF FISH FUNCTION TO CHANGE PERMEABILITY
*--------TO STRESS STATE

DEF PERM_VAR
K11MAX=0.
K22MAX=0.
;
WHILE_STEPPING
  LOOP I (1,IZONES)
     LOOP J (1,JZONES)
       IF MODEL(I,J) # 1 THEN
          X_APER = EX_6(I,J)+((SYY(I,J)+PP(I,J)-EX_3(I,J))/100E9)
          Y_APER = EX_6(I,J)+((SXX(I,J)+PP(I,J)-EX_2(I,J))/100E9)
          X_APER =MAX(X_APER,EX_6(I,J))
          Y_APER =MAX(Y_APER,EX_6(I,J))
        K11(I,J) = (((X_APER)^3) / (12*EX_4(I,J)*1E-3))
        K22(I,J) = (((Y_APER)^3) / (12*EX_5(I,J)*1E-3))
        K11MAX = 10 * EX_8(I,J)
        K22MAX = 10 * EX_9(I,J)
        K11(I,J) = MIN(K11(I,J),K11MAX)
        K22(I,J) = MIN(K22(I,J),K22MAX)
      END_IF
    END_LOOP
  END_LOOP
END

*--------SET RUNNING CONDITIONS
SET FORCE 5E4 CLOCK 10000 STEP 100000
SET FLOW ON
SET MECH ON
SET NMECH 500
HIS NSTEP=500

SOLVE AUTO ON AGE 2.592E6
TIT
BMT3, TUNNEL EXCAVATION, FLOW TIME = 30 DAYS
SAVE 30DAYS.SAV

SOLVE AUTO ON AGE 3.456E6
TIT
BMT3, TUNNEL EXCAVATION AND FLOW EQUILIBRIUM, FLOW TIME=40 DAYS
SAVE 40DAYS.SAV
```

```
**************************************************
*
*--------THERMAL PART-----------------------------------------------
*
* Thermal source applied as infinite linear source,
* width=b.h. diameter, height=5 m gives q=117.5 W/m^2
* if applied as a boundary flux.
* 1993-04-05
**************************************************


REST 40DAYS.SAV

INI TEMP=27

DEF T_INI
  LOOP I (1,IZONES)
     LOOP J (1,JZONES)
       IF MODEL(I,J)#1 THEN
         TEMPZ=0.25*(TEMP(I,J)+TEMP(I,J+1)+TEMP(I+1,J)+TEMP(I+1,J+1))
         EX_1(I,J) = TEMPZ
       END_IF
    END_LOOP
  END_LOOP
END

;
DEF TEMP_DO
  LOOP I (1,IZONES)
     LOOP J (1,JZONES)
       IF MODEL(I,J)#1 THEN
         TEMPZ=0.25*(TEMP(I,J)+TEMP(I,J+1)+TEMP(I+1,J)+TEMP(I+1,J+1))
         TEMPD=TEMPZ-EX_1(I,J)
         K11(I,J)=K11(I,J)*(1.0+3.2E-2*TEMPD)
         K22(I,J)=K22(I,J)*(1.0+3.2E-2*TEMPD)
       END_IF
    END_LOOP
  END_LOOP
END
DEF FREEZE
  LOOP I (1,IZONES)
     LOOP J (1,JZONES)
       IF MODEL(I,J)#1 THEN
          EX_15(I,J)=PP(I,J)+(SXX(I,J)+SYY(I,J)+SZZ(I,J))/3.0
       END_IF
    END_LOOP
  END_LOOP
END

DEF N_PP
  LOOP I (1,IZONES)
     LOOP J (1,JZONES)
       IF MODEL(I,J)#1 THEN
          PP(I,J)=EX_15(I,J)-(SXX(I,J)+SYY(I,J)+SZZ(I,J))/3.0
          II=I
           JJ=J
           PPP=PP(I,J)
          COMMAND
            INI PP PPP I=II J=JJ
          END_COMMAND
       END_IF
    END_LOOP
  END_LOOP
END
```

```
DEF DECAY
    THINI=0.0
    DECONST=-6.342E-10
    DECAY=EXP(DECONST*(THTIME-THINI))
END

APPLY FLUX=117.5 HIST DECAY I=1 J=9,14

*----------ASSIGN THERMAL PROPERTIES TO THE EXCAVATED TUNNEL
APPLY CONVECTION 27. 7. FROM 1,19 TO 1,25


*---------ASSIGN THERMAL BOUNDARY CONDITIONS

FIX TEMP 27 I=1,22 J=36 *TOP BOUNDARY

SET FLOW OFF
SET MECH OFF

SET THERM ON

T_INI
SET IMPLICIT ON THDT 2E4
HIS NSTEP 250
STEP 1577
SAVE 1YTHONLY.SAV
FREEZE
SET THERM OFF
SET FLOW OFF
SET MECH ON
SET NMECH 1
WATER BULK 1
SET IMPLICIT OFF
STEP 5000

SAVE 1YMEONLY.SAV

WATER BULK 2E8
N_PP
TEMP_DO
INI PP=0.0 MARK I=1,7 J=18,26
INI PP=4.6595E6 J 36
SET MECH OFF FLOW ON
SET NGW 256
STEP 1000000

SAVE 1YFLOW.SAV

REST 1YFLOW.SAV
SET FLOW OFF
SET MECH OFF

SET THERM ON

T_INI
SET IMPLICIT ON THDT 2E4
HIS NSTEP 250
STEP 4731
SAVE 4YTHONLY.SAV
SET THERM OFF
SET FLOW OFF
SET MECH ON
SET NMECH 1
WATER BULK 1
SET IMPLICIT OFF
STEP 5000
```

```
SAVE 4YMEONLY.SAV

WATER BULK 2E8
N_PP
TEMP_DO
INI PP=0.0 MARK I=1,7 J=18,26
INI PP=4.6595E6 J 36
SET MECH OFF FLOW ON
SET NGW 256
STEP 1000000
SAVE 4YFLOW.SAV
```

List of SKB reports

Annual Reports

1977-78
TR 121
KBS Technical Reports 1 – 120
Summaries
Stockholm, May 1979

1979
TR 79-28
The KBS Annual Report 1979
KBS Technical Reports 79-01 – 79-27
Summaries
Stockholm, March 1980

1980
TR 80-26
The KBS Annual Report 1980
KBS Technical Reports 80-01 – 80-25
Summaries
Stockholm, March 1981

1981
TR 81-17
The KBS Annual Report 1981
KBS Technical Reports 81-01 – 81-16
Summaries
Stockholm, April 1982

1982
TR 82-28
The KBS Annual Report 1982
KBS Technical Reports 82-01 – 82-27
Summaries
Stockholm, July 1983

1983
TR 83-77
The KBS Annual Report 1983
KBS Technical Reports 83-01 – 83-76
Summaries
Stockholm, June 1984

1984
TR 85-01
Annual Research and Development Report 1984
Including Summaries of Technical Reports Issued during 1984. (Technical Reports 84-01 – 84-19)
Stockholm, June 1985

1985
TR 85-20
Annual Research and Development Report 1985
Including Summaries of Technical Reports Issued during 1985. (Technical Reports 85-01 – 85-19)
Stockholm, May 1986

1986
TR 86-31
SKB Annual Report 1986
Including Summaries of Technical Reports Issued during 1986
Stockholm, May 1987

1987
TR 87-33
SKB Annual Report 1987
Including Summaries of Technical Reports Issued during 1987
Stockholm, May 1988

1988
TR 88-32
SKB Annual Report 1988
Including Summaries of Technical Reports Issued during 1988
Stockholm, May 1989

1989
TR 89-40
SKB Annual Report 1989
Including Summaries of Technical Reports Issued during 1989
Stockholm, May 1990

1990
TR 90-46
SKB Annual Report 1990
Including Summaries of Technical Reports Issued during 1990
Stockholm, May 1991

1991
TR 91-64
SKB Annual Report 1991
Including Summaries of Technical Reports Issued during 1991
Stockholm, April 1992

1992
TR 92-46
SKB Annual Report 1992
Including Summaries of Technical Reports Issued during 1992
Stockholm, May 1993

1993
TR 93-34
SKB Annual Report 1993
Including Summaries of Technical Reports Issued during 1993
Stockholm, May 1994

1994

TR 94-33

SKB Annual Report 1994

Including Summaries of Technical Reports Issued during 1994.
Stockholm, May 1995

List of SKB Technical Reports 1995

TR 95-01

Biotite and chlorite weathering at 25°C. The dependence of pH and (bi) carbonate on weathering kinetics, dissolution stoichiometry, and solubility; and the relation to redox conditions in granitic aquifers

Maria Malmström[1], Steven Banwart[1], Lara Duro[2], Paul Wersin[3], Jordi Bruno[3]
[1] Royal Institute of Technology, Department of Inorganic Chemistry, Stockholm, Sweden
[2] Universidad Politécnica de Cataluña, Departmento de Inginería Química, Barcelona, Spain
[3] MBT Tecnología Ambiental, Cerdanyola, Spain
January 1995

TR 95-02

Copper canister with cast inner component. Amendment to project on Alternative Systems Study (PASS), SKB TR 93-04

Lars Werme, Joachim Eriksson
Swedish Nuclear Fuel and Waste Management Co, Stockholm, Sweden
March 1995

TR 95-03

Prestudy of final disposal of long-lived low and intermediate level waste

Marie Wiborgh (ed.)
Kemakta Konsult AB, Stockholm, Sweden
January 1995

TR 95-04

Spent nuclear fuel corrosion: The application of ICP-MS to direct actinide analysis

R S Forsyth[1], U-B Eklund[2]
[1] Caledon-Consult AB, Nyköping, Sweden
[2] Studsvik Nuclear AB, Nyköping, Sweden
March 1995

TR 95-06

Palaeohydrological implications in the Baltic area and its relation to the groundwater at Äspö, south-eastern Sweden – A literature study

Bill Wallin
Geokema AB, Lidingö, Sweden
March, 1995

TR 95-07

Äspö Hard Rock Laboratory Annual Report 1994

SKB
April 1995

TR 95-08

Feasibility study for siting of a deep repository within the Storuman municipality

Swedish Nuclear Fuel and Waste Management Co., Stockholm
January 1995

TR 95-09

A thermodynamic data base for Tc to calculate equilibrium solubilities at temperatures up to 300°C

Ignasi Puigdomènech[1], Jordi Bruno[2]
[1] Studsvik AB, Nyköping, Sweden
[2] Intera Information Technologies SL, Cerdanyola, Spain
April 1995

TR 95-10

Investigations of subterranean microorganisms. Their importance for performance assessment of radioactive waste disposal

Karsten Pedersen[1], Fred Karlsson[2]
[1] Göteborg University, General and Marine Microbiology, The Lundberg Institute, Göteborg, Sweden
[2] Swedish Nuclear Fuel and Waste Management Co., Stockholm, Sweden
June 1995

TR 95-11

Solute transport in fractured media – The important mechanisms for performance assessment

Luis Moreno, Björn Gylling, Ivars Neretnieks
Department of Chemical Engineering and Technology, Royal Institute of Technology, Stockholm, Sweden
June 1995

TR 95-12
Literature survey of matrix diffusion theory and of experiments and data including natural analogues
Yvonne Ohlsson, Ivars Neretnieks
Department of Chemical Engineering and Technology, Royal Institute of Technology, Stockholm, Sweden
August 1995

TR 95-13
Interactions of trace elements with fracture filling minerals from the Äspö Hard Rock Laboratory
Ove Landström[1], Eva-Lena Tullborg[2]
[1] Studsvik Eco & Safety AB
[2] Terralogica AB
June 1995

TR 95-14
Consequences of using crushed crystalline rock as ballast in KBS-3 tunnels instead of rounded quartz particles
Roland Pusch
Clay Technology AB
February 1995

TR 95-15
Estimation of effective block conductivities based on discrete network analyses using data from the Äspö site
Paul R La Pointe[1], Peter Wallmann[1], Sven Follin[2]
[1] Golder Associates Inc., Seattle, WA, USA
[2] Golder Associates AB, Lund, Sweden
September 1995

TR 95-16
Temperature conditions in the SKB study sites
Kaj Ahlbom[1], Olle Olsson[1], Stefan Sehlstedt[2]
[1] Conterra AB
[2] MRM Konsult AB
June 1995

TR 95-17
Measurements of colloid concentrations in the fracture zone, Äspö Hard Rock Laboratory, Sweden
Anna Ledin, Anders Düker, Stefan Karlsson, Bert Allard
Department of Water and Environmental Studies,Linköping University, Linköping, Sweden
June 1995

TR 95-18
Thermal evidence of caledonide foreland, molasse sedimentation in Fennoscandia
Eva-Lena Tullborg[1], Sven Åke Larsson[1], Lennart Björklund[1], Lennart Samuelsson[2], Jimmy Stigh[1]
[1] Department of Geology, Earth Sciences Centre, Göteborg University, Göteborg, Sweden
[2] Geological Survey of Sweden, Earth Sciences Centre, Göteborg, Sweden
November 1995

TR 95-19
Compaction of bentonite blocks. Development of technique for industrial production of blocks which are manageable by man
Lars-Erik Johannesson, Lennart Börgesson, Torbjörn Sandén
Clay Technology AB, Lund, Sweden
April 1995

TR 95-20
Modelling of the physical behaviour of water saturated clay barriers. Laboratory tests, material models and finite element application
Lennart Börgesson[1], Lars-Erik Johannesson[1], Torbjörn Sandén[1], Jan Hernelind[2]
[1] Clay Technology AB, Lund, Sweden
[2] FEM-Tech AB, Västerås, Sweden
September 1995

TR 95-21
Conceptual model for concrete long time degradation in a deep nuclear waste repository
Björn Lagerblad, Jan Trägårdh
Swedish Cement and Concrete Research Institute
February 1994

TR 95-22
The use of interaction matrices for identification, structuring and ranking of FEPs in a repository system. Application on the far-field of a deep geological repository for spent fuel
Kristina Skagius[1], Anders Ström[2], Marie Wiborgh[1]
[1] Kemakta, Stockholm, Sweden
[2] Swedish Nuclear Fuel and Waste Management Co, Stockholm, Sweden
November 1995

TR 95-23
Spent nuclear fuel. A review of properties of possible relevance to corrosion processes
Roy Forsyth
Caledon Consult AB
April 1995

TR 95-24
Studies of colloids and their importance for repository performance assessment
Marcus Laaksoharju[1], Claude Degueldre[2], Christina Skårman[1]
[1] GeoPoint AB, Sollentuna, Sweden
[2] University of Geneva, Switzerland
December 1995

TR 95-25
Sulphate reduction in the Äspö HRL tunnel
Marcus Laaksoharju (ed.)
GeoPoint AB, Sollentuna, Sweden
December 1995

TR 95-26
The Äspö redox investigations in block scale. Project summary and implications for repository performance assessment
Steven Banwart (ed.)
Dept. of Civil and Environmental Engineering, University of Bradford, UK
November 1995

TR 95-27
Survival of bacteria in nuclear waste buffer materials. The influence of nutrients, temperature and water activity
Karsten Pedersen[1], Mehrdad Motamedi[1], Ola Karnland[2]
[1] Department of General and Marine Microbiology, the Lundberg Institute, Göteborg University, Göteborg, Sweden
[2] Clay Technology AB, Lund, Sweden
December 1995

TR 95-28
DECOVALEX I – Test Case 2: Calculation of the Fanay-Augères THM Test – Thermomechanical modelling of a fractured rock volume
Lennart Börgesson[1], Jan Hernelind[2]
[1] Clay Technology AB, Lund, Sweden
[2] Fem-Tech AB, Västerås, Sweden
December 1995

TR 95-29
DECOVALEX I – Test Case 3: Calculation of the Big Ben Experiment – Coupled modelling of the thermal, mechanical and hydraulic behaviour of water-unsaturated buffer material in a simulated deposition hole
Lennart Börgesson[1], Jan Hernelind[2]
[1] Clay Technology AB, Lund, Sweden
[2] Fem-Tech AB, Västerås, Sweden
December 1995